Functional regions within a Q/N rich prion domain driving prion replication in the mammalian cytosol

Dissertation

zur

Erlangung des Doktorgrades (Dr. rer. nat.)

der

Mathematisch-Naturwissenschaftlichen Fakultät

der

Rheinischen Friedrich-Wilhelms-Universität Bonn

vorgelegt von

Yvonne Dürnberger

aus

Neuwied

Bonn 2016

Angefertigt mit Genehmigung der Mathematisch-Naturwissenschaftlichen Fakultät der

Rheinischen Friedrich-Wilhelms-Universität Bonn

1. Gutachterin: Prof. Dr. Ina Vorberg

2. Gutachter: Prof. Dr. Walter Witke

Tag der Promotion: 06.04.2017

Erscheinungsjahr: 2017

Table of contents

Summary

Prions are proteinaceous infectious agents that replicate by recruiting and converting homotypic soluble proteins into growing aggregates. Prions in mammals cause transmissible spongiform encephalopthies and are composed of membrane-bound PrP. In addition to prions in mammals, infectious protein aggregates were also identified in lower eukaryotes. Prion domains of lower eukaryotes are often enriched in glutamine (Q) and asparagine (N) residues and are usually located in unstructured regions. Interestingly, approximately one percent of human protein-coding genes contain Q/N rich prion-like domains. Until recently, it was unclear if prion replication is possible in the mammalian cytosol. By expressing the prion domain of *Saccharomyces cerevisiae* Sup35 in mouse neuroblastoma cells, our group could already show that Q/N rich prions can replicate in the mammalian cytosol. Yet, which regions within the Q/N rich prion domain of Sup35 specifically drive prion induction, propagation and inheritance in mammalian cells was so far unclear. Therefore, the aim of this study was to identify the essential regions that are required for the individual steps of prion replication in the mammalian cytosol. Surprisingly, we found that the aminoterminal region essential for prion activity in yeast, was dispensable for prion replication in the mammalian cytosol and even helped to retain the protein in its soluble state. Instead, we identified a carboxyterminal region with a lower Q/N content as the crucial region for prion replication in mammalian cells, a region that was shown not to influence prion formation in yeast. Interestingly, we found that in mammalian cells all prion activity was governed by only one distinct region, whereas in yeast, prion replication processes were depending on separate elements. Combined, these findings indicate that prion domains active in mammalian cells differ from the ones active in yeast, and suggest that studies on prionogenic behavior of prion or prion-like proteins should be undertaken in the correct environment. Our data provides a more detailed insight into the requirements for cytosolic prion replication in the mammalian cytosol, and will help to better predict proteins with prion-like properties that might be the cause for diseases of so far unknown etiology in mammals.

1.Introduction

1.1 Prion diseases

Prions were first described by Stanly Prusiner in 1982 as the causative agent for prion diseases, also known as transmissible spongiform encephalopathies (TSEs). Prions are proteinaceous infectious particles that replicate independently of nucleic acids (Prusiner 1982). In his protein-only hypothesis, Prusiner postulates that the cellular prion protein (PrP^{C}) undergoes a post-translational conformational change to its misfolded isoform (PrP^{Sc}) that serves as a template for continuous conversion of further cellular PrP^{C} monomers (Griffith 1967, Prusiner 1998). TSEs are fatal neurodegenerative disorders that affect humans and other mammals. In humans they include Creutzfeldt-Jakob disease (CJD), variant CJD, fatal familial insomnia (FFI), Gerstmann-Sträussler-Scheinker syndrome (GSS) and kuru. Scrapie in goats and sheep, bovine spongiform encephalopathy (BSE) in cattle and chronic wasting disease (CWD) in deer and elk (Prusiner 1998), account for TSEs in mammals. Prion diseases can be acquired, as observed for kuru and variant CJD, sporadic, resulting from spontaneous conversion to the prion isoform, or familial, as a result of mutations in the PrP gene (*PRNP*). TSE pathology is characterized by the deposition of misfolded PrP aggregates in the central nervous system (CNS) and lymphoreticular system, as well as histopathological hallmarks such as neuronal vacuolation and degeneration (Prusiner 1998). Prion diseases have a very long incubation time before clinical symptoms are noticeable. They can be discriminated from other misfolding disorders through their unique infectivity and transmissibility within and between species (Aguzzi and Heikenwalder 2006).

1.2 PrP: structure and replication

PrP is encoded by the highly conserved *PRNP* gene, which shows more than 80 % sequence homology from amphibians to mammals (Basler et al. 1986). PrP expression was found in skeletal muscle, kidney, heart, secondary lymphoid organs and the CNS (Aguzzi and Heikenwalder 2006). So far, the cellular prion protein has been associated with a wide array of physiological functions, including signaling cascades, neuronal survival, apoptosis, immunomodulation and microRNA metabolism (Gibbings et al. 2012, Linden et al. 2012). PrP consists of 254 amino

acids (aa), has an aminoterminal signal peptide (SP) for endoplasmic reticulum (ER) translocation and is tethered to the outer leaflet of the plasma membrane by a carboxyterminal glycosylphosphatidylinositol (GPI) anchor (Fig. 1).

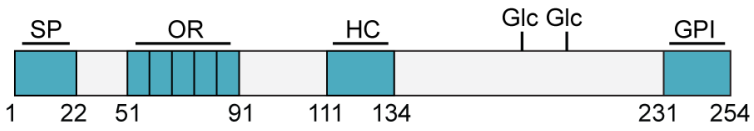

Figure 1. Primary sequence of PrP. PrP consists of 254 amino acids and contains an ER signal peptide (SP, aa 1-22), an octapeptide repeat region (OR, aa 51-91), consisting of five octapeptide repeats, a hydrophobic core region (HC, aa 111-134), two glycosylation (Glc) sites (aa 181, 197) and a GPI anchor. Numbers refer to amino acids.

The aminoterminal part of the protein is unstructured but contains two distinct regions: The octapeptide repeat region that consists of five oligopeptide repeats (OR, PHGGGWGQ, aa 51-91) and a downstream hydrophobic core region (HC, aa 111-134) (Aguzzi and Heikenwalder 2006). The carboxyterminal part of the protein is mainly α-helical and contains two glycosylation (Glc) sites. Replication of PrP^{Sc} occurs through the process of seeded polymerization (Come et al. 1993, Caughey et al. 1995) (Fig. 2).

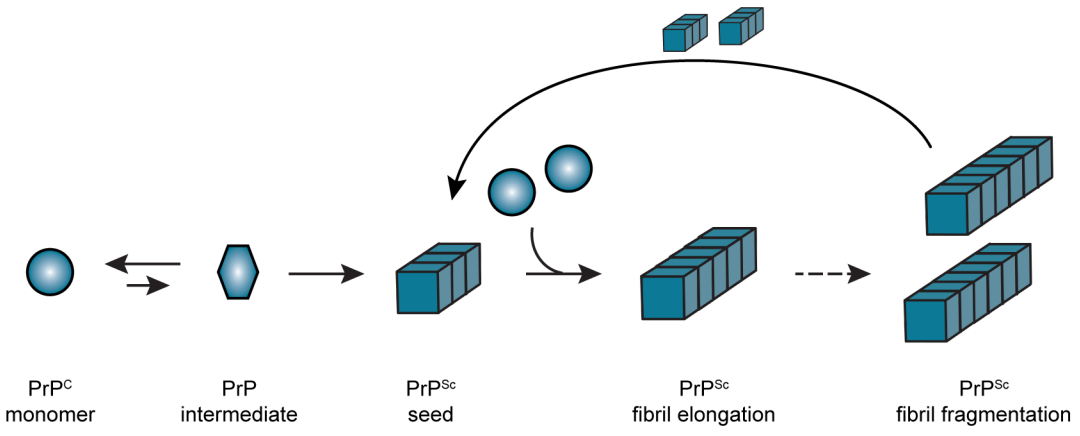

Figure 2. PrP^{Sc} replication by seeded polymerization. On rare occasions, PrP^{C} monomers spontaneously convert to the misfolded isoform PrP^{Sc} via a PrP intermediate. PrP^{Sc} seeds subsequently serve as templates to bind and convert further PrP^{C} monomers to the misfolded isoform. In secondary nucleation events, growing amyloid fibrils are fragmented into smaller entities that function as new conversion sites.

PrP is hypothesized to exist in equilibrium between PrP^C and a PrP intermediate, where the PrP^C monomer is favored. On rare occasions, PrP^C undergoes a conformational change to its misfolded isoform PrP^{Sc}. Spontaneously formed misfolded conformers bind soluble PrP^C monomers and template their conversion into the prion isoform, leading to continuously growing fibrils with so-called amyloid-structure. Amyloid fibrils have a distinct conformation. They are usually 6-12 nm in diameter, rigid and non-branching (Serpell 2000, Serpell et al. 2000, Stefani and Dobson 2003). Each amyloid fibril consists of two to six protofilaments that are twisted around each other forming a supercoiled structure (Serpell 2000, Serpell et al. 2000, Stefani and Dobson 2003). Furthermore, each protofilament comprises a number of β-sheets that run perpendicular to the fibril axis (Shewmaker et al. 2008, Shewmaker et al. 2009). In secondary nucleation events, the growing amyloid fibril is fragmented into smaller infectious entities that function as new seeds for the conversion of further PrP^C monomers (Orgel 1996, Knowles et al. 2009). Interestingly, Caughey and colleagues demonstrated in 2005, that non-fibrillar particles comprising 14-28 PrP molecules are the most infectious (Silveira et al. 2005). In contrast to the mainly α-helical PrP^C, PrP^{Sc} aggregates are rich in β-sheets, resulting in increased heat-, detergent- and protease-resistance. While PrP^C is sensitive to proteinase K digestion, PrP^{Sc} contains a proteolytic protected carboxyterminal core (aa 90 – 231) (Prusiner et al. 1984, Oesch et al. 1985). The proteinase K resistance of PrP^{Sc} is broadly used to distinguish the two isoforms (Oesch et al. 1985, Gasset et al. 1992).

1.3 The species barrier and prion strains

Prions are transmissible within one species and sometimes also between species. However, in interspecies transmissions, usually prolonged incubation times are observed, known as the ‘’species barrier’’ (Bruce 1993, Bruce et al. 1994, Sweeting et al. 2010). The species barrier is predominantly determined by polymorphisms in PrP (Scott et al. 1993, Schatzl et al. 1995, Priola et al. 2001). The severity of the species barrier and the duration of incubation time can be highly variable, depending on the conformational degree of overlap between the infectious and normal prion protein (Collinge and Clarke 2007, Beringue et al. 2008).

The existence of prion strains was first demonstrated in 1961 (Pattison and Millson 1961). In 1992, Bessen and Marsh detected that strains isolated from outbred Syrian

golden hamsters differed in the biochemical and physical properties of PrP^{Sc} (Bessen and Marsh 1992). Prion strains differ in their incubation period as well as type, severity and distribution of pathological changes in the brain and are associated with a characteristic lesion profile (Fraser and Dickinson 1968, Bruce 1993). Additionally, prion strains exhibit differences in the biochemical properties of PrP^{Sc}, such as electrophoretic mobility of PrP^{Sc} after proteinase K digestion, stability towards denaturing agents and ratio of glycoforms (Beringue et al. 2008). Strain-specific phenotypes, including biochemical properties as well as pathology, are stably propagated from mouse to mouse (Telling et al. 1996, Beringue et al. 2008). In 2001, Soto and coworkers invented a new method for *in vitro* replication of prions, termed "Protein Misfolding Cyclic Amplification" (PMCA). Using PMCA it was demonstrated that prion strain phenotypes are also stably propagated *in vitro* (Saborio et al. 2001, Castilla et al. 2005). However, the underlying mechanisms that result in the initial formation of diverse prion strains are still unknown.

1.4 Protein misfolding diseases

The conformational change from natively folded or unfolded protein into a misfolded isoform is not only observed for prion proteins. Proteins that exhibit prion-like properties are associated with many neurodegenerative diseases, including Alzheimer's disease (AD), Parkinson's disease (PD) and type 2 diabetes (Soto 2012). The largest group among the protein misfolding diseases (PMDs) is associated with the formation of amyloid aggregates. Interestingly, even though these aggregation-prone proteins share the formation of this particular amyloidogenic molecular structure, they share no obvious sequence similarities (Chiti and Dobson 2006). To date, a great number of proteins was shown to form amyloid conformations under specific conditions, arguing that the ability to form into an amyloid structure is a generic property of all proteins whose propensity can, however, vary depending on the sequence (Chiti and Dobson 2006). Similar to PrP, amyloids are formed by seeded polymerization. Interestingly, several disease-associated amyloids are, on a molecular und cellular level, also transmissible between cells (Walker and Jucker 2015), and thus share some prion-like characteristics. Yet, in contrast to PrP, there is no epidemiological proof of transmission from one individual to another (Aguzzi and Rajendran 2009, Cushman et al. 2010).

1.5 Prions in lower eukaryotes

Besides the mammalian prion protein, several proteins in lower eukaryotes have been identified that are capable of converting into a prion isoform (Table 1).

Table 1. Prions in lower eukaryotes

Protein	Prion isoform	Cellular function	Reference
Sup35	[PSI+]	Translation termination	(Wickner 1994)
Ure2	[URE3]	Regulation of nitrogen catabolism	(Wickner 1994)
Rnq1	[PIN+]	So far unknown	(Sondheimer and Lindquist 2000)
HET-s*	[Het-s]	Heterokaryon incompatibility in the prion form; no function in the non-prion form	(Coustou et al. 1997)
Swi1	[SWI+]	Chromatin remodeling	(Du et al. 2008)
Cyc8	[OCT+]	Repression of transcription	(Patel et al. 2009)
Mot3	[MOT+]	Regulation of transcription	(Alberti et al. 2009)
Sfp1	[ISP+]	Transcription factor	(Rogoza et al. 2010)
Mod5	[MOD+]	tRNA isopentenyltransferase	(Suzuki et al. 2012)

All listed proteins are capable of folding into amyloid fibrils (Wickner et al. 2015). * All prions except [Het-s] were found in *Saccharomyces cerevisiae (S. cerevisiae)*. [Het-s] was discovered in *Podospora anserina*.

Yeast prions are a very useful tool to analyze prion characteristics and their replication, as they share many mammalian prion properties. However, except for the oligopeptide repeats in PrP and the oligopeptide repeat region (OPR) of the *Saccharomyces cerevisiae (S. cerevisiae)* prion Sup35, PrP and the so far identified yeast prions share no sequence similarities. Unlike PrP, yeast prions are found in the cytosol and will therefore most likely differ from PrP in their replication. Yeast prions can be toxic to the host (McGlinchey et al. 2011), but in contrast to PrP, some have also been reported to have beneficial functions (Newby and Lindquist 2013). Two of the most extensively studied yeast prions are Ure2 and Sup35 (Ross, Minton, et al.

2005). The soluble form of Ure2 is a negative regulator of enzymes and transporters needed for the utilization of poor nitrogen sources (Wickner 1994). Sup35 functions as a translation termination factor. However, protein activity is lost upon conversion to the prion isoform, leading to a read-through of stop codons (Uptain and Lindquist 2002). In a reporter assay, the prion isoform induced read-through of stop-codons is used to distinguish the soluble from the prion phenotype (Chernoff et al. 1995) (Fig. 3).

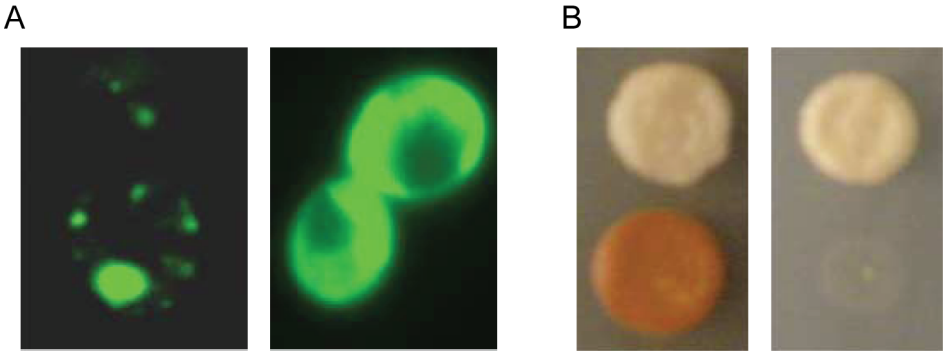

Figure 3. Representation of Sup35 prions in yeast. A. Immunofluorescence staining of Sup35 fused to a GFP tag. Prion isoform (left), soluble isoform (right). **B.** Growth of yeast cells expressing the prion isoform (upper panel) of Sup35 and the soluble isoform (lower panel) on YPD medium with (left) or without (right) adenine. From Tuite and Cox (2003).

In this color assay, the prion isoform of Sup35 reads through a premature stop codon in the *ade1-14* allele, resulting in growth of white colonies on solid rich medium (YPD). In its soluble form, however, translation of adenine is prematurely halted, leading to the accumulation of metabolic byproducts and the formation of red colonies. The assay can be altered to select only strains carrying the prion isoform by growing yeast strains on medium deprived of adenine (Fig. 3B).

Similar to the mammalian prion, yeast prions propagate by seeded polymerization (Fig. 2). The first step, conversion of the soluble isoform to the prion conformer, is a very rare event in yeast, with a frequency of ~ 10^{-7} (Lancaster et al. 2010). In analogy to PrP, prion fibrils are fragmented into smaller entities, offering numerous new conversion sites. In yeast, fragmentation depends on the heat-shock protein Hsp104 in a concentration-dependent manner. Moderate amounts of Hsp104 are required to fragment assembled fibrils into smaller entities. Depletion of Hsp104 or excess

amounts on the other hand have been shown to cure the prion phenotype. This demonstrates that prion propagation in yeast depends on a well-balanced ratio of Sup35 and Hsp104 (Chernoff et al. 1995). In the final step, the generated propagons are distributed to the daughter cell or are naturally transmitted during mating (Uptain and Lindquist 2002). As yeast prions are not naturally transmitted to neighboring cells, their infectivity is assessed by cytoduction. Cytoduction is a process of cytoplasmic mixing without nuclei fusion, where it was shown that the prion phenotype is induced in a former non-prion bearing cell by mixing with cytoplasm of a prion-bearing cell (Aigle and Lacroute 1975, Wickner 1994).

In line with the strain-phenomenon observed for mammalian prions (Bruce 1993), yeast prions can also adopt different conformations (Derkatch et al. 1996, Schlumpberger et al. 2001, Tanaka et al. 2004). In yeast, prion strains are often referred to as "variants", to distinguish them from the variety of laboratory yeast strains. For Sup35, prion variants are mostly distinguished by the loss of the protein's translation termination function and are classified as strong, moderate or weak (Derkatch et al. 1996). Strong Sup35 variants contain less soluble Sup35 compared to weak variants (Kochneva-Pervukhova et al. 2001). Strong Sup35 variants also show a higher efficiency in cell-free conversion assays (Uptain et al. 2001), where yeast lysates with no prion phenotype are converted to the prion isoform by mixing with yeast lysates showing the prion phenotype (Paushkin et al. 1997). In analogy to mammalian prion strains, yeast prion variants also show distinct physical properties *in vitro* (Chien and Weissman 2001), though upon further passaging their characteristics are lost in a cell-free environment (Uptain et al. 2001). Yeast prion variants also show differences in their amyloid core structures (Toyama et al. 2007).

In yeast, prion properties are conferred by the prion domain (PrD). The PrD is a modular structure that retains its prion activity even when fused to other proteins (Li and Lindquist 2000, Baxa et al. 2002, MacLea and Ross 2011). Although the exact molecular structures that govern prion propensities have so far, not been entirely identified, extensive research over the last decade unraveled the fundamentals of PrDs (Li and Lindquist 2000, Alberti et al. 2009). Two major theories were put forward. In the first theory, the PrD is a large, disordered region in which many weak interactions drive aggregation (Toombs et al. 2012). In the second theory, aggregation is facilitated by a small, highly aggregation-prone domain that is embedded in a large, disordered region enriched in glutamine (Q) and asparagine

(N) residues (Sabate et al. 2015). Whether any of the two theories is ultimately correct, or different types of PrDs exist, has so far not been established.

1.6 Structure of Sup35

The prion phenomenon associated with Sup35 was first discovered in 1965 by Brian Cox, who described it as a non-chromosomal epigenetic element that does not segregate in a Mendelian fashion (Cox 1965). The full-length *S. cerevisiae* Sup35 protein comprises 685 amino acids and consists of three domains: the aminoterminal N domain, the middle M domain and the carboxyterminal C domain (Fig. 4).

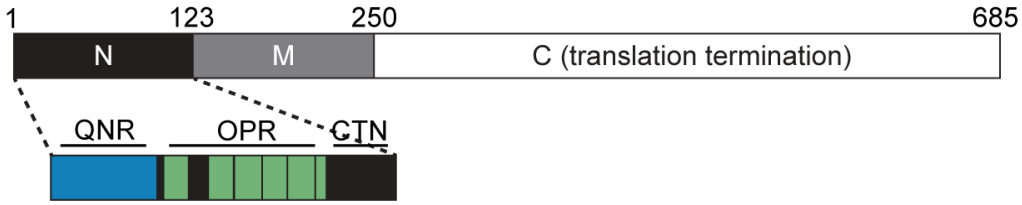

Figure 4. Primary sequence of Sup35. Sup35 consists of three domains: The aminoterminal N domain, the middle M domain and the carboxyterminal C domain. The N domain is responsible for the prion activity and can be subdivided into a Q/N rich region (QNR), an oligopeptide repeat region (OPR) and a carboxyterminal N domain (CTN). The M domain is highly charged, influences the proteins solubility and stabilizes the amyloid fibril. The C domain encodes the translation termination function, but is dispensable for the prion characteristics of the protein. Numbers refer to amino acids.

The C domain (aa 251-685) encodes the translation termination function of the protein, but is otherwise dispensable for its prion properties (Ter-Avanesyan et al. 1993). The highly charged M domain influences the solubility of Sup35 and promotes mitotic stability of the prion state, possibly through interactions with Hsp104 (Liu et al. 2002). The N domain is rich in glutamine and asparagine residues and contains the PrD (Ter-Avanesyan et al. 1993, Ter-Avanesyan et al. 1994, Derkatch et al. 1996). The N domain can be further subdivided into three regions: the especially glutamine- (32%) and asparagine- (24%) rich region (QNR, aa 1-39), the oligopeptide repeat region (OPR), consisting of five and a half imperfect oligopeptide repeats (R1 - R6, PQGGYQQ-YN, aa 40-97) and the carboxyterminal N domain (CTN), also rich in glutamine (19%) and asparagine (23%) residues (aa 98-123).

1.7 Defining the prion domain

In recent years, extensive studies have been conducted to define and characterize PrDs. In general, most PrDs are described to be rich in glutamine and asparagine residues, contain only a few charged and hydrophobic amino acids and are located in an unstructured region (DePace et al. 1998, Alberti et al. 2009, Du 2011). Studies on Sup35 soon identified the N domain as the critical region for the appearance of the prion phenotype (Glover et al. 1997, King et al. 1997). Interestingly, in 2005, Ross and coworkers demonstrated that scrambling the PrD of Sup35 does not disrupt its prion propensity, arguing that it is the amino acid composition rather than the primary sequence that determines prion characteristics (Ross, Edskes, et al. 2005). These findings were later confirmed by Shewmaker and colleagues, who demonstrated that the molecular structure of normal and shuffled Sup35 prions most likely resembles an in-register β-sheet (Shewmaker et al. 2008, Shewmaker et al. 2009). However, even in shuffling studies, differences in prion characteristics, such as prion frequency and stability, were observed, indicating that although composition is of great importance, the primary sequence plays a major role, too.

On the basis of primary sequence, numerous mutation and deletion studies were performed to define minimal regions within the N domain that are capable of inducing and propagating the prion phenotype. Many different yeast strains and prion variants were used, leading to minor variations in the experimental outcomes. Though differences in experimental setups complicate direct comparisons, some conclusion can be drawn. *De novo* aggregation of overexpressed NM (Sup35 that lacks its C domain) was found to depend on the QNR and the first two repeats of the OPR (aa 1-64) in two separate studies (Osherovich et al. 2004, Shkundina et al. 2006). Similar results were found by King and coworkers, who identified the first 61 amino acids to be required for *de novo* aggregation (King 2001). These results are in agreement with the finding that expression of Sup35 with mutations in the first 34 amino acids of the QNR cure the prion phenotype (DePace et al. 1998). However, in studies conducted by Parham and colleagues, the QNR and the entire OPR (aa 1-97) were needed for aggregation (Parham et al. 2001). The same region (aa 1-97) was also discovered in the same study to be crucial for aggregate maintenance, data that agrees with findings from Osherovich (aa 1-97) and Shkundina (aa 1-83) (Parham et al. 2001, Osherovich et al. 2004, Shkundina et al. 2006). Interestingly, in studies conducted by Chang and colleagues, only the QNR

and the first repeat (aa 1-53) were required for prion infectivity (Chang et al. 2008). In accordance with the previous data, Toyama and coworkers could show that the first 40 or, depending on the prion variant, the first 70 amino acids were protected from hydrogen-deuterium exchange experiments, arguing that those residues were part of the protected amyloid core region and thus crucial for aggregation (Toyama et al. 2007). Interestingly, one single glycine to aspartic acid point mutation in the second repeat (aa 58) was shown to eliminate the prion phenotype, suggesting that the second repeat has a crucial function for aggregate fragmentation and consequently maintenance (Doel et al. 1994, Osherovich et al. 2004). Combined, these findings suggest that *in vitro* and in yeast, the QNR and the first two repeats are essential for *de novo* induction of prions, whereas the OPR is required for fragmentation and maintenance.

1.8 Mammalian proteins with putative prion-like domains

Based on compositional similarities of yeast PrDs, several prediction algorithms were generated to identify proteins with putative prion-like domains (PrLDs) (Alberti et al. 2009, Espinosa Angarica et al. 2014, Lancaster et al. 2014). Surprisingly, these algorithms predict PrLDs in one percent of human protein-coding genes (King et al. 2012). Amongst them are many RNA-binding proteins such as TDP-43 and FUS that form cytoplasmic inclusions in PMDs like amyotrophic lateral sclerosis (ALS) and frontotemporal lobar degeneration (FTLD). TDP-43 is involved in transcriptional regulation and splicing of RNA (Buratti and Baralle 2008, Buratti and Baralle 2010). TDP-43 is intrinsically aggregation-prone, but aggregation can be prevented upon deletion of its carboxyterminal PrLD (King et al. 2012). FUS functions in transcriptional regulation and RNA homeostasis (Bertolotti et al. 1996, Zinszner et al. 1997, Kasyapa et al. 2005). Similar to TDP-43, aggregation of FUS is promoted by its aminoterminal PrLD (Couthouis et al. 2011, Sun et al. 2011). The high abundance of prion-like proteins in the human proteome suggests that prion-like behavior might be an evolutionary conserved feature. The aggregation-prone nature of many RNA-binding proteins is hypothesized to be involved in long-term memory similar to *Aplysia* Cytoplasmic Polyadenylation Element Binding protein (CPEB) (Si et al. 2003, Shorter and Lindquist 2005, Si et al. 2010). The PrLDs of RNA-binding proteins are also suggested to function in P-body and stress granules formation, as already

reported for TIA-1 (Gilks et al. 2004, King et al. 2012). However, whether mammalian proteins with PrLDs can truly fold into self-templating prions remains elusive.

1.9 NM as a model system in mammalian cells

The only known mammalian prion to date is the membrane-anchored PrP. Until recently, it was unclear if prion replication is possible in the mammalian cytosol. NM has no translation termination function and exhibits no sequence homology to mammalian proteins, making it a very suitable model to study cytosolic prion replication without a loss of function phenotype. The NM model system was established in our laboratory by transducing the mouse neuroblastoma cell line N2a with lentiviral particles coding for NM carboxyterminally fused to a hemagglutinin-tag (HA-tag). In this system, NM was shown to reside in its soluble state, with no detectable spontaneous aggregation (Krammer et al. 2009). Upon addition of *in vitro* fibrillized recombinant NM to the cell culture medium, aggregation of NM could be induced (Krammer et al. 2009). This is in analogy to experiments in yeast, where purified NM was seeded with NM aggregates derived from yeast cells carrying the prion isoform, and afterwards used to successfully induce the prion phenotype in yeast (King and Diaz-Avalos 2004). In N2a cells, induced aggregates stably propagate to daughter cells and act as infectious entities that horizontally transmit to bystander cells (Krammer et al. 2009, Hofmann et al. 2013). For successful propagation, high-molecular weight conformers must be fragmented into smaller entities. In yeast, Hsp104 was shown to be one of the major components responsible for fragmentation and consequently, maintenance of the prion phenotype (Chernoff et al. 1995). Intriguingly, to date no mammalian homologue of Hsp104 has been identified, suggesting that fragmentation is facilitated by a different, and so far unknown machinery in mammalian cells. Limiting dilution cloning of cells stably propagating NM aggregates revealed morphologically and biochemically different aggregate types that were stably propagated, reminiscent of prion variants in yeast (Krammer et al. 2009). Interestingly, cell extracts from NM-HA aggregate bearing cell clones could induce the prion phenotype in yeast (Krammer et al. 2009). Though induction was less efficient compared to inductions with extracts derived from yeast carrying the prion isoform, the results demonstrated that NM aggregates derived from mammalian cells function as true prions (Tanaka et al. 2004, Brachmann et al. 2005, Krammer et al. 2009). Combined, these results illustrate that NM prions behave as

infectious entities in mammalian cells and fulfill the entire life cycle of cytosolic prions. Thus, the NM system provided proof-of-principle that cytosolic prion replication is possible in mammalian cells (Fig. 5).

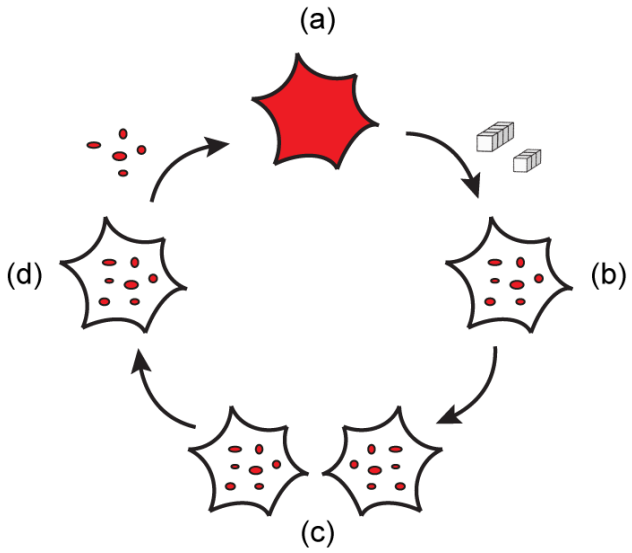

Figure 5. Scheme depicting the cytosolic NM prion life cycle. (a) The prion precursor protein resides in its soluble state, (b) aggregation is induced upon addition of exogenous NM fibrils, (c) aggregates are fragmented and propagons inherited by daughter cells, (d) propagons invade neighboring cells and induce a self-perpetuating prion state of the prion precursor protein.

1.10 Objective

Extensive research has been conducted to identify and further characterize domains that govern prion properties, so-called prion or prion-like domains. Prion domains are often enriched in glutamine and asparagine, lack charged amino acids and are usually located in unstructured regions. Early on the N domain was identified as the prion domain of Sup35 and later on further subcategorized into regions crucial for *de novo* aggregation and maintenance of the prion phenotype in yeast. Based on these and other experiments performed *in vitro* and in yeast, several algorithms have been developed to detect so far unknown prion-like proteins in lower eukaryotes as well as in mammals. Interestingly, algorithms have predicted that one percent of the human proteome contain prion-like domains. Yet, whether domains that share compositional similarity to yeast prion domains also govern prion-like properties in mammalian cells has not been analyzed so far. The aim of this study was to identify

essential elements required for the individual steps of cytosolic prion replication in mammalian cells using the already established NM N2a cell model. In this study, NM proteins with deletions or a point mutation in the N domain of Sup35 should be stably expressed in mouse neuroblastoma cell line N2a. The individual cell lines should be screened for events of spontaneous aggregation by high-throughput confocal microscopy to detect rare events of prion induction. Aggregation of the ectopically expressed NM mutants should be induced by either exogenous recombinant NM fibrils or endogenous NM prions and should be analyzed for differences in the induction efficiencies compared to the full-length protein. Following successful aggregate induction, the NM mutant cell lines should be monitored for aggregate maintenance. To complete the prion replication cycle, the infectious properties of NM mutants should be investigated by coculture experiments of cells with and without aggregates. Combined, this research should present a more detailed insight into sequence requirements for cytosolic prion replication in the mammalian context. This knowledge will help to optimize prediction algorithms for the search of so far unknown prion-like proteins in mammals.

2. Materials and methods

2.1 Biological safety

Genetic engineering and work with genetically modified organisms was conducted under biosafety containment level 2 according to the German *Gentechnikgesetz* (August 31st, 2015). All contaminated materials and solutions were collected, decontaminated and disposed following the official rules.

2.2 Chemicals

All chemicals were purchased from Carl Roth (Karlsruhe, Germany) or Sigma-Aldrich (Steinheim, Germany), unless stated otherwise.

2.3 Molecular biological methods

2.3.1 Polymerase chain reaction (PCR)

Kapa Hifi PCR kit Kapa Biosytems, Cape Town, South Africa

For amplification or modification of DNA constructs, Kapa Hifi PCR kit was used with a specific primer pair according to the manufacturer's instructions (Table 2).

Table 2: Oligodeoxynucleotides

Name	**Sequence (5' - 3')**
NM-HA_linker	GTC GAC TTA AGC GTA ATC TGG TAC GTC GTA TGG GTA GAA TTC AAC TTC GTC ATC CAC
TS9	TAA AGG ATC CGT CGC CAC CAT GTC CGA TTC AAA CCA AGG
TS2	ATA TTG AAT TCA ACT TCG TCA TCC ACT TCT TC
N-domain_EcoRI_addition	GAA TTC ACC TTG AGA CTG TGG TT
NM_del_1-39_fwd	GGA TCC GTC GCC ACC ATG CAA CCT GCA GGT GG
NM_del_39-123_fwd	TAC AAT GCT CAA ATG TCT TTG AAC GAC TTT C
NM_del_39-123_rev	GTC GTT CAA AGA CAT TTG AGC ATT GTA AGC

NM_del_75-123_fwd	CAA CAG TAT AAT ATG TCT TTG AAC GAC TTT C
NM_del_75-123_rev	GTC GTT CAA AGA CAT ATT ATA CTG TTG CTG G
NM_del_98-123_fwd	CCA CAA GGT GGC ATG TCT TTG AAC GAC TTT C
NM_del_98-123_rev	GTC GTT CAA AGA CAT GCC ACC TTG TGG ATT G

2.3.2 Enzymatic digestion of plasmid DNA

Restriction enzymes and buffers New England Biolabs, Ipswich, USA

For each reaction, approximately 1 µg plasmid DNA was digested. The appropriate buffer was chosen according to the restriction enzymes used for individual experiments. The reagents were mixed according to the manufacturer's instructions and incubated for 3 - 4 h at 37 °C.

2.3.3 Enzymatic ligation of DNA

T4 DNA ligase and buffer New England Biolabs, Ipswich, USA

Vector DNA and insert DNA were ligated at a molar ratio of 1:3 with a combined amount of approximately 100 ng. DNA, ligase and buffer were mixed according to the manufacturer's instructions and incubated for 1 h at room temperature (RT) or overnight (O/N) at 16 °C.

2.3.4 Agarose gel electrophoresis

1x TAE buffer	40 mM Tris/HCl, pH 7.6 20 mM Acetic acid 1 mM EDTA in H_2O_{bidest}
Agarose	Biozym, Hessisch Oldendorf, Germany
6x DNA Loading buffer	Peqlab, Erlangen, Germany
1 kb DNA ladder	Carl Roth, Karlsruhe, Germany
GelRED	Biotium, Hayward, USA

To prepare agarose gels, 1 - 3 % agarose was melted in TAE buffer. The appropriate amount of GelRED (1:10000) was added and the agarose solution was poured into an electrophoresis chamber (Peqlab, Erlangen, Germany) equipped with a comb.

After the gel was solidified, the chamber was filled with TAE buffer and the comb removed. DNA samples supplemented with DNA loading buffer were loaded into the wells along with 3 µl of DNA marker as a reference for the size of the DNA fragments. The gel was run at 80 - 100 V for 60 - 90 min, depending on the agarose concentration and the size of the gel. Images of the gel were taken with a gel documentation system (Stella, Raytest, Straubenhardt, Germany) using UV illumination and a digitally controlled video camera.

2.3.5 DNA extraction from agarose gels

Gel Extraction Kit	Qiagen, Venlo, Netherlands

DNA was visualized with the UV transilluminator (Biostep, Burkhardtsdorf, Germany). The appropriate DNA band was cut out and DNA was extracted from residual agarose using the Gel Extraction Kit according to the manufacturer's instructions.

2.3.6 Generation of chemically competent *E.coli*

LB medium	2 % LB Broth-agar in H_2O_{bidest}

To generate chemically competent bacteria, 2 ml of LB medium were inoculated with one colony of DH5α or BL21 *Escherichia coli* (*E.coli*) and incubated in a shaker at 220 rpm O/N at 37 °C (LT-X Lab-Therm, Kuhner Shaker, Aachen, Germany). The next day, 100 ml of LB medium were inoculated with 500 µl of the O/N culture and shaken at 220 rpm and 37 °C until an OD_{600} of 0.3 was reached (LT-X Lab-Therm, Kuhner Shaker, Aachen, Germany). The bacteria were cooled on ice for 10 min and afterwards centrifuged at 1500 x g for 10 min at 4 °C (Heraeus Multifuge X3R, Thermo Scientific, Waltham, USA). The supernatant was discarded and the bacteria were carefully resuspended in 10 ml 0.1 M $MgCl_2$. As the bacteria are sensitive after $MgCl_2$ and the subsequent $CaCl_2$ treatment, all following steps were conducted on ice. The bacteria were centrifuged at 1500 x g for 10 min at 4 °C and the supernatant was discarded. The bacteria pellet was resuspended in 20 ml 0.1 M $CaCl_2$ and incubated for 20 min on ice. Centrifugation was repeated and the pellet resuspended in 1 ml 0.1 M $CaCl_2$ supplemented with 15 % glycerol. Cells were snap frozen in 50 µl aliquots and stored at -80 °C until further use.

2.3.7 Transformation of chemically competent *E.coli*

Depending on the experiment, either DH5α or BL21 *E.coli* were thawed and incubated with 10 - 50 ng plasmid DNA or half of the ligation mixture for 30 min on ice (Table 3). Afterwards, the bacteria were exposed to heat shock for 42 sec at 42 °C and subsequently cooled for 1 - 2 min on ice. 1 ml LB medium was carefully added and the bacteria were shaken at 300 rpm for 30 - 60 min at 37 °C (Thermomixer Compact, Eppendorf, Hamburg, Germany). To remove excess medium, the bacteria were spun down at 514 x g for 3 min at RT (Eppendorf Centrifuge 5417R, Hamburg, Germany). Most of the supernatant was discarded and the bacteria pellet was resuspended in the remaining medium. The bacteria were plated onto LB agar plates supplemented with either 100 µg/ml Kanamycin or Ampicillin, depending on the transformed plasmid. The plates were incubated O/N at 37 °C and could afterwards be stored at 4 °C.

Table 3: Plasmids

Construct	Tag	Vector Backbone
NM	HA	pJ602
NM Δ 1-39	HA	pJ602
NM Δ 39-123	HA	pJ602
NM Δ 75-123	HA	pJ602
NM Δ 98-123	HA	pJ602
NM G58D	HA	pJ602
NM Δ 39-57	HA	pJ602 (DNA 2.0, Menlo Park, USA)
NM Δ 39-74	HA	pJ602 (DNA 2.0, Menlo Park, USA)
NM Δ 75-97	HA	pJ602 (DNA 2.0, Menlo Park, USA)
NM	HA	pRRL.sin.PPT.CMV.Wpre (Follenzi and Naldini 2002)
NM Δ 1-39	HA	pRRL.sin.PPT.CMV.Wpre
NM Δ 39-123	HA	pRRL.sin.PPT.CMV.Wpre
NM Δ 75-123	HA	pRRL.sin.PPT.CMV.Wpre

NM Δ 98-123	HA	pRRL.sin.PPT.CMV.Wpre
NM G58D	HA	pRRL.sin.PPT.CMV.Wpre
NM Δ 39-57	HA	pRRL.sin.PPT.CMV.Wpre
NM Δ 39-74	HA	pRRL.sin.PPT.CMV.Wpre
NM Δ 75-97	HA	pRRL.sin.PPT.CMV.Wpre
	HA	pRRL.sin.PPT.CMV.Wpre
	GFP	pRRL.sin.PPT.CMV.Wpre
NM Δ 39-123		pMK (Geneart, Waltham, USA)
N		pMK (Geneart, Waltham, USA)
N	HA	pJ602
N	Myc	pJ602
NM Δ 138-250	HA	pJ602 (DNA 2.0, Menlo Park, USA)
NM Δ 138-250	Myc	pJ602
M	Myc	pcDNA3.1 (Thermo Scientific, Waltham, USA)
		pMDl.g/pRRE (Follenzi and Naldini 2002)
		pMD2.VSVG (Follenzi and Naldini 2002)
		pRSV-Rev (Follenzi and Naldini 2002)
NM		pNOTAG (Jens Tyedmers, University Heidelberg)

2.3.8 Cultivation of bacteria and preparation of plasmid DNA

Plasmid Mini Kit Qiagen, Venlo, Netherlands

Plasmid Maxi Kit Qiagen, Venlo, Netherlands

One bacteria colony cultivated on LB agar plates was used to inoculate either 5 ml (mini culture) or 200 ml (maxi culture) LB medium supplemented with 100 µg/ml of the appropriate antibiotic. The culture was grown at 180 rpm O/N at 37 °C (LT-X Lab-Therm, Kuhner Shaker, Aachen, Germany). The following day, plasmid DNA was isolated from the cultures using either the Plasmid Mini or Maxi Kit according to the manufacturer's instructions. Plasmid DNA was resuspended in 50 µl

(Mini Kit) or 300 µl (Maxi Kit) of the supplied buffer and DNA concentration was determined using the Nanodrop (Thermo Scientific, Waltham, USA). Plasmid DNA was stored at -20 °C.

2.3.9 DNA sequence analysis

DNA sequencing was conducted using the GATC Biotech Sanger sequencing service (Konstanz, Germany). Sequence information was analyzed using the Serial Cloner 2.6.1 Software.

2.4 Cell culture

Cell culture was performed under sterile conditions in a sterile hood with sterile medium, glass and plastic ware. Cells were cultured in a cell incubator (HERAcell 240i, Thermo Scientific, Waltham, USA) at 37 °C in a humidified 5 % CO_2 atmosphere.

2.4.1 Thawing of cells

N2a culture medium	Dulbecco's Modified Eagle Medium (DMEM) + GlutaMAX (Gibco, Waltham, USA) 10 % Fetal Calf Serum (FCS) (Biochrom, Kenilworth, USA)
Hek293T/17 culture medium	Iscove's Modified Dulbecco's Medium (IMDM) 10 % FCS (Biochrom, Kenilworth, USA) 1 % Penicillin/Streptomycin (Gibco, Waltham, USA) 3.024 g/L Sodium bicarbonate

Cells frozen in liquid nitrogen were thawed, resuspended in culture medium and centrifuged at 314 x g for 5 min at RT (Heraeus Multifuge X3R, Thermo Scientific, Waltham, USA) (Table 4). The supernatant was discarded and the cell pellet was resuspended in culture medium. Cells were plated on cell culture flasks or on dishes and cultured as described (2.4.2).

Table 4: Cell lines

Cell line	Property	Reference
N2a	Murine neuroblastoma cell line	ATCC CCL 131; Butler et al. (1988)
N2a NM-HA	N2a cells expressing NM-HA	Generated in this study
N2a NM-HA^{agg} clone 5A	N2a cell clone producing NM-HA aggregates	Generated in this study
N2a NM-HA^{agg} clone 7A	N2a cell clone producing NM-HA aggregates	Generated in this study
N2a NM-HA^{agg} clone 10A	N2a cell clone producing NM-HA aggregates	Generated in this study
N2a NM-HA^{agg} clone 5B	N2a cell clone producing NM-HA aggregates	Generated in this study
N2a NM-HA Δ 1-39	N2a cells expressing NM-HA Δ 1-39	Generated in this study
N2a NM-HA^{agg} Δ 1-39 clone 5A	N2a cell clone producing NM-HA Δ 1-39 aggregates	Generated in this study
N2a NM-HA^{agg} Δ 1-39 clone 1B	N2a cell clone producing NM-HA Δ 1-39 aggregates	Generated in this study
N2a NM-HA^{agg} Δ 1-39 clone 2B	N2a cell clone producing NM-HA Δ 1-39 aggregates	Generated in this study
N2a NM-HA^{agg} Δ 1-39 clone 5D	N2a cell clone producing NM-HA Δ 1-39 aggregates	Generated in this study
N2a NM-HA Δ 39-123	N2a cells expressing NM-HA Δ 39-123	Generated in this study
N2a NM-HA Δ 75-123	N2a cells expressing NM-HA Δ 75-123	Generated in this study
N2a NM-HA^{agg} Δ 75-123 clone 8H-13	N2a cell clone producing NM-HA Δ 75-123 aggregates	Generated in this study
N2a NM-HA^{agg} Δ 75-123 clone 8H-23	N2a cell clone producing NM-HA Δ 75-123 aggregates	Generated in this study

N2a NM-HA^{agg} Δ 75-123 clone 64H-3	N2a cell clone producing NM-HA Δ 75-123 aggregates	Generated in this study
N2a NM-HA^{agg} Δ 75-123 clone 64H-20	N2a cell clone producing NM-HA Δ 75-123 aggregates	Generated in this study
N2a NM-HA Δ 98-123	N2a cells expressing NM-HA Δ 98-123	Generated in this study
N2a NM-HA G58D	N2a cells expressing NM-HA G58D	Generated in this study
N2a NM-HA Δ 39-57	N2a cells expressing NM-HA Δ 39-57	Generated in this study
N2a NM-HA Δ 39-74	N2a cells expressing NM-HA Δ 39-74	Generated in this study
N2a NM-HA Δ 75-97	N2a cells expressing NM-HA Δ 75-97	Generated in this study
N2a NM-GFP	N2a cells expressing NM-GFP	Hofmann et al. (2013)
N2a NM-GFP^{agg} clone 2CG11	N2a cell clone producing NM-GFP aggregates	Hofmann et al. (2013)
N2a-GFP Δ 1-39	N2a cells expressing NM-GFP Δ 1-39	Peer-Hendrik Kuhn, Stefan Lichtenthaler, Munich
N2a NM-GFP Δ 75-123	N2a cells expressing NM-GFP Δ 75-123	Peer-Hendrik Kuhn, Stefan Lichtenthaler, Munich
Hek293T/17	Human embryonic kidney cells, expressing simian virus 40 large T antigen, clone 17	ATCC CRL-11268, Graham et al. (1977)

2.4.2 Culturing of cells

PBS	Gibco, Waltham, USA
Trypsin-EDTA, 0.05 %	Gibco, Waltham, USA

Cells were grown in cell culture flasks or dishes containing culture medium and passaged every 3 - 4 days. For passaging, the medium was aspirated, the cells were washed with PBS and incubated in Trypsin-EDTA for 5 min. Trypsin was inactivated by adding at least one volume of cell culture medium. After resuspension, the cells were centrifuged at 314 x g for 5 min at RT (Heraeus Multifuge X3R, Thermo Scientific, Waltham, USA) and the supernatant was discarded. The pellet was resuspended in approximately 5 ml of cell culture medium and, if needed, the cell number was determined using the automated cell counter (TC 20, BioRAD, Hercules, USA). The cell suspension was plated on fresh cell culture flasks, dishes or multi-well plates and cells were cultivated in a cell incubator (2.4).

2.4.3 Cryoconservation of cells

For cryoconservation, cells were detached as described (2.4.2) and pelleted at 314 x g for 5 min at 4 °C (Heraeus Multifuge X3R, Thermo Scientific, Waltham, USA). Cell pellets were resuspended in FCS + 10 % DMSO and transferred into cryogenic vials. Vials were frozen O/N at -80 °C and transferred into liquid nitrogen the following day. Cells were kept in liquid nitrogen for long-term storage.

2.4.4 Transient transfection of cells

Efectene Transfection Reagent Kit	Qiagen, Venlo, Netherlands
Lipofectamine 2000 Transfection Reagent	Thermo Scientific, Waltham, USA

For transient transfection of cells, Effectene Transfection Reagent Kit or Lipofectamine 2000 Transfection Reagent were used according to the manufacturer's instructions.

2.4.5 Production of lentiviral particles

0.1 % TE buffer	1 mM Tris/HCl, pH 8.0 0.1 mM EDTA, pH 8.0 in H_2O_{bidest}
2x HBSS	281 mM NaCl 100 mM HEPES 1.5 mM Na_2HPO_4, pH 7.12 in H_2O_{bidest}
5x Polyethylene glycol	25 mM Polyethylene glycol 0.2 M NaCl 2 mM Tris/HCl, pH 7.5 in H_2O_{bidest}

During lentiviral production and transduction of cells with lentiviral particles, two sets of gloves, arm protection, safety goggles and a surgical mask were worn at all times. To immediately decontaminate liquid waste, liquid waste was collected in 1 l glass bottles already prepared with 500 ml 20 % SDS (10 % SDS final concentration) and afterwards autoclaved following the official guidelines. During centrifugation steps, centrifugation buckets were always sealed with the appropriate lids.

Table 5: Lentiviral plasmids and their function

Plasmid	**Amount of DNA (µg) for transfection of 7x 15 cm dishes**	**Function**
pMDl.g/pRRE	112	Packaging plasmid
pRSV-Rev	44	Rev encoding plasmid
pMD2.VSVG	63	Envelop plasmid
pRRL.sin.PPT.CMV.NM-HA mutant.Wpre	175	Expression plasmid

Lentiviral particles were produced using the method of Follenzi and Naldini (2002). To generate viral particles, approximately 7.5 x 10^6 Hek293T/17 cells were plated on 7x 15 cm dishes and grown in 25 ml Hek293T/17 medium (~ 40 % confluency). Cells were grown for 5 - 7 h and afterwards transfected using the calcium phosphate precipitation method. For transfection, 7645 µl 0.1 % TE buffer, 875 µl 2.5 M $CaCl_2$ and the lentiviral plasmids (Table 5) were mixed in a 50 ml conical tube. The mixture was applied drop wise to 7875 µl vigorously vortexed 2x HBSS in a 50 ml conical tube using a serological pipette to produce DNA – calcium - phosphate precipitates. The transfection solution was evenly distributed on the culture dishes in a drop wise manner. 12 - 16 h post transfection, the medium was replaced with fresh culture medium. The day after, the medium was collected and the cells were cultured for another 24 h in fresh medium. To remove residual cells and cell debris, the collected medium was centrifuged at 690 x g for 5 min at 4 °C (Heraeus Multifuge X3R, Thermo Scientific, Waltham, USA) and the supernatant was stored at 4 °C. The following day, the medium was collected again and centrifuged as described before. At this point cells were discarded. The combined supernatant was filtered through a 0.22 µm Corning bottle-top vacuum filter, mixed with 5x PEG (1x PEG final concentration) and incubated O/N at 4 °C in aliquots in 50 ml conical tubes. The next day, the precipitated viral particles were centrifuged at 1500 x g for 30 min at 4 °C and the supernatant was discarded. The pellets were carefully combined and again centrifuged at 1500 x g for 5 min at 4 °C. The supernatant was discarded and the lentiviral particles were carefully resuspended in 800 - 1000 µl PBS, depending on the pellet size. Aliquots were stored at -80 °C.

2.4.6 Lentiviral transduction of mammalian cells

Transduction medium	5 % FCS (Biochrom, Kenilworth, USA) 8 µg/ml Polybrene (Merck Millipore, Billerica, USA) in DMEM (Gibco, Waltham, USA)

Prior to transduction, 8 x 10^4 cells were plated on one well of a 24 - well plate and cultured O/N. On the day of transduction, culture medium was replaced with transduction medium and the appropriate amount of lentiviral particles was added to the cells. The well plate containing the cells and viral particles was centrifuged at 800 x g for 10 min at RT (Heraeus Multifuge X3R, Thermo Scientific, Waltham, USA)

and afterwards cultured for 24 h. The next day, the medium was exchanged with fresh culture medium and the cells were expanded. Aliquots of generated stable cell lines were frozen in liquid nitrogen to be used for future experiments as described (2.4.3).

2.4.7 Immunofluorescence staining and confocal microscopy analysis of N2a cells

High Precision Microscope Cover Glass, No 1.5H	Marienfeld Superior, Lauda-Königshofen, Germany
Microplate, 96 - well, µ-clear, F-Bottom, black	Greiner Bio-One, Kremsmünster, Austria
Hoechst 33342	Molecular Probes, Eugene, USA
HCS CellMask Blue Stain	Molecular Probes, Eugene, USA
Aqua Polymount	Polysciences, Warrington, USA
Superfrost Plus Microscopic Slides	Thermo Scientific, Waltham, USA

For immunofluorescence staining, N2a cells were grown on coverslips or 96 - well plates coated with Poly-L-lysine. To this end, coverslips or 96 - well plates were coated with Poly-L-lysine in PBS (1:100) O/N at RT. The following day Poly-L-lysine was discarded and the coverslips or 96 - well plates were washed three times with PBS before the cells were plated. Cells were grown for at least 24 h and treated according to the individual experiments. Cells were fixed with 4 % paraformaldehyde for 10 min (coverslips) or 15 min (96 - well plates) at RT. Cells were rinsed three times with PBS and afterwards permeabilized for 5 min (0.1 % Triton X-100, coverslips) or 10 min (0.5 % Triton X-100, 96 - well plates) at RT. After three washing steps, the cells were blocked with 2 % goat serum in PBS for 1 h at RT. NM was detected by staining with the indicated primary antibody diluted in 2 % blocking solution O/N at 4 °C (Table 6). Unbound antibody was removed by washing the cells three times for 5 min in PBS. Subsequently, the cells were incubated with the appropriate fluorophore - coupled secondary antibody in blocking solution (1:500) for 1 h at RT (Table 7). After three washing steps with PBS for 5 min, nuclei were stained with Hoechst 33342 in PBS (1:10000) for 5 min at RT. For automated confocal microscopy, cytoplasm was visualized using HCS CellMask Blue Stain (1:5000) in PBS for 10 min at RT. The cells were rinsed six times with PBS and one

time with H_2O_{bidest} before they were mounted on microscopic slides. Microscopic slides were stored at 4 °C. Cells stained on 96 - well plates were kept in PBS at 4 °C. Confocal microscopy was performed using the LSM 700 (Zeiss, Jena, Germany) or the upright LSM 700 (Zeiss, Jena, Germany). For high-throughput analysis, cells were imaged with an automatic confocal microscope (Cell Voyager 6000, Yokogawa, Tokyo, Japan). Image analysis was performed using the Cell Profiler cell image analysis software.

Table 6: Primary antibodies

Antibody	Origin	Specificity	Dilution	Reference
Anti–hemagglutinin (HA) F7	Mouse monoclonal	Epitope of hemagglutinin (YPYDVPDYA)	IF 1:200	Santa Cruz Biotechnology, Santa Cruz, USA
Anti-hemagglutinin (HA) (3F10)	Rat monoclonal	Epitope of hemagglutinin (YPYDVPDYA)	WB 1:1000	Roche Diagnostics, Basel, Switzerland
Anti-hemagglutinin (HA) Alexa 647	Mouse monoclonal	Epitope of hemagglutinin (YPYDVPDYA)	IF 1:200	Biozol, Eching, Germany
Anti–actin (C4)	Mouse monoclonal	Chicken gizzard actin, all six known vertebrate isoactins	WB 1:5000	MP Biomedicals, Eschwede, Germany
Anti–NM (4A5) (hybridoma supernatant)	Rat monoclonal	M domain of Sup35 (aa 229-247)	WB 1:10	Provided by Dr. Kremmer, Helmholtz Zentrum, Munich, Germany
Anti–Myc-tag	Rabbit polyclonal	Epitope of c-myc (EQKLISEEDL)	IF 1:500	Abcam, Cambridge, UK

Table 7: Secondary antibodies

Antibody	Origin	Specificity	Dilution	Reference
Horseradish peroxidase (HRP) conj. anti-rat IgG	Goat	Rat IgG	1:10000	Dianova, Hamburg, Germany
Horseradish peroxidase (HRP) conj. anti-mouse IgG	Goat	Mouse IgG	1:10000	Dianova, Hamburg, Germany
Alexa Fluor 488-conj. anti-mouse	Goat	Mouse IgG	1:500	Life Technologies, Darmstadt, Germany
Alexa Fluor 594-conj. anti-mouse	Goat	Mouse IgG	1:500	Life Technologies, Darmstadt, Germany
Alexa Fluor 488-conj. anti-rabbit	Goat	Rabbit IgG	1:500	Life Technologies, Darmstadt, Germany
Alexa Fluor 568-conj. anti-rabbit	Goat	Rabbit IgG	1:500	Life Technologies, Darmstadt, Germany

2.4.8 Aggregate induction by recombinant NM fibrils

For aggregate induction, recombinant NM protein was prepared as described (2.5.8). To generate fibrils, the NM protein was thawed and rotated head-over-tail at 50 rpm for 24 h at 4 °C (LD-76, Labinco, DG Breda, Netherlands) at a concentration of 10 - 100 µM (monomer concentration), depending on the experiment. To dissociate fibrils into smaller fragments more likely to enter the cell, NM fibrils were sonicated for 3 min (5 sec on, 1 sec off) in an ice-cold water bath, with the amplitude set to 10 % (Sonicator Sonoplus, Bandelin, Berlin, Germany). Fibrils were added to the cells (1 or 10 µM final concentration, monomer concentration) seeded on 24 - well plates the day before. After 24 h, the medium was exchanged and the cells were further passaged or directly analyzed.

2.4.9 Aggregate maintenance analysis

To analyze the maintenance of NM aggregates over several passages, N2a full-length NM-HA and NM-HA mutant cells at passage three were seeded on 24 - well plates and grown O/N. Recombinant NM fibrils were generated as described (2.4.8, 2.5.8) and added to the cells for 24 h (10 µM, monomer concentration). After fibril induction, cells were expanded to T25 - flasks and grown until passage nine post induction. During the cultivation at passage one, three, six and nine post induction, cells were also seeded on Poly-L-lysine coated 96 - well plates for immunofluorescence analysis (2.4.7).

2.4.10 Time-lapse analysis

4 - well chamber slides Nunc, Thermo Scientific, Waltham, USA

N2a cells expressing full-length and mutant NM-GFP were seeded on 24 - well plates 24 h prior to induction with 10 µM recombinant NM fibrils (monomer concentration) (2.4.8). Cells were grown for another two passages and afterwards plated on 4 - well chamber slides. After 24 h, time-lapse images were taken over a period of 15 h using a wide-field fluorescence microscope (Zeiss, Jena, Germany) at 37 °C and 5 % CO_2.

2.4.11 Limiting dilution cloning

For limiting dilution cloning, cells were detached and the cell number was determined as described (2.4.2). The cells were diluted to a final concentration of 10 cells/ml and seeded (100 µl/well) on 96 - well plates. Cells were cultured for approximately 10 days and afterwards, single cell clones were selected. Single cell clones were expanded to 24 - and subsequently 6 - well plates. To detect NM aggregate bearing cell clones, clones were seeded on 96 - well plates and analyzed by immunofluorescence staining (2.4.7). Each cell clone was frozen in liquid nitrogen as described (2.4.3).

2.4.12 Generation of full-length and mutant N2a NM-HA^{agg} cell clones

Effectene Transfection Reagent Kit	Qiagen, Venlo, Netherlands

Aggregate induction was performed as previously described (2.4.8). To enhance the fibril induction rate, fibrils were mixed with the appropriate amount of Effectene transfection reagents used for transfection in 24 - well plates (see manufacturer's instructions), prior to addition to N2a cells. After three passages, the percentage of aggregate bearing cells in the N2a NM-HA expressing bulk populations was determined (2.4.7). Aggregate bearing single cell clones were afterwards generated by limiting dilution cloning (2.4.11). For NM mutant NM-HA^{agg} Δ 75-123, a second limiting dilution cloning step was necessary as the first round resulted in mitotically instable cell clones. Cell clones were frozen in liquid nitrogen for future experiments.

2.4.13 Coculture analysis

N2a NM-HA^{agg} donor clones were cocultured with N2a NM-GFP^{sol} recipient cells (ratio 1.5:1) on Poly-L-lysine coated coverslips (1.25 x 10^5 total cells) or 96 - well plates (2.5 x 10^4 total cells). After 42 h, cells were fixed and stained as described (2.4.7). Confocal images were taken with the LSM 700 (Zeiss, Jena, Germany), the upright LSM 700 (Zeiss, Jena, Germany) or the automatic confocal microscope (Cell Voyager 6000, Yokogawa, Tokyo, Japan), respectively.

2.5 Protein biochemical methods

2.5.1 Preparation of protein lysates from mammalian cells

Lysis buffer	150 mM NaCl 50 mM Tris/HCl, pH 7.5 0.5 % NP-40 in H_2O_{bidest} Protease inhibitor (complete, EDTA free, Roche Diagnostics, Basel, Switzerland)

Cells were detached from cell culture dishes (2.4.2) and centrifuged at 314 x g for 5 min at 4 °C (Heraeus Multifuge X3R, Thermo Scientific, Waltham, USA). Cell pellets were washed in ice-cold PBS and either lysed directly or stored at -20 °C until

further use. Cell pellets were resuspended in the appropriate amount of lysis buffer freshly supplemented with protease inhibitor (1 x T75 – flasks: 1 ml; 1 x 6 – well: 100 µl; 1x 24 – well: 50 µl) and lysed for 30 min on ice. Cell debris was spun down at 514 x g for 3 min at 4 °C (Eppendorf Centrifuge 5417R, Hamburg, Germany) and the supernatant was transferred into a fresh tube. Protein lysates were either used directly or stored at -20 °C.

2.5.2 Bradford protein assay

Quick Start Bradford Assay	BioRAD, Hercules, USA
Quick Start Bovine Serum Albumin Standard Set	BioRAD, Hercules, USA

To determine the protein concentration of cell lysates, the Bradford protein assay was used. A clear 96 - well plate was prepared with 5 µl of a 1:10 dilution of the protein lysate in H_2O_{bidest} in duplicates, a BSA standard dilution series ranging from 62.5 - 2000 µg/ml and a H_2O blank control. The chemical reaction was started by addition of 250 µl Bradford reagent, resulting in a protein concentration dependent color change in each sample. After 5 min incubation, the absorbance was measured at 595 nm with the plate reader (FLUOstar Omega, BMG Labtech, Offenburg, Gemany). Protein concentrations were calculated by generating a standard curve from the measured absorbance of the standard concentrations using MARS data analysis software.

2.5.3 Discontinuous sodium dodecyl sulfate - polyacrylamide gel electrophoresis (SDS-PAGE)

3x Sample buffer	90 mM Tris/HCl, pH 6.8 7 % SDS 30 % Glycerol 20 % β-mercaptoethanol Bromphenol blue in H_2O_{bidest}
20x NuPAGE MOPS SDS Running Buffer (Thermo Scientific, Waltham, USA)	50 mM MOPS 50 mM Tris 0.1 % SDS 1 mM EDTA pH 7.7
10x Tris/Glycine/SDS Electrophoresis Buffer (BioRAD, Hercules, USA)	25 mM Tris 192 mM Glycine 0.1 % SDS pH 6.8
4x NuPAGE LDS Sample Buffer	Thermo Scientific, Waltham, USA
NuPAGE 12 % Bis-Tris Protein Gels	Thermo Scientific, Waltham, USA
Any kD Mini-PROTEAN TGX Precast Gels	BioRAD, Hercules, USA
PageRuler Plus Prestained Protein Ladder	Thermo Scientific, Waltham, USA
InstantBlue Protein Stain	C.B.S Scientific, San Diego, USA

To separate proteins by size, SDS-PAGE was performed. The BioRAD system was used for all protein samples, except for the limited proteolysis samples that were run on 12 % NuPAGE gels, as a higher resolution was required. For both systems, protein samples were mixed with their respective sample buffer and heated for 5 min or 10 min (in the case of limited proteolysis experiments) at 95 °C. Samples and 4 µl of marker were loaded onto the gel and run at 30 mA for 1 h (Any kD Mini-PROTEAN TGX Precast Gels) or 2.5 h (NuPAGE 12 % Bis-Tris Protein Gels). Gels were either stained with InstantBlue or further used for Western Blotting. To directly detect

proteins, gels were stained with InstantBlue for 15 – 60 min and afterwards washed with H_2O_{bidest}.

2.5.4 Sedimentation assay

Lysis Buffer	10 mM Tris/HCl, pH 7.5 100 mM NaCl 10 mM EDTA 0.5 % Triton X-100 0.5 % Sodium Deoxycholate Protease inhibitor (complete, EDTA free, Roche Diagnostics, Basel, Switzerland)
TNE Buffer	50 mM Tris/HCl, pH 7.5 150 mM NaCl 5 mM EDTA

For the sedimentation assay, cells were plated on 6 cm dishes for 24 h and, depending on the assay, incubated with 10 µM *in vitro* fibrillized NM (monomer concentration) for 24 h (2.4.8) or left untreated. Cells were detached as described (2.4.2) and lysed in 200 µl lysis buffer for 20 min on ice. Cell lysates were centrifuged at 1000 x g for 1 min at 4 °C to remove cell debris (Eppendorf Centrifuge 5417R, Hamburg, Germany). To separate the soluble from the insoluble fraction, the supernatant was centrifuged at 20000 x g for 20 min at 4 °C. Proteins in the soluble supernatant fraction were precipitated with Methanol O/N at -20 °C. The insoluble pellet fraction was washed once with lysis buffer and the centrifugation step was repeated. The pellet was stored at -20 °C. The following day, the precipitated soluble fraction was centrifuged at 2120 x g for 25 min at 4 °C and the supernatant discarded. The insoluble and soluble fractions were resuspended in 17 µl or 100 µl TNE buffer, respectively. Fractions were supplemented with sample buffer and heated for 5 min at 95 °C as described (2.5.3). The entire insoluble and 1/6 of the soluble fraction were loaded onto SDS gels.

2.5.5 Semi-denaturing detergent - agarose gel electrophoresis (SDD-AGE)

Lysis Buffer	50 mM Tris/HCl, pH 7.5 150 mM NaCl 1 % NP-40 Protease inhibitor (complete, EDTA free, Roche Diagnostics, Basel, Switzerland)
4x Sample Buffer	2x TAE buffer (2.3.4) 20 % Glycerol 8 % SDS Bromphenol blue
Running Buffer	1x TAE buffer 0.1 % SDS
TBS	25 mM Tris/HCl, pH 7.6 137 mM NaCl in H_2O_{bidest}
Thick blot filter papers	BioRAD, Hercules, USA
Protran BA 83 Nitrocellulose 0.2 µm	Whatman, Maidstone, UK

To verify the amyloid nature of NM aggregates, the SDD-AGE assay (Kryndushkin et al. 2003) was performed. Cells were harvested as described (2.4.2) and lysed for 30 min on ice (T75 – flasks: 50 – 500 µl lysis buffer, depending on the expression level of the individual protein). Cell debris was removed by centrifugation at 514 x g for 2 min at 4 °C (Eppendorf Centrifuge 5417R, Hamburg, Germany). The supernatant was incubated with sample buffer for 5 min at RT. Samples were loaded on an 1.5 % agarose gel supplemented with 0.1 % SDS submerged in running buffer to separate monomeric and SDS-resistant protein polymers. The gel was run at 15 V O/N at 4 °C in an electrophoresis chamber (Peqlab, Erlangen, Germany). On the following day, a nitrocellulose membrane, ten thick blot filter papers and eight whatman papers were cut into the size of the gel. The membrane, four of the whatman papers and one long whatman paper, to be used as a wick, were immerged in TBS. The agarose gel was briefly washed with water to remove excess running buffer. Ten dry thick blot filter papers, four dry whatman papers, one pre-wetted whatman paper and the membrane were stacked in a dry electrophoresis chamber

on top of each other. The agarose gel was carefully slid onto the membrane taking care to avoid bubble formation under the gel that would hinder the transfer. The three remaining pre-wetted whatman papers were placed on top of the gel. The wick was draped on top of the stack with both ends immerged in TBS. As a weight, a full 500 ml glass bottle was placed on top and capillary transfer proceeded O/N at RT. On the next day, the membrane was further processed by standard Western blotting methods (2.5.7).

2.5.6 Limited proteolysis

Lysis Buffer	50 mM Tris/HCl, pH 7.5 150 mM NaCl 0.5 % NP-40
1 % Pefabloc	Roche, Mannheim, Germany in H_2O_{bidest}

Cells were harvested as described (2.4.2) and lysed in lysis buffer (1/3 T75 – flask: 80 µl) on ice for 30 min. Cell debris was spun down at 514 x g for 2 min at 4 °C (Eppendorf Centrifuge 5417R, Hamburg, Germany) and the protein concentration of the supernatant was determined as described (2.5.2). Protein lysates (100 – 300 µg protein) and *in vitro* fibrillized recombinant NM (500 ng) (2.4.8) were partially digested with the appropriate amount of freshly thawed chymotrypsin for 1 h on ice using protein:protease ratios between 1:250 - 1:1000 (cell lysates) and 1:1 – 1:50000 (NM fibrils) in a total volume of 25 – 50 µl. The reaction was stopped by addition of 1 % Pefabloc (0.04 % final concentration) and the appropriate amount of 4x SEB buffer. Samples were heated for 10 min at 95 °C and loaded onto 12 % SDS gels. The gel was afterwards processed by standard Western blotting methods (2.5.7).

2.5.7 Immunochemical detection of proteins via Western blot

1x Blotting buffer	20 % Methanol 25 mM Tris 192 mM Glycine in H_2O_{bidest}
10x TBST	250 mM Tris/HCl, pH 7.6 1.37 M NaCl 0.05 % TWEEN-20 in H_2O_{bidest}
Protran BA 83 nitrocellulose 0.2 µm	Whatman, Maidstone, UK
Pierce ECL solution	Thermo Scientific, Waltham, USA
Amersham ECL Prime Western Blotting Detection Reagent	GE Healthcare Life Sciences, Chicago, USA
10x ReBlot Plus Strong Antibody Stripping Solution	Merck Millipore, Billerica, USA

SDS gels were prepared as previously described (2.5.3). For Western blotting, a nitrocellulose membrane and six whatman papers were cut to the size of the gel and pre-equilibrated in blotting buffer together with the gel. Gel, membrane, whatman papers and 2 pre-wetted sponge pads were stacked in perforated plastic plates and placed into a wet blotter (PerfectBlue, Tank-Electroblotter Web, Peqlab, Erlangen, Germany). The electric protein transfer was conducted at 300 mA for 60 min (Perfect Blue small) or 800 mA for 70 min (Perfect Blue medium). After blotting, the membrane was blocked in 5 % milk powder in 1x TBST for 60 minutes. The blocking buffer was discarded and the membrane was incubated with the primary antibody diluted in blocking buffer O/N at 4 °C (Table 6). The next day, unbound antibody was removed by washing three times in 1x TBST for 10 min. After the washing steps, the membrane was incubated with the corresponding secondary HRP-conjugated antibody diluted in blocking buffer for 1 h at RT (Table 7). The membrane was washed three times in 1x TBST for 10 min and afterwards incubated in 2 ml ECL solution for 1 min. The membrane was placed between a transparent plastic wrap and the light signal of the luminescence reaction was detected using a transilluminator machine (Stella, Raytest, Straubenhardt, Germany).

To detect a second protein of interest, the membrane was stripped to remove bound antibodies. To this end, the membrane was washed with H_2O_{bidest} for 10 min and afterwards incubated twice with 1x ReBlot Plus Strong Antibody Stripping Solution (1:10 in H_2O_{bidest}) for 20 min. The membrane was washed three times with 1x TBST, blocked in blocking buffer for 30 min and incubated with the respective antibodies as described above.

2.5.8 Production and purification of recombinant NM protein

Protein Purification Buffer A	10 mM Tris/HCl, pH 7.2 8 M Urea in H_2O_{bidest}
Protein Purification Buffer B	10 mM Tris/HCl, pH 7.2 8 M Urea 1 M NaCl in H_2O_{bidest}
Protein Purification Buffer C	5 mM KPhos, pH 7.2 8 M Urea in H_2O_{bidest}
Protein Purification Buffer D	500 mM KPhos, pH 7.2 8 M Urea in H_2O_{bidest}

Table 8: Program Q-sepharose and CHT resin columns

Time in min	Flow ml/min	% Buffer B/D
0	3.0	5
30	3.0	10
90	3.0	50
105	3.0	99
120	3.0	100

To produce recombinant NM protein, BL21 *E.coli* were transformed with the pNOTAG-NM plasmid as described (2.3.7). The following day, all bacteria colonies

were collected and used to inoculate 3 l LB medium supplemented with 100 µg/ml Ampicillin. The bacteria were shaken at 180 rpm and 37 °C (LT-X Lab-Therm, Kuhner Shaker, Aachen, Germany) until an OD_{600} of 0.6 was reached. At that point, gene expression was induced by addition of 1 M IPTG and the bacteria were shaken at 180 rpm for 3 - 4 h at 30 °C (LT-X Lab-Therm, Kuhner Shaker, Aachen, Germany). The bacteria were spun down at 3488 x g for 15 min at RT (Heraeus Multifuge X3R, Thermo Scientific, Waltham, USA), the supernatant was discarded and the pellet directly used or stored at -80 °C until further use. The bacteria pellet from 1 l of culture was resuspended in 50 ml of buffer A and lysed at 180 rpm for at least 30 min at 37 °C (LT-X Lab-Therm, Kuhner Shaker, Aachen, Germany). Afterwards, the suspension was centrifuged at 30000 x g for 20 min at 25 °C to remove any insoluble material. The supernatant was applied to a Q-sepharose column pre-equilibrated with buffer A. Unbound material was removed by washing with 5 column volumes of buffer A. Proteins were gradually eluted according to their ionic strength by applying a gradient of buffer A and B (Table 8). The eluted material was collected in 5 ml fractions that were analyzed by SDS-PAGE as described (2.5.3). Fractions containing the NM protein were pooled and loaded onto a CHT resin column pre-equilibrated with buffer C. The column was washed with 2 column volumes of buffer C to remove unbound material. The bound protein was eluted from the CHT resin by applying a gradient of buffer C and D (Table 8). Samples were again collected in 5 ml fractions and their protein content was analyzed by SDS-PAGE. Fractions containing the NM protein were pooled and dialyzed three times against 1x PBS at 4 °C. Protein concentration was determined and 1 ml aliquots with a concentration of 100 µM (monomer concentration) were stored at -80 °C.

2.6 Image data analysis and statistics

2.6.1 Image data analysis

Confocal images captured with the LSM 700, upright LSM 700 or wide-field fluorescence microscope (Zeiss, Jena, Germany) were processed using Zen 2010 (black edition) or Zen 2012 (blue edition) software (Zeiss, Jena, Germany). For statistical analysis, confocal image sets were obtained using the Cell Voyager CV6000 (Yokogawa, Tokyo, Japan) with 40x magnification. Images were analyzed with Cell Profiler 2.1 image analysis software. To this end, an image analysis routine

was developed. In brief, nuclei and the corresponding cytoplasm were identified based on morphology parameters and the intensity of Hoechst 33342 and HCS CellMask staining, respectively. Full-length and mutant NM expressing cells were distinguished from non-expressing cells by intensity levels of immunofluorescently labeled NM. To identify aggregates, pixels were classified using the Ilastik segmentation toolkit. The number of full-length or mutant NM expressing cells as well as aggregate bearing cells was determined.

2.6.2 Statistical analysis

All data displayed in bar graphs are depicted as the mean. For statistically analyzed data, at least three biological replicates ($n \geq 3$) were analyzed and at least 5000 cells per cell population were imaged. Error bars represent the standard deviation (SD) or the upper limit of the confidence interval as indicated. For statistical analysis the Cochran-Mantel-Haenszel test with continuity correction or the t-test were used as indicated. Longitudinal analysis of aggregate loss was performed using Cox proportional hazard model. A p-value of ≤ 0.05 was considered statistically significant.

3. Results

3.1 Determining the prion domain of NM in mammalian cells

Sup35 is the best-studied yeast prion to date and it is comprised of three domains. In prior studies, the carboxyterminal C domain was found to encode the translation termination function of the protein, whereas the aminoterminal N domain and the middle M domain were reported to encode its prion propensities (Ter-Avanesyan et al. 1993, Ter-Avanesyan et al. 1994, Liu et al. 2002). Previous studies have already shown that NM is able to propagate as a prion in mammalian cells (Krammer et al. 2009, Hofmann et al. 2013), demonstrating the capacity of mammalian cells to replicate cytosolic prions. Since then, reports have further confined the PrD to the N domain and, depending on the publication, different amino acid stretches within this region. In mammalian cells however, no such definition of the PrD has been published so far. To first analyze whether the propensity to form polymers in mammalian cells is encoded in only one of the two domains, we constructed one mutant encoding only the N domain, one mutant encoding only the M domain and one mutant coding for NM Δ 138-250, which has been shown to maintain the prion phenotype in *S. cerevisiae* (Bradley and Liebman 2004) (Fig. 6A). All constructs were carboxyterminally tagged with either an HA-tag (full-length NM) or a Myc-tag (mutants). To first explore the expression of full-length NM and the three mutants, we transiently transfected N2a cells and analyzed them by immunofluorescence staining after 48 h (Fig. 6B). Full-length NM and all mutants showed diffuse cytosolic expression. Interestingly, mutants with deletions of the entire or part of the M domain were also expressed in the nucleus, suggesting that the M domain helps to retain NM in the cytosol.

It was previously shown that *in vitro* fibrillized recombinant NM seeds can enter the cell and induce aggregation of endogenous NM in yeast as well as in mammalian cells (King and Diaz-Avalos 2004, Tanaka et al. 2004, Krammer et al. 2009). To test if aggregation could be induced in our three mutants, we transiently transfected N2a cells with full-length NM and the three deletion mutants and incubated them 48 h post transfection with *in vitro* fibrillized recombinant NM for 24 h (Fig. 7A). Full-length NM and the three mutants demonstrated punctate aggregates in the cytosol (Fig. 7B).

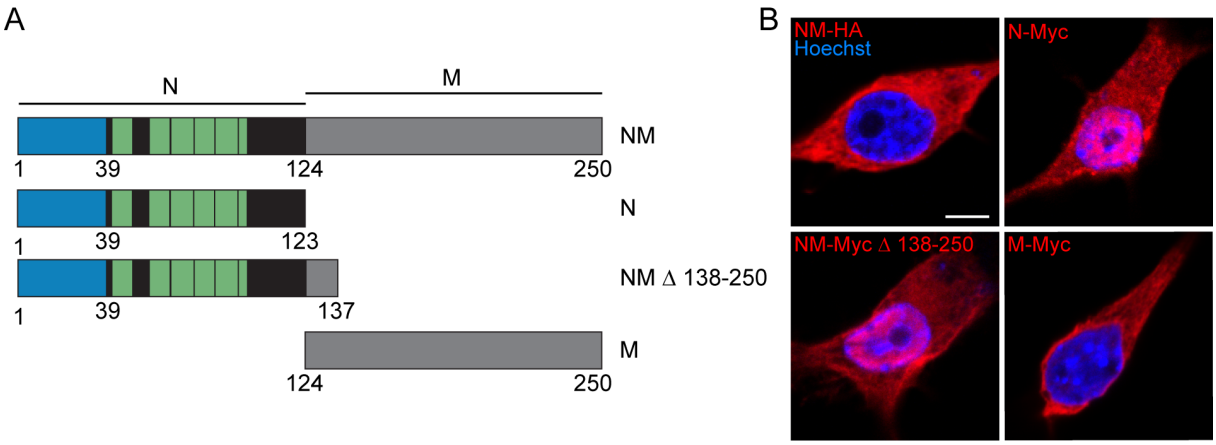

Figure 6. Full-length NM and mutants are expressed and retain their soluble state. **(A)** Scheme of full-length NM and the three deletion mutant constructs: NM, encoding the entire N and M domain; N, with a deletion of the entire M domain; NM Δ 138-250, with a deletion of the entire M domain except for the first 14 amino acids; M, with a deletion of the entire N domain. Numbers refer to amino acids. **(B)** Immunofluorescence staining of N2a cells transiently transfected with full-length NM and mutants for 48 h. NM was detected using either mAb anti-HA or pAb anti-Myc as indicated (red). Nuclei were visualized with Hoechst (blue). Scale bar: 5 µm.

Only the mutant lacking the entire N domain remained diffusely expressed without any signs of aggregation. Noticeably, mutants with an entire or partial deletion of the M domain showed punctate aggregates in the nucleus in addition to the cytosol (Fig. 7B, arrows). A finding that is in line with the previously observed expression pattern.

To determine whether aggregation could also be induced by endogenous NM prions, we transiently transfected N2a cell clone 2CG11 stably producing NM-GFP aggregates (Hofmann et al. 2013) with full-length NM and the three deletion mutants (Fig. 8A). Full-length NM and the mutants showed decoration of the endogenous NM-GFP prions in the cytosol. As before, only the deletion mutant encoding only the M domain remained diffusely expressed without colocalization with NM-GFP aggregates. In line with previous results, mutants with deletions of the entire or part of the M domain also displayed aggregates in the nucleus (Fig. 8B, arrows). Interestingly, in those cells, NM-GFP aggregates were only detected in the cytosol.

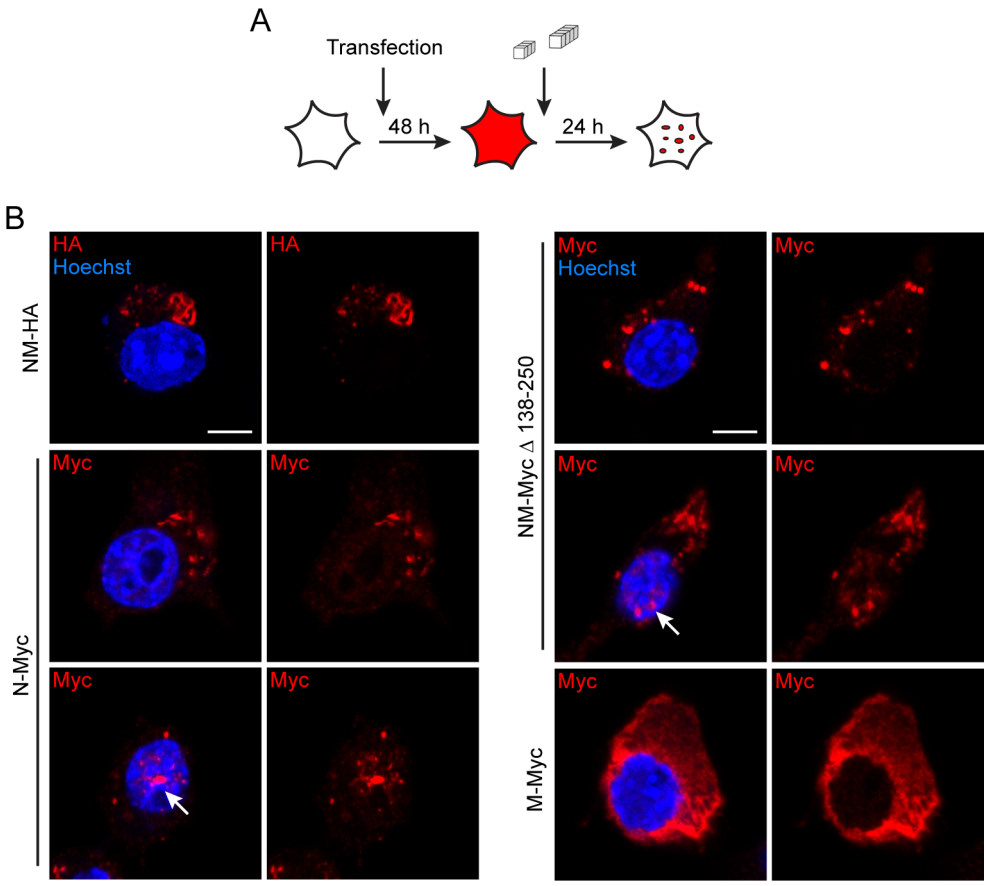

Figure 7. Aggregate induction by addition of exogenous recombinant NM fibrils. **(A)** Experimental setup. N2a cells were transiently transfected with full-length NM or mutants and incubated after 48 h with 10 µM (monomer concentration) *in vitro* fibrillized recombinant NM for 24 h. **(B)** Immunofluorescence staining of transiently transfected N2a cells. NM was detected using either mAb anti-HA or pAb anti-Myc as indicated (red). Nuclei were visualized with Hoechst (blue). Arrows mark intranuclear aggregates. Scale bar: 5 µm.

To rule out the possibility that the sizable GFP-tag sterically hindered aggregate induction, we performed the same experiment with N2a cell clone NM-HA^{agg} 5A stably producing NM-HA aggregates (Fig. 9). Confirming the previous results, mutants with a deletion of the entire or part of the M domain showed decoration of the endogenous NM-HA aggregates in the cytosol and additionally punctate intranuclear aggregates (Fig. 9, arrows). Again, no colocalization with endogenous aggregates could be observed for the mutant encoding only the M domain.

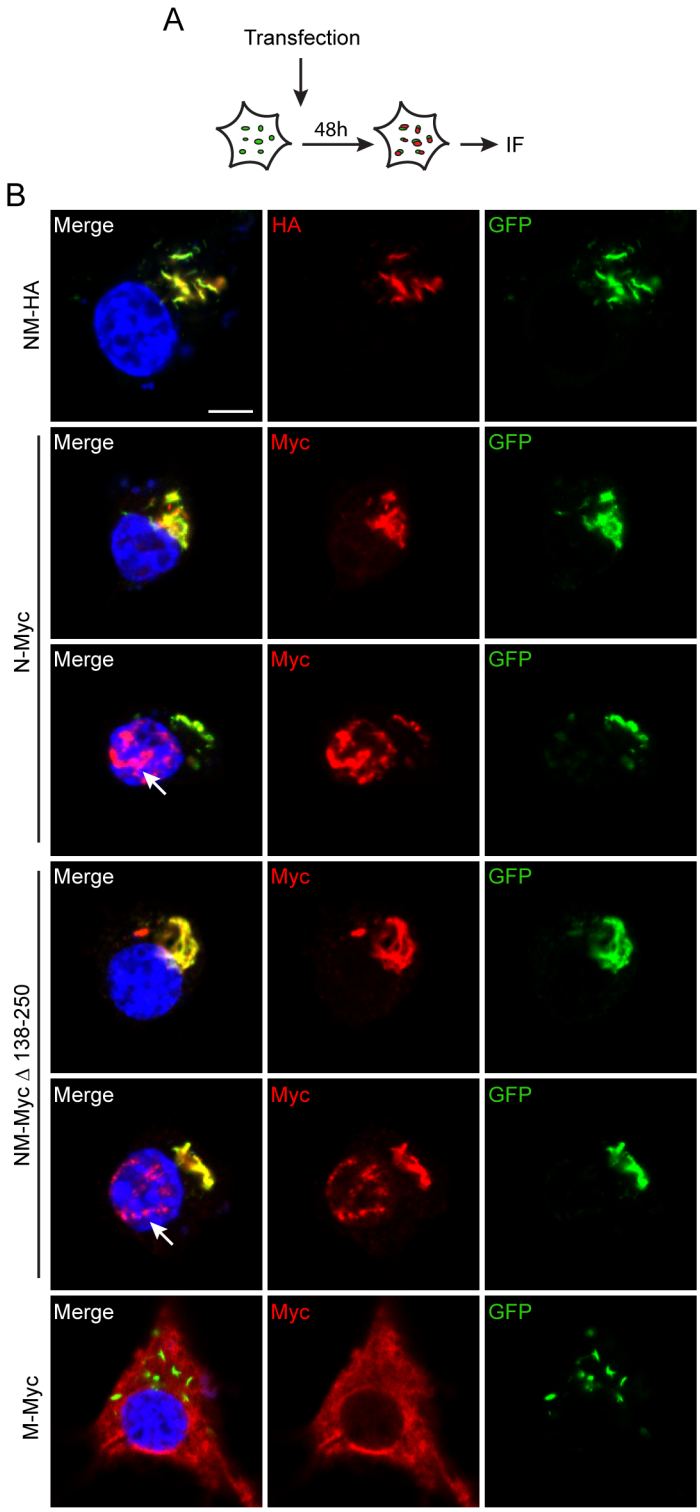

Figure 8. Aggregate decoration of endogenous NM-GFP prions. (A) Experimental setup. N2a cells stably producing NM-GFP prions were transiently transfected with full-length NM or mutant constructs for 48 h. **(B)** Immunofluorescence staining of N2a cell clone NM-GFP^{agg} 2CG11 transiently transfected with full-length NM or mutant constructs. NM was detected using either mAb anti-HA or pAb anti-Myc as indicated (red). GFP is depicted in green. Nuclei were visualized with Hoechst (blue). Arrows mark intranuclear aggregates. Scale bar: 5 µm.

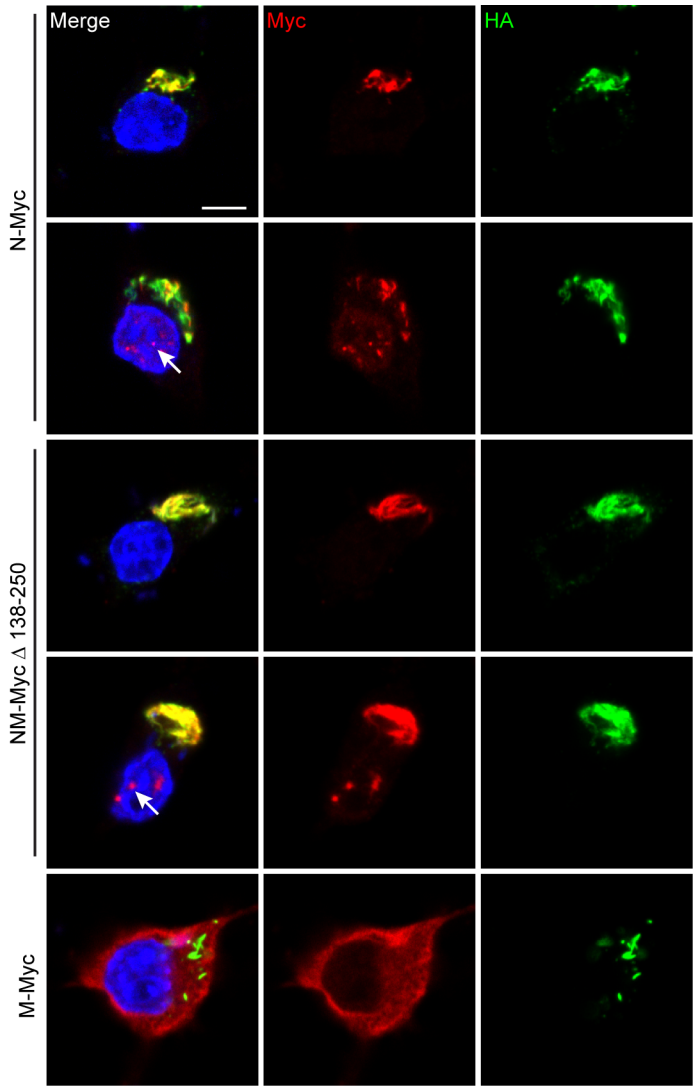

Figure 9. Aggregate decoration of endogenous NM-HA prions. Immunofluorescence staining of N2a cell clone NM-HA^{agg} 5A transiently transfected with mutant constructs for 48 h. NM was detected using either pAb anti-Myc (red) or mAb anti-HA (green) as depicted. Nuclei were visualized with Hoechst (blue). Arrows mark intranuclear aggregates. Scale bar: 5 µm.

In summary, these findings demonstrate that the M domain itself is not capable of forming self-replicating polymers whether induced by exogenous fibrils or endogenous prions. The N domain on the other hand is sufficient to form aggregates and carries the PrD of NM in mammalian cells as well as in yeast. Nevertheless, intracellular localization of the protein appears to be influenced by expression of the M domain. Based on these results we decided to focus the identification of functional domains crucial for cytosolic prion replication on the N domain, albeit also expressing the M domain to restrict expression to the cytoplasm.

3.2 Generation of N2a cell lines stably expressing full-length NM and NM mutants

To identify functional regions required for cytosolic prion replication within the N domain of Sup35, eight NM mutants were generated based on mutants that had previously been studied in yeast (Osherovich et al. 2004): NM Δ 1-39, lacking the QNR; NM Δ 39-123, with a deletion of the entire OPR (R1 – R6) and the CTN; NM Δ 75-123, lacking repeats 4 – 6 and the CTN; NM Δ 98-123, lacking only the CTN; NM G58D, carrying a point mutation in repeat 2; NM Δ 39-57, with a deletion of repeat 1 and partially of repeat 2; NM Δ 39-74, lacking repeats 1 - 3 and NM Δ 75-97, with a deletion of repeats 4 – 6 (Fig. 10).

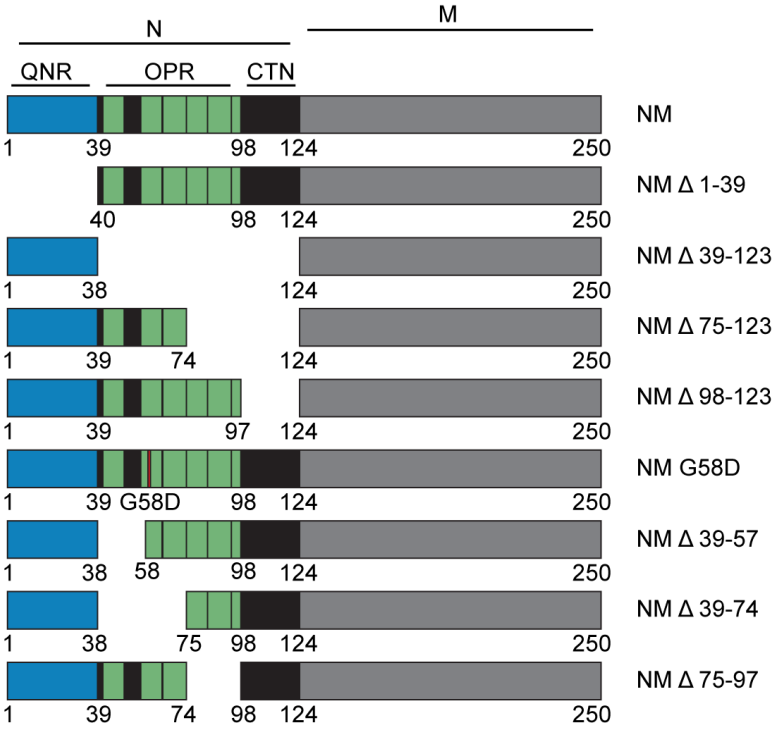

Figure 10. Scheme of full-length NM and NM mutants. Full-length NM and eight NM mutants were analyzed in this study. QNR: aa 1-39, R1: aa 41-49, R2: aa 56-64, R3: aa 65-74, R4: aa 75-83, R5: aa 84-93, R6: aa 94-97, CTN: aa 98-123. NM Δ 1-39, with a deletion of the QNR; NM Δ 39-123, with a deletion of the entire OPR (R1 – R6) and the CTN; NM Δ 75-123, with a deletion of repeats 4 – 6 and the CTN; NM Δ 98-123, with a deletion of the CTN; NM G58D, with a glycine to aspartic acid point mutation in repeat 2; NM Δ 39-57, with a deletion of repeat 1 and part of repeat 2; NM Δ 39-74, with a deletion of repeat 1 – 3 and NM Δ 75-97, with a deletion of repeats 4 – 6. Numbers refer to amino acids.

The NM mutants were generated using mutation specific primers or were purchased from the indicated manufacturers (methods, Table 2 and 3). NM constructs were carboxyterminally tagged with an HA-tag and cloned into the mammalian expression vector pJ602. To generate stable cell lines expressing full-length NM and NM mutants using lentiviral transduction, NM constructs were additionally cloned into the lentiviral expression vector pRRL.sin.PPT.CMV.Wpre (Follenzi and Naldini 2002).
To obtain stable cell lines expressing full-length NM and NM mutants, we produced lentiviral particles encoding the NM constructs. N2a cells were transduced with the lentiviral particles and analyzed by immunofluorescence staining (Fig. 11A).

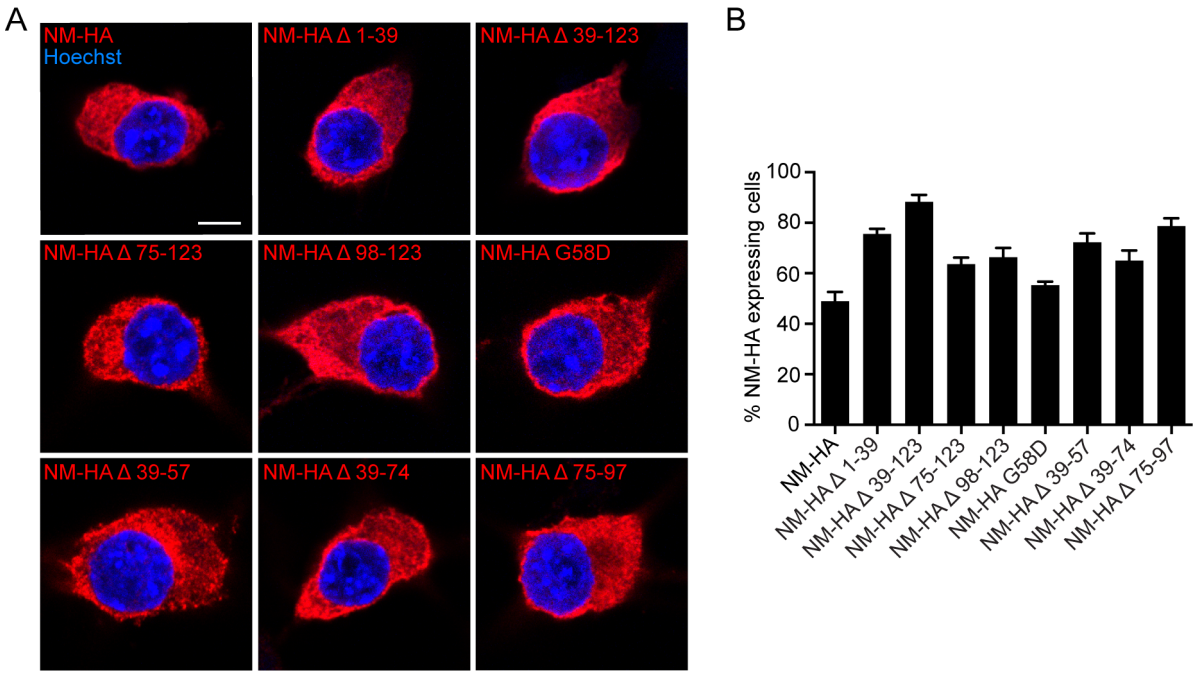

Figure 11. N2a cells stably express full-length NM and NM mutants. **(A)** Immunofluorescence staining of N2a cells stably expressing full-length NM and NM mutants. NM was detected using mAb anti-HA (red). Nuclei were visualized with Hoechst (blue). Scale bar: 5 µm. **(B)** Percentage of cells in the bulk population (passage one post thawing) expressing full-length and mutant NM. Bars represent mean values ± SD (n = 3).

All cell lines showed stable and diffuse ectopic expression of full-length and mutant NM throughout the cytosol. No expression in the nucleus was detected. We performed high-throughput analysis to determine the transduction rate of the stable full-length and mutant NM-HA cell lines. To this end, we stained the cells in a 96 - well plate and imaged them with an automated confocal microscope (Cell Voyager 6000, Yokogawa, Tokyo, Japan) (methods, 2.4.7). Image analysis was

performed using the Cell Profiler cell image analysis software (methods, 2.6.1). The analysis demonstrated that at least ~ 48 % of the cells showed clear expression of full-length NM and NM mutants (Fig. 11B).

These initial results demonstrate the generation of a useful tool for further studies on functional domains for cytosolic prion replication in a mammalian cell line.

3.3 Deletion of the QNR increases the rate of spontaneous aggregation

The previous images showed that full-length NM and NM mutants are diffusely expressed throughout the cytosol. However, upon closer examination of the immunofluorescence data, in individual cells spontaneously formed aggregates were detected in cell line NM-HA Δ 1-39 (Fig. 12A).

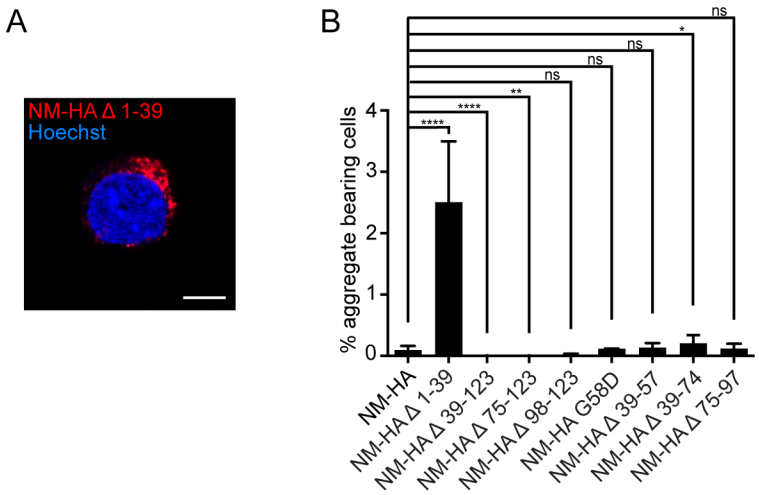

Figure 12. Deletion of the QNR increases the rate of spontaneous aggregation. (A) Immunofluorescence staining of the stable N2a cell line expressing NM-HA Δ 1-39. NM was detected using mAb anti-HA (red). Nuclei were visualized with Hoechst (blue). Scale bar: 5 µm. **(B)** Percentage of cells that express the transgene and spontaneously form NM aggregates at passage one post thawing. Bars represent mean values ± SD (n = 3, three individual cryogenic vials were thawed). At least 14000 cells were imaged per cell population. For statistical analysis the Cochran-Mantel-Haenszel test was performed (* $p \leq 0.05$, ** $p \leq 0.01$, **** $p \leq 0.0001$, ns: not significant).

To determine the frequency of spontaneous aggregation in full-length NM and NM mutant cell lines, we performed high-throughput analysis of the cell populations at passage one post thawing (Fig. 12B). The quantitative assessment showed that

approximately 2.5 % of cells expressing NM Δ 1-39 were bearing NM aggregates, whereas aggregates were rare in the other cell lines. Only extremely rare events (≤ 0.2 %) were detected for full-length NM or NM mutants with deletions within the OPR (NM Δ 39-57, NM Δ 39-74, NM Δ 75-97). However, lowest spontaneous aggregation frequencies (≤ 0.02 %) were detected for NM mutants lacking the last three repeats of the OPR and/or the CTN (NM Δ 39-123, NM Δ 75-123, NM Δ 98-123).

To verify the aggregation state of full-length NM and NM mutants, we separated soluble from insoluble proteins by sedimentation assay and performed Western blot analysis (Fig. 13).

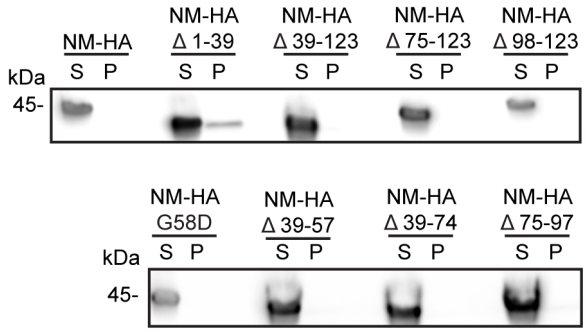

Figure 13. Sedimentation assay of N2a cells stably expressing full-length NM or NM mutants. Sedimentation assay of N2a cell lines stably expressing full-length or mutant NM. NM was detected using mAb anti-HA. S: supernatant, P: pellet.

All NM cell populations displayed a clear signal in the soluble fraction, confirming expression of full-length NM and NM mutants by biochemical analysis. Small size differences in the NM bands correspond to the deletions found in each mutant. Only NM Δ 1-39 additionally showed a signal in the insoluble fraction, thereby verifying the aggregated nature of the observed spontaneously formed conformers.

To determine if the rate of spontaneous aggregation would vary in consecutive passages and if spontaneously formed aggregates were stable over time, we quantitatively assessed the percentage of aggregate bearing cells at passage 1, 3, 5, 7, 10 and 13 post thawing (Fig. 14). Generally, the highest percentage of cells harboring spontaneously formed aggregates was detected at passage one. Towards later passages, the amount of aggregate bearing cells was steadily decreasing, indicating that spontaneous aggregation is merely an early event and spontaneously formed aggregates do not accumulate over time. Lowest frequencies of

spontaneously formed aggregates were again detected for NM mutants lacking the last three repeats of the OPR and/or the CTN (NM Δ 39-123, NM Δ 75-123, NM Δ 98-123).

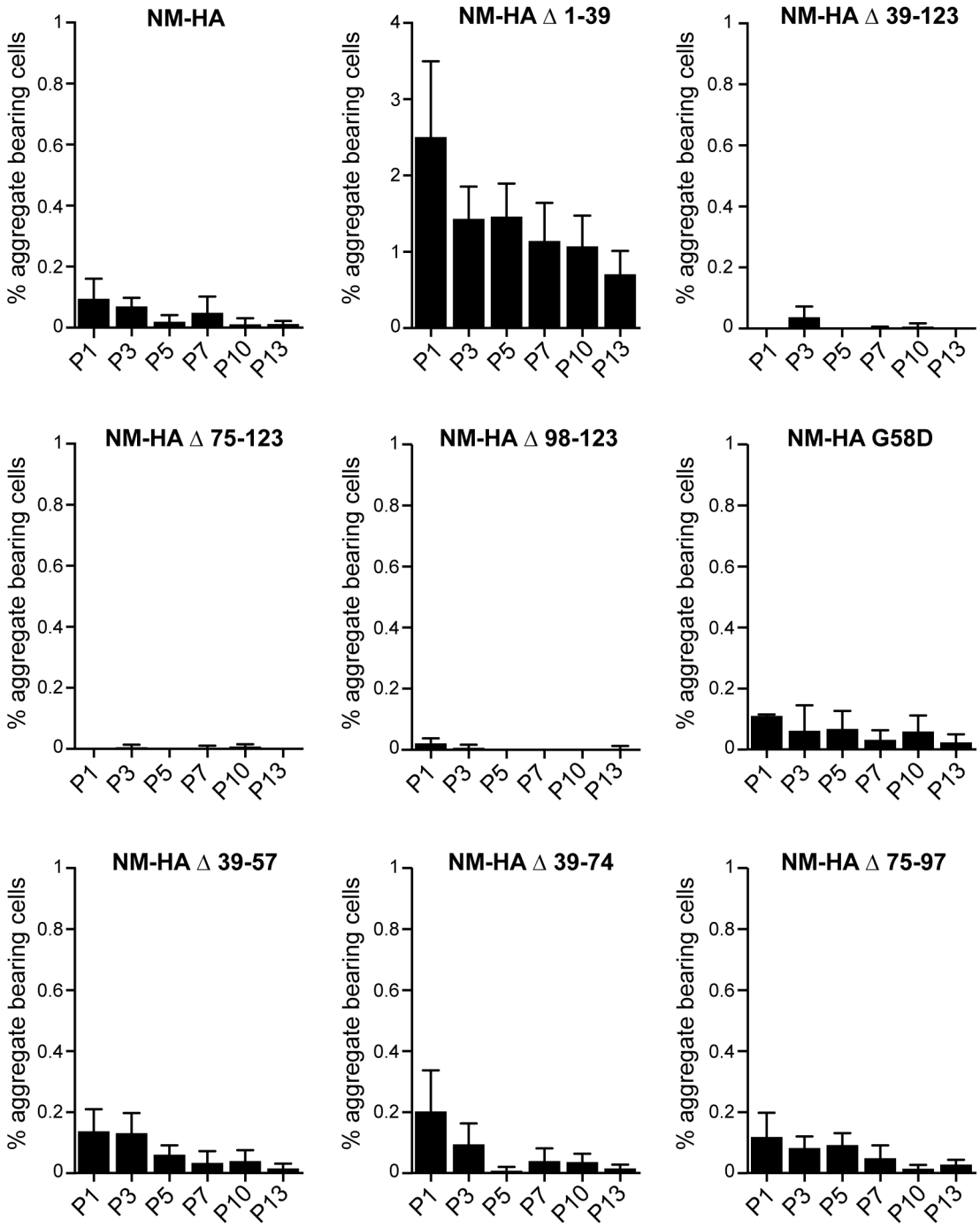

Figure 14. Spontaneous aggregation of full-length NM and NM mutants over consecutive passages. Quantitative analysis of cells that express the NM transgene and spontaneously form aggregates at passage 1, 3, 5, 7, 10, 13 post thawing. Note variations in scaling. Bars represent mean values ± SD (n = 3). P: passage.

In yeast, the frequency of prion induction is increased with a higher expression level of the respective prion protein (Derkatch et al. 1996). To analyze whether the elevated rate of spontaneous aggregation observed in N2a cell line NM-HA Δ 1-39 was due to higher expression of the NM mutant, we first determined full-length NM and NM mutant expression levels in the stable cell populations (Fig. 15)

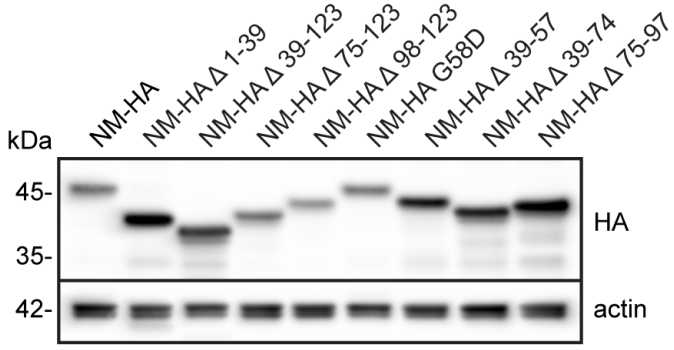

Figure 15. Expression of full-length NM and NM mutants in stable cell populations. Expression levels of full-length NM or NM mutants in N2a cell populations. NM was detected using mAb anti-HA. Actin was visualized with mAb anti-actin.

Differences in the expression levels correlated with the percentage of cells expressing full-length and mutant NM in the stable N2a cell populations (Fig. 11B, 15). The slight banding pattern visible underneath some NM signals is most likely due to protein degradation observed already by Paushkin and colleagues in 1996 (Paushkin et al. 1996). To test the influence of expression levels on the rate of spontaneous aggregation, we transiently transfected N2a cell populations expressing full-length NM and NM mutants Δ 75-123 and Δ 98-123 with expression plasmids encoding the same NM construct (Fig. 16A). Upon transient transfection the expression was increased almost three-fold in all cell populations (Fig. 16B).

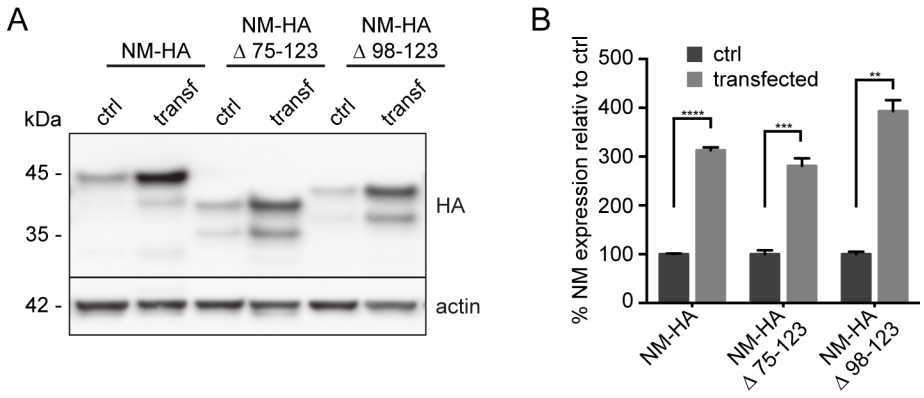

Figure 16. Expression levels of full-length NM and NM mutants upon transient transfection of stable N2a cell populations. N2a cell populations expressing full-length NM and NM mutants Δ 75-123 or Δ 98-123 were transiently transfected with expression plasmids encoding the respective NM protein. **(A)** Ctrl: cell populations before transfection, transf: same cell population after transfection with the respective NM construct. NM was detected with mAb anti-HA. Actin was visualized with mAb anti-actin. **(B)** Quantitative analysis of NM expression shown in A (three separate transfections). For statistical analysis, the t-test was performed (** $p \leq 0.01$, *** $p \leq 0.001$, **** $p \leq 0.0001$).

We performed high-throughput analysis of the control und transiently transfected cell populations (Fig. 17) and detected that the rate of spontaneous aggregation was only insignificantly altered, indicating that the expression level itself was not the cause for the increase in spontaneously formed aggregates in N2a cell line NM-HA Δ 1-39.

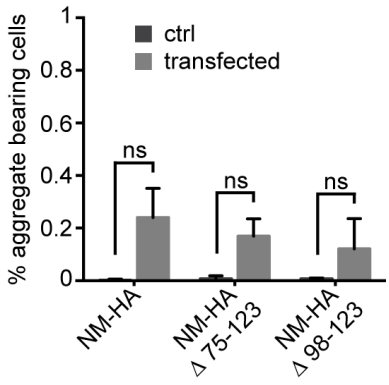

Figure 17. Influence of the expression level on spontaneous aggregation. Spontaneous aggregation of stable full-length and mutant NM expressing cell lines compared to the untransfected control cell lines. At least 5000 cells were analyzed per cell population. For statistical analysis, the Cochran-Mantel-Haenszel test was performed (n = 3, three separate transfections). At least 5000 cells were imaged per cell population Ctrl: control, ns: not significant.

In conclusion, the data indicate that the QNR helps to retain the prion precursor protein in its soluble state and has an inhibitory effect on aggregation in the mammalian cell environment.

3.4 The last three repeats of the OPR and the CTN are essential for initial aggregate formation

In the previous experiments, we could show that full-length NM and NM mutants were clearly expressed in the cytosol and, with very few exceptions, remained soluble throughout multiple passages. Next, to investigate which functional domains of NM are important for the induction of aggregates, we analyzed whether aggregation could be induced by endogenous NM-GFP prions. We therefore transiently transfected N2a cell clone 2CG11 stably producing NM-GFP aggregates with full-length NM and NM mutant constructs and screened the cells for NM-HA aggregates (Fig. 18).

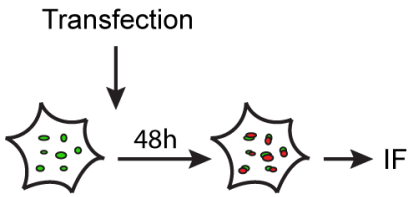

Figure 18. Experimental setup to study decoration of endogenous NM-GFP prions by NM-HA. N2a cell clone 2CG11 stably producing NM-GFP aggregates was transiently transfected with full-length NM or NM mutant constructs. Cells were fixed 48 h post transfection and screened for NM-HA aggregates.

Colocalization of NM-HA with NM-GFP prions was observed for all NM mutants, except for NM deletion mutant NM Δ 39-123, where aggregation was essentially abolished (≤ 1%) (Fig. 19). Though all except one NM mutant showed clear decoration of endogenous NM-GFP prions, decoration efficiencies appeared to be highly divers.

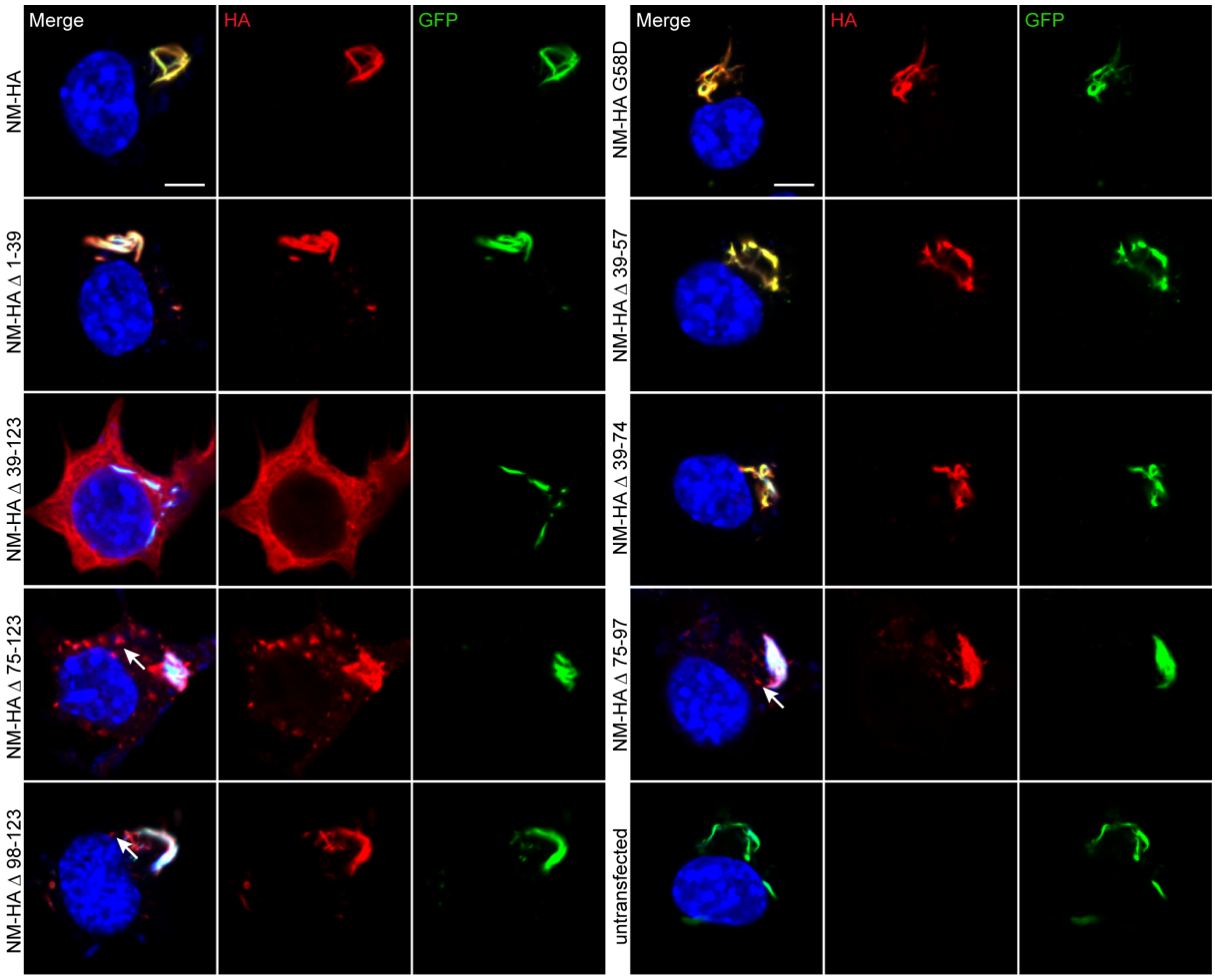

Figure 19. Full-length NM and NM mutants colocalize with endogenous NM-GFP prions. Immunofluorescence staining of N2a cell clone 2CG11 stably producing NM-GFP prions transiently transfected with HA-tagged full-length NM or NM mutant constructs. Cells were fixed 48 h post transfection. NM was detected using mAb anti-HA (red). GFP is depicted in green. Nuclei were visualized with Hoechst (blue). Note that some NM-GFP aggregates also brightly stained with Hoechst. Arrows mark NM-HA aggregate puncta not colocalizing with NM-GFP prions. Scale bar: 5 µm.

For full-length NM, NM Δ 1-39, NM G58D and NM deletion mutants with a deletion of the aminoterminal OPR (NM Δ 39-57, NM Δ 39-74) a high majority of cells showed decoration of NM-GFP prions (≥ 50%). For NM mutants with a deletion of the carboxyterminal OPR and/or CTN (NM Δ 75-123, NM Δ 98-123, NM Δ 75-97) only very few cells with NM-HA aggregates were found (≤ 5%). Interestingly, in those cell lines aggregates only partially colocalized with NM-GFP prions. Small NM-HA aggregate puncta were often found separated from NM-GFP aggregates (Fig. 19, arrows), suggesting that NM-GFP prions could template the conversion to the

aggregated NM-HA isoform but only inefficiently co-aggregated with those NM mutants. Note that large NM-GFP aggregates occasionally stained with the double-stranded DNA dye Hoechst, probably due to dye being trapped in high molecular weight conformers.

To analyze if aggregation of ectopically expressed NM could also be induced by addition of exogenous seeds, we induced aggregation of full-length NM and NM mutants in the stable N2a cell lines by incubation with *in vitro* fibrillized recombinant NM (Fig. 20A).

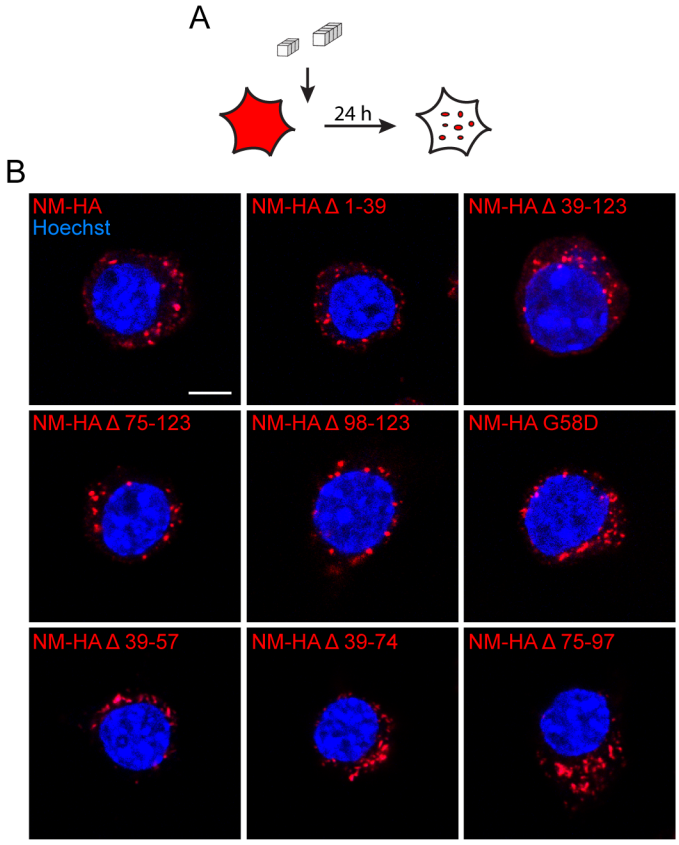

Figure 20. Exogenous NM fibrils induce full-length NM and NM mutant aggregates. **(A)** Experimental setup. N2a cells stably expressing full-length NM or NM mutants were incubated with 1 µM (monomer concentration) *in vitro* fibrillized NM for 24 h. **(B)** Immunofluorescence staining of N2a cells stably expressing full-length NM or NM mutants incubated with NM fibrils. NM was detected using mAb anti-HA (red). Nuclei were visualized with Hoechst (blue). Scale bar: 5 µm. Note that recombinant NM fibrils do not stain with mAb anti-HA.

Punctate aggregates were found in full-length NM and all NM mutant cell populations (Fig. 20B). Aggregates sometimes clustered together near the nucleus and at times

were spread throughout the entire cytosol. However, no localization could directly be attributed to one NM mutant.

To confirm the aggregation state of NM, we performed sedimentation assays using the stable full-length or mutant NM expressing cell lines 24 h after induction with *in vitro* fibrillized recombinant NM (Fig. 21).

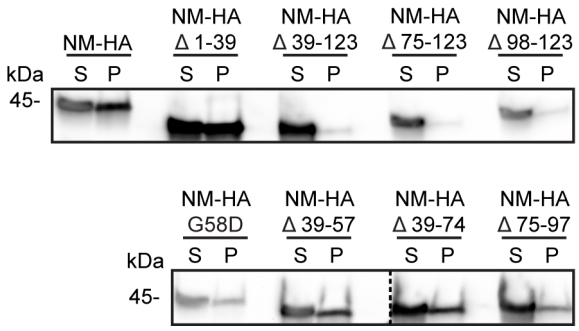

Figure 21. Sedimentation assay of stable N2a cells expressing full-length NM or NM mutants after induction with NM fibrils. Sedimentation assay of stable N2a cell lines expressing full-length and mutant NM incubated with 10 µM (monomer concentration) *in vitro* fibrillized NM for 24 h. NM was detected using mAb anti-HA. Additional lanes were excised for presentation purposes as indicated by the dotted line. S: supernatant, P: pellet.

For full-length NM and all NM mutants, a signal in the insoluble fraction was detected, confirming the aggregated state of the observed puncta. Interestingly, though aggregates were clearly formed, a major part of the protein was still found in the soluble fraction, indicating that not the entire pool of NM was converted into insoluble conformers. The amount of insoluble protein in full-length NM and NM mutants showed great differences, indicating that aggregate induction efficiencies varied between the NM mutants.

To quantify the induction efficiencies in full-length NM and NM mutants, we performed high-throughput analysis on the stable N2a cell lines at passage one after aggregate induction by *in vitro* fibrillized recombinant NM (Fig. 22).

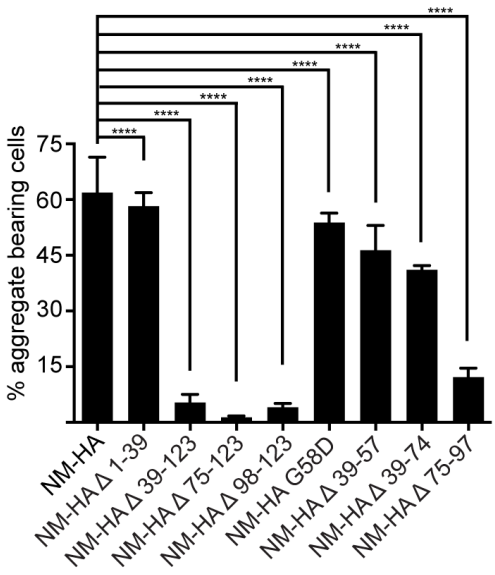

Figure 22. Aggregate induction efficiencies of full-length NM and NM mutants. Stable N2a cells expressing full-length NM and NM mutants were incubated with 10 µM (monomer concentration) recombinant NM fibrils for 24 h and analyzed by immunofluorescence staining at passage one post induction. Bars represent mean values ± SD (n = 3, three separate induction experiments). At least 12500 cells per cell population were imaged. For statistical analysis the Cochran-Mantel-Haenszel test was performed (**** $p \leq 0.0001$).

In full-length NM expressing cells aggregates were detected in approximately 60 % of the cells. Comparable results were observed for NM mutants with either a deletion of the QNR or a point mutation in the second repeat (NM Δ 1-39: 58 %, NM G58D: 54 %). NM mutants lacking only part of the OPR showed a reduced number of aggregate bearing cells compared to full-length NM and interestingly, the effect was more pronounced with a closer proximity of the deletion to the carboxyterminus of the N domain (NM Δ 39-57: 46 %, NM Δ 39-74: 41 %, NM Δ 75-97: 12 %). The strongest effect was seen in NM mutants with deletions of the CTN with or without additional deletions of the last three repeats of the OPR (NM Δ 39-123, NM Δ 75-123, NM Δ 98-123, ≤ 5 %).

In summary, the data demonstrates that the last three oligopeptide repeats and the CTN play a major role for the template-mediated conformational change to the prion isoform.

3.5 The last three oligopeptide repeats and the CTN contribute to vertical transmission

Our prior results showed that the last three repeats of the OPR and the CTN are of great importance for the templated conversion to the prion isoform. Besides aggregation, one striking feature of prions is the continual propagation of the prion phenotype to daughter cells. Propagation is facilitated by fragmentation of high molecular weight polymers into smaller entities (Krauss and Vorberg 2013). In cell culture models, functional fragmentation and propagation is determined by analyzing the amount of aggregate bearing cells over several passages. To assess the mitotic stability of the newly formed conformers, we analyzed stable N2a cells expressing full-length NM or NM mutants for nine passages after aggregate induction with NM fibrils (Fig. 23A). Full-length NM and NM mutants demonstrated the same variations in the initial amount of aggregate bearing cells as already observed in Figure 22 (Fig. 23B). As before, full-length NM, NM with a deletion of the QNR and NM with a point mutation in the second repeat (NM Δ 1-39 and NM G58D, respectively) showed the highest amount of aggregate bearing cells, whereas only few aggregates could be detected for NM mutants lacking the last three oligopeptide repeats and/or the CTN (NM Δ 39-123, NM Δ 75-123, NM Δ 98-123, NM Δ 75-97). Independent of the initial amount of cells with aggregates, full-length NM and NM mutants showed a gradual decline in aggregate bearing cells over time, which appeared to stabilize between passages six and nine for full-length NM, NM Δ 1-39 and NM G58D. Interestingly, even in N2a cell populations with a very low initial number of aggregate bearing cells, few cells with aggregates could still be detected after nine passages.

We used the Cox proportional hazard model to statistically analyze differences in the mitotic stability of NM mutants compared to full-length NM (Fig. 24). A higher fold change indicates a higher probability of aggregate bearing cells being lost over time. In general, mutations in NM decreased the mitotic stability of aggregates. NM mutants lacking the last three repeats of the OPR or the CTN (NM Δ 98-123, NM Δ 75-97, fold change > 1) were the least heritable.

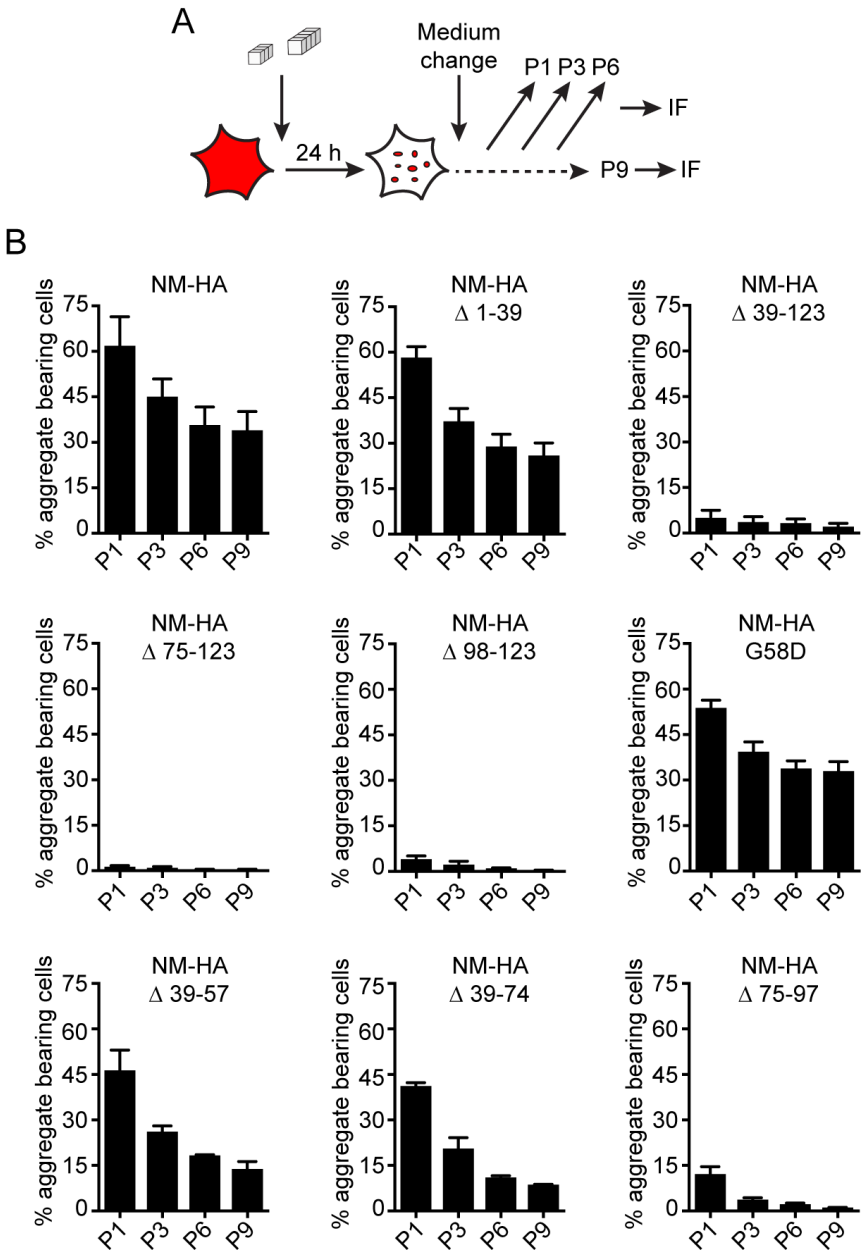

Figure 23. Full-length NM and NM mutant aggregates are maintained over several passages. (A) Experimental setup. Stable N2a cells expressing full-length NM or NM mutants were incubated with 10 µM (monomer concentration) *in vitro* fibrillized recombinant NM for 24 h and grown for nine passages. Cells at passage 1, 3, 6 and 9 were stained and analyzed by automated confocal microscopy. **(B)** Percentage of full-length NM or NM mutant expressing N2a cells harboring aggregates over consecutive passages (n = 3, three independent induction experiments). P: passage.

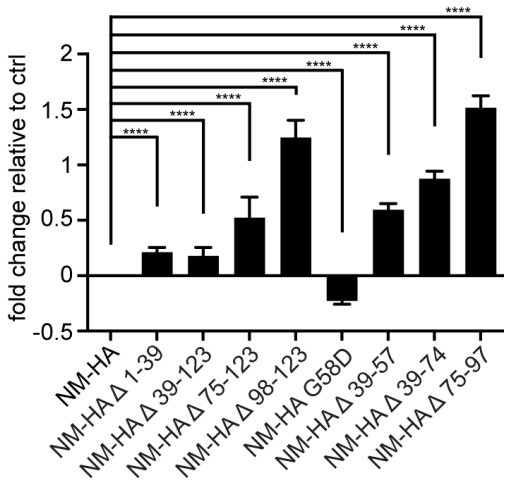

Figure 24. Fold change of the loss of NM mutant aggregate bearing cells over time compared to full-length NM. Fold change of the probability for NM mutant cell populations to loose aggregate harboring cells over time compared to full-length NM. Bars represent mean values. Error bars represent the upper limit for the confidence interval (n = 3). Ctrl: control. Cox proportional hazard model was performed for statistics (cell count >12500, **** $p \leq 0.0001$).

However, a high fold change was also seen in NM mutant NM Δ 75-123, lacking both regions, NM Δ 39-57, lacking repeat 1 and parts of repeat 2, and NM Δ 39-74, lacking repeats 1 – 3 (fold change > 0.5 and < 1). Interestingly, NM G58D showed even increased mitotic stability (fold change > -0.5 and < 0) compared to full-length NM, contradictory to previous findings where the point mutation resulted in prion loss in yeast (Kochneva-Pervukhova et al. 1998). These findings indicate, that in contrast to yeast, NM maintenance in mammalian cells does not depend on the second oligopeptide repeat.

To directly examine the fate of full-length NM and NM mutant aggregates upon cell division, we generated N2a cell lines stably expressing full-length NM and NM mutants NM Δ 1-39 and NM Δ 75-123 with a carboxyterminal GFP-tag. Aggregation was induced by addition of recombinant NM fibrils and the cells were subsequently subjected to life cell imaging two passages post induction (Fig. 25). All cell populations showed distinct NM-GFP aggregates that were distributed to both daughter cells upon cell division, confirming that mutant NM, lacking either the QNR or the last three repeats and the CTN, could still be propagated to the progeny.

In conclusion, these findings show that the last three repeats of the OPR and the CTN mainly contribute to mitotic stability of the prion isoform.

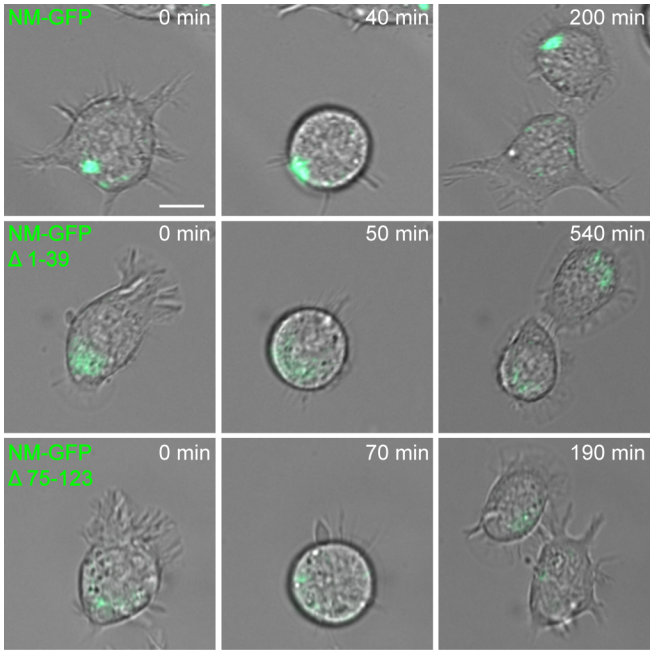

Figure 25. Full-length NM and NM mutant aggregates are bidirectionally transmitted to daughter cells. Time-lapse analysis of stable N2a cell lines expressing full-length NM or NM mutants Δ 1-39 and Δ 75-123 with a carboxyterminal GFP-tag (green). N2a cells were exposed to 10 µM (monomer concentration) recombinant NM fibrils for 24 h. Cells were subjected to life cell imaging for a total of 15 hours two passages post induction. Min: minutes; scale bar: 10 µm.

3.6 NM mutants exhibit infectious properties and horizontally transmit the aggregate phenotype to bystander cells

In contrast to their behavior in yeast, full-length NM prions were shown to infect neighboring cells and induce a self-perpetuating prion state (Hofmann et al. 2013). In the previous experiments we could already show that template-mediated aggregation and the subsequent propagation of aggregates were impaired by deletions of the last three oligopeptide repeats and the CTN, while deletion of the QNR had rather opposite effects. To further investigate the infectivity of mutated NM, we first had to increase the amount of aggregate bearing cells in our stable cell lines. Transfection reagents have already been shown to facilitate the uptake of fibrillized proteins into cells (Nonaka et al. 2010). Thus, we incubated the stable N2a cell lines expressing full-length NM or NM mutants with NM fibrils mixed with Effectene reagents (Fig. 26).

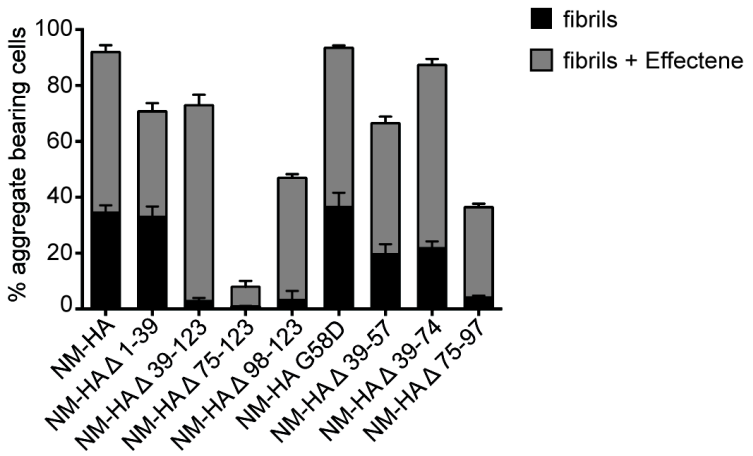

Figure 26. Increased aggregate induction efficiency by Effectene reagents. 10 µM (monomer concentration) *in vitro* fibrillized recombinant NM was solely or in combination with Effectene reagents added to stable N2a cells expressing full-length NM or NM mutants for 24 h. Aggregate induction efficiencies were determined at passage three post induction. At least 400 cells per treatment were analyzed.

Mixing NM fibrils with Effectene reagents drastically increased the induction rates in full-length NM and NM mutant expressing stable cell lines. Interestingly, the increase in aggregate bearing cells was not equal in all NM mutants. NM Δ 39-123, lacking the entire OPR and the CTN, showed the most striking change, with an increase of over 25-fold. Though the number of aggregate bearing cells was drastically increased for all NM mutants, the stable N2a cell line expressing NM Δ 75-123 still exhibited less than 8 % of NM aggregate bearing cells. Thus, we performed limiting dilution cloning using the aggregate bearing full-length NM and NM Δ 1-39 and NM Δ 75-123 N2a bulk populations generated with the use of Effectene reagents to generate cell clones with a high number of aggregate bearing cells. For full-length NM, we analyzed a total of 24 clones, 14 of which produced aggregates in 80-100 % of the cells. For NM Δ 1-39, we tested 20 clones and obtained 16 clones stably propagating aggregates in 80-100 % of total cells. Due to the low amount of aggregate bearing cells in the NM Δ 75-123 expressing cell line, we analyzed 144 clones but obtained only two clones with 40-70 % stably propagating aggregates, indicating deficits in mitotic stability. We therefore performed sub-cloning, using the two clones obtained after the first round of limiting dilution cloning. We screened 86 clones, 21 of which showed aggregates in at least 50 % of the cells. For full-length NM as well as the two NM mutants, four clones or subclones were chosen, exhibiting aggregates in over 80 % of the cells (Fig. 27).

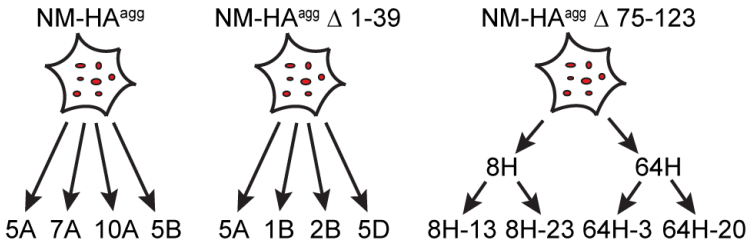

Figure 27. Cloning strategy to isolate N2a cell clones with stably propagating NM aggregates. Full-length NM and NM mutant cell populations were exposed to 10 µM (monomer concentration) recombinant NM fibrils mixed with Effectene reagents. Single cell clones were subsequently isolated by limiting dilution cloning. For NM Δ 75-123, a second cloning step was included as the first round resulted in clones with only weak mitotic stability of NM aggregates. For full-length NM and NM mutants, four clones/subclones were chosen that produced aggregates in over 80 % of total cells.

Confocal microscopy analysis of the cell clones revealed morphological diverse aggregate phenotypes (Fig. 28). Most cell clones produced small punctate aggregates, whereas others contained larger, fibrillar conformers. In addition, in some of the clones aggregates appeared to be restricted to one area, whereas in others aggregation was observed throughout the entire cytosol. However, neither morphological phenotypes nor specific cellular localizations could be directly attributed to individual deletions in NM. Multiple stably propagating phenotypic aggregate variants were already observed in yeast as well as in mammalian cells (Tanaka et al. 2004, Krammer et al. 2009) and are most likely the result of variations in expression levels, clonal differences and the conformational diversity of the NM fibrils used to induce aggregation.

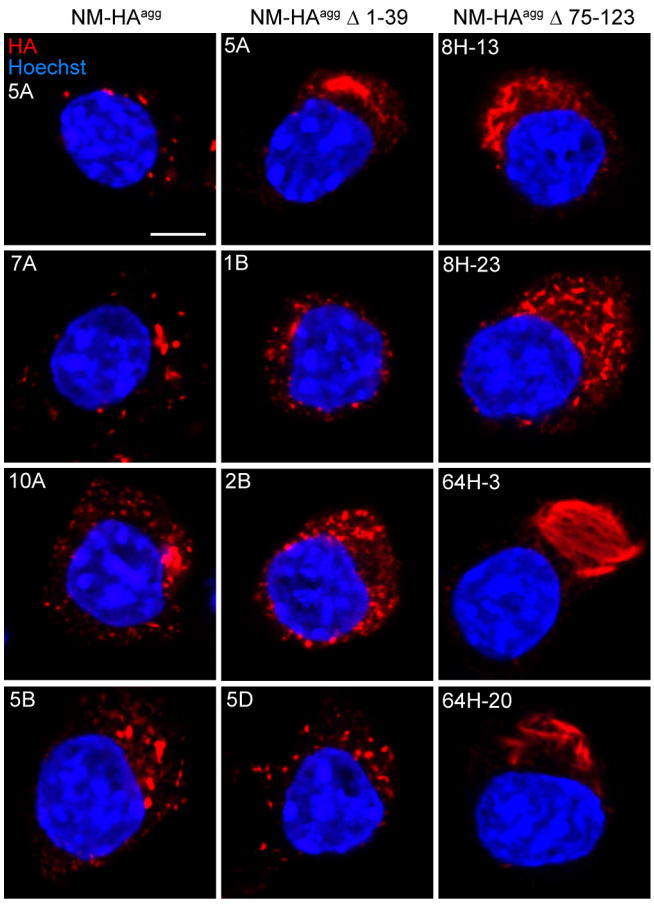

Figure 28. Full-length NM and NM mutant cell clones stably propagate NM aggregates. Confocal microscopy analysis of single cell clones isolated by limiting dilution cloning. For full-length and mutant NM four clones/subclones were analyzed. NM was detected using mAb anti-HA (red). Nuclei were stained with Hoechst (blue). Scale bar: 5 µm.

To confirm the amyloid nature of the aggregates, we performed semi-denaturing detergent - agarose gel electrophoresis (SDD-AGE) (Kryndushkin et al. 2003). For full-length NM and the NM mutants one single cell clone and the corresponding soluble NM-HA expressing bulk cell line were analyzed (Fig. 29). A distinct monomeric signal was detected for all soluble NM-HA expressing bulk cell lines. The single cell clones on the other hand showed large SDS resistant smears, confirming the amyloidogenic nature of the NM aggregates. Interestingly, the amyloid bands of full-length NM and NM mutant cell clones showed differences in the dominant size of the amyloid, suggesting the occurrence of different variants.

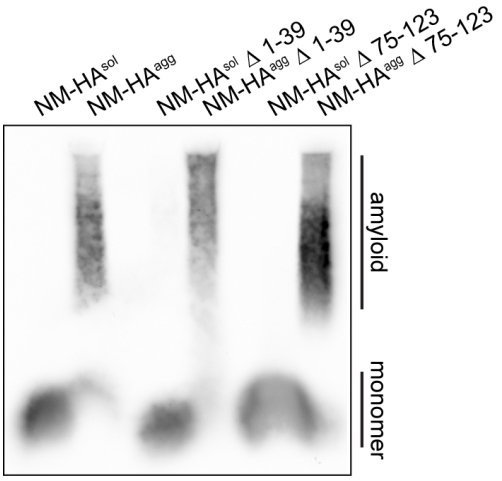

Figure 29. Full-length NM and NM mutant cell clones produce NM aggregates of amyloid nature. SDD-AGE assay of cell lysates from N2a NM-HA^{agg} clone 7A, Δ 1-39 clone 5D, Δ 75-123 subclone 8H-23 and the corresponding soluble NM-HA expressing bulk cell lines. NM was detected using mAb anti-HA.

Next, we used the full-length NM and NM mutant cell clones to investigate the infectivity of the NM aggregates. We therefore cocultured the aggregate bearing full-length NM and NM mutant cell clones with N2a cells expressing soluble NM-GFP for 42 h and screened for the appearance of NM-GFP aggregates (Fig. 30A). NM-GFP aggregates were induced by all cell clones except for NM-HA^{agg} Δ 75-123 subclone 64H-3, exhibiting especially large aggregates (Fig. 30B). It was already shown that transmission of the aggregate phenotype to bystander cells appears to be more efficient when donor cells produce small punctate aggregates (Hofmann et al. 2013), an observation that most likely explains the lack of infectivity of that specific clone.

To detect differences in the infectivity of full-length and mutant NM, we performed quantitative assessment of the intercellular aggregate induction rate of full-length NM and NM mutant cell clones (Fig. 31). Collectively, the induction rates were very low for full-length NM and the NM mutants. However, NM deletion mutant NM Δ 1-39 showed a significantly higher induction rate in comparison to the full-length NM control, suggesting that the QNR has, if any, a rather inhibiting effect on aggregate dissemination. Notably, direct comparison of aggregate induction rates is challenging due to clonal effects that might influence intercellular transmission of the aggregate phenotype (Hofmann et al. 2013).

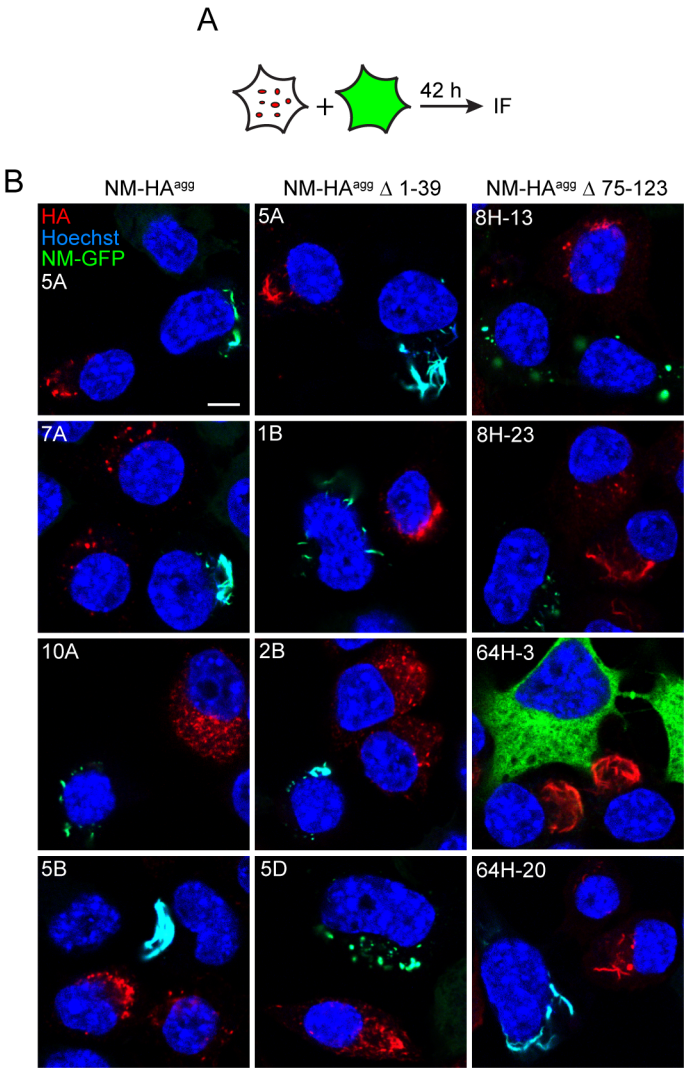

Figure 30. Coculture of N2a full-length and mutant NM-HA^{agg} cell clones with N2a NM-GFP^{sol} cells. (A) Experimental setup. Clones harboring NM-HA aggregates were cocultured with N2a cells expressing NM-GFP for 42 h on coverslips**. (B)** Immunofluorescence staining of N2a full-length or mutant NM-HA^{agg} donor cell clones cocultured with N2a NM-GFP^{sol} recipient cells. Images were screened for cells with NM-GFP aggregates. NM-HA was detected using mAb anti-HA (red). Nuclei were stained with Hoechst (blue). GFP is depicted in green. Note that large NM-GFP aggregates also brightly stained with Hoechst dye. Scale bar: 5 µm.

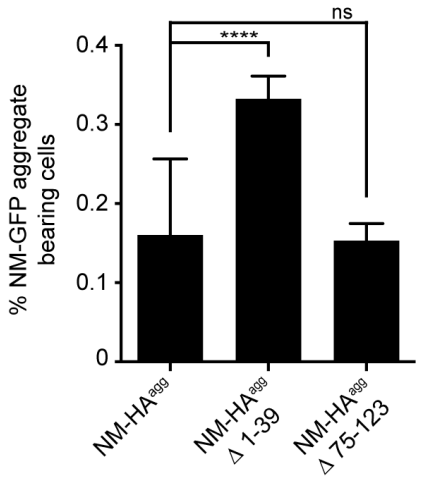

Figure 31. Quantification of the intercellular aggregate induction rate of full-length NM and NM mutant cell clones. Percentage of NM-GFP aggregate bearing recipient cells after 42 h coculture with full-length NM and NM mutant donor cells. Bars represent mean values of the combined data from the four NM full-length and NM mutant clones/subclones ± SD (n = 4). Cell count > 79000, **** $p \leq 0.0001$, ns: not significant, Cochran-Mantel-Haenszel test.

In summary, these results demonstrate that neither the QNR nor the last three oligopeptide repeats and the CTN are essential for intercellular transmission of the prion phenotype.

3.7 The QNR is not part of the proteolytic protected core of full-length NM aggregates

In vitro, the first 40 residues of NM, including the QNR, were experimentally identified as the amyloid core (Toyama et al. 2007). However, previous results from our study suggest a rather insignificant role of the QNR in the process of aggregation. To determine the tightly packed core region in our NM aggregates, we performed limited proteolysis using cell lysates form N2a NM-HA^{agg} clone 7A, Δ 1-39 clone 5D, Δ 75-123 subclone 8H-23 and the respective NM-HA expressing soluble bulk cell lines (Fig. 32A). Cell lysates were digested with decreasing amounts of chymotrypsin with the protease to total protein ratio ranging from 1:250 to 1:1000. Chymotrypsin preferentially cleaves at the carboxyterminus of aromatic amino acids (phenylalanine, tryptophan, tyrosine), residues that are with one exception only found in the N domain (Fig. 32B).

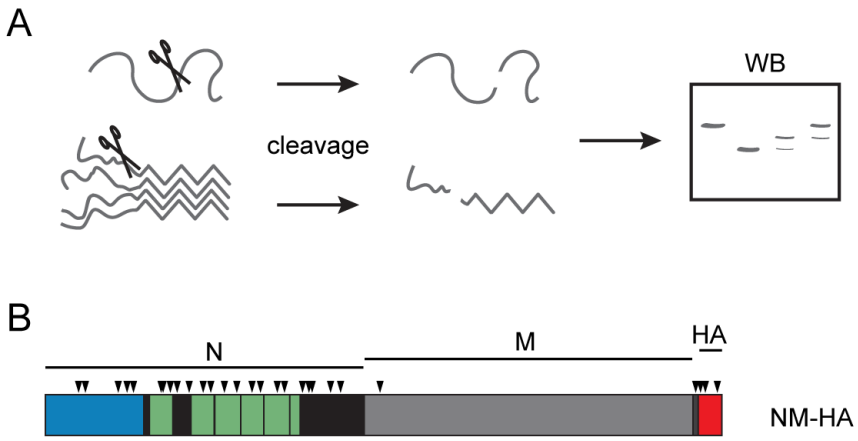

Figure 32. Experimental setup to determine the amyloid core of full-length NM and NM mutants. (A) Limited proteolytic digestion of cell lysates from N2a cells expressing soluble NM or producing NM aggregates. Proteins were analyzed by SDS PAGE and Western Blot. WB: Western blot. **(B)** Preferential cleavage sites of chymotrypsin. Arrowheads mark cleavage sites. Dark grey: EcoRI restriction site, red: HA-tag.

Aggregated full-length NM and NM mutant protein displayed a much higher resistance to proteolytic digestion compared to the soluble isoforms (Fig. 33), in line with previous reports (Paushkin et al. 1996). As expected, the level of degradation was increased with higher amounts of chymotrypsin, resulting in protein fragments with a lower molecular weight. Surprisingly, no degradation products were detected for NM-HA^{agg} Δ 1-39 and only weak fragments for Δ 75-123, that were most likely the result of residual soluble protein. In undigested soluble full-length NM, a second band was visible approximately 7 kDa below the band representing full-length NM. A similar band pattern was detected for undigested soluble NM Δ 75-123. Additional bands in the undigested samples with a lower molecular weight were most likely the result of partial degradation of the NM protein, resulting from the absence of protease inhibitor in the lysis buffer. To interpret and compare fragment sizes between full-length NM and NM mutants more precisely, we repeated the experiment and this time loaded the NM-HA^{sol} and NM-HA^{agg} samples on one gel each (Fig. 34). For aggregated full-length NM, a very low band (~ 30 kDa) that was most likely the result of residual soluble protein, and two only slightly digested fragments (~ 38, 41 kDa) in addition to the full-length protein appeared on the blot. Interestingly, the most prominent fragment (~ 38 kDa) had the same size as undigested NM Δ 1-39.

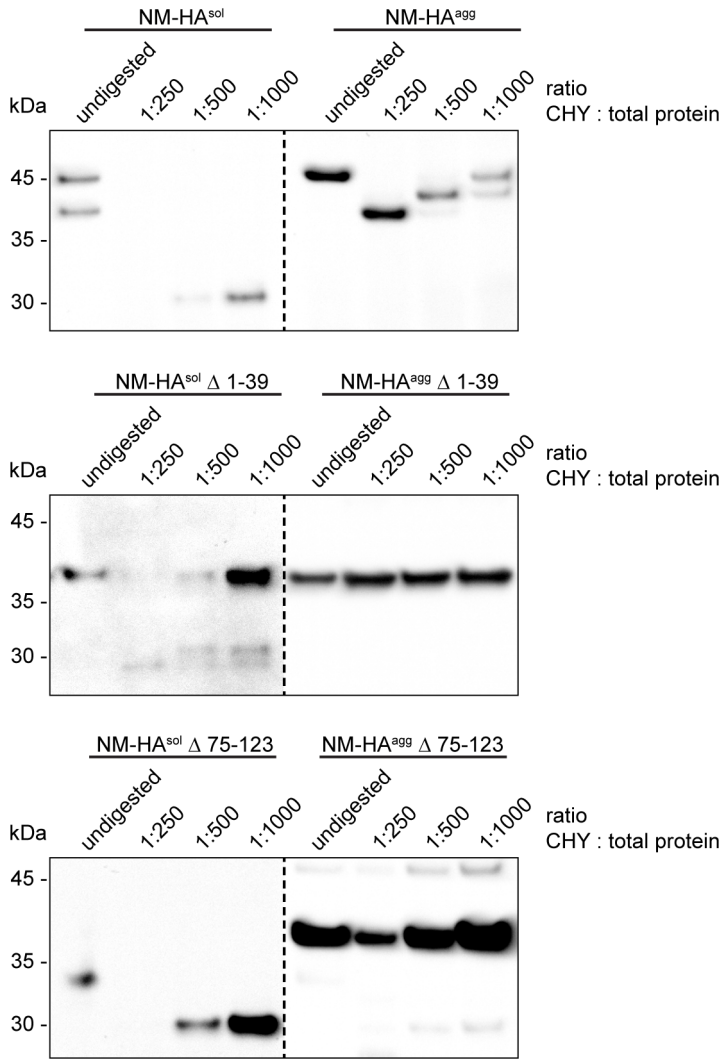

Figure 33. Proteolytic digestion of soluble and aggregated full-length NM and NM mutants. Proteolytic digestion of cell lysates from N2a NM-HA^{agg} clone 7A, Δ 1-39 clone 5D, Δ 75-123 subclone 8H-23 and the corresponding soluble NM-HA expressing bulk cell lines. Cell lysates were treated with chymotrypsin at the indicated protease to total protein ratios or left untreated. For size comparison samples from cells expressing soluble full-length NM-HA/NM-HA mutants and aggregated full-length NM-HA/NM-HA mutants were loaded on the same gel. NM was detected using 4A5 anti-M domain antibody (epitope: aa 229-247). CHY: chymotrypsin.

As chymotrypsin preferentially cleaves in the aminoterminal half of NM and proteins on the membrane were detected with an antibody binding the carboxyterminal M domain (aa 229-247), this finding suggests that in full-length NM the QNR region is accessible to digestion.

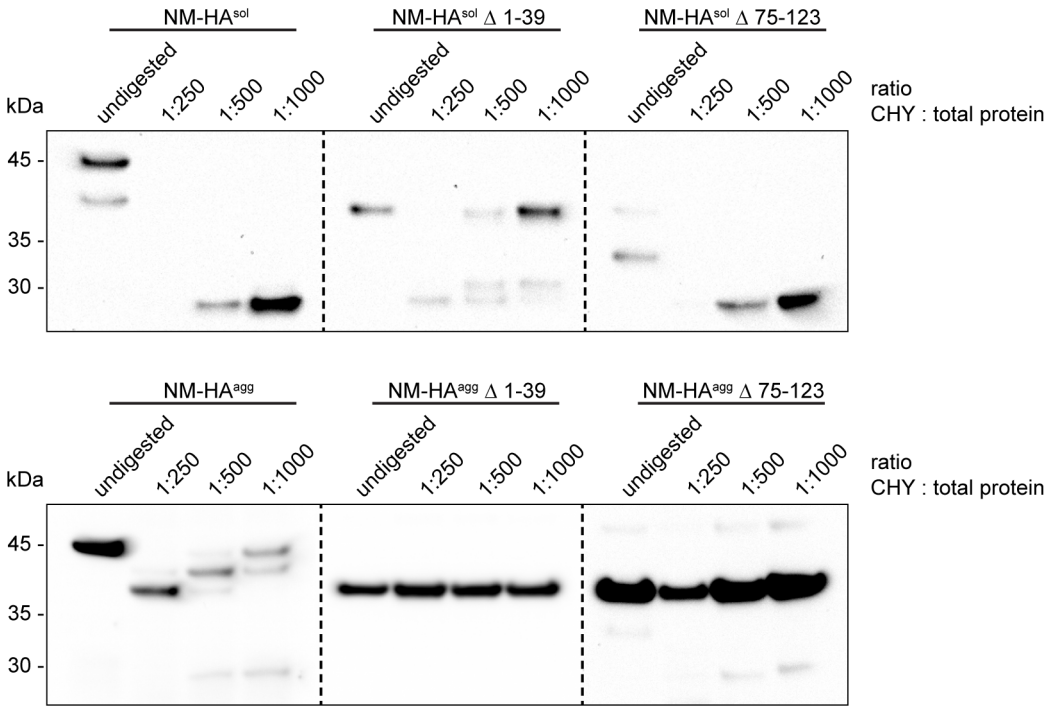

Figure 34. Comparing full-length NM and NM mutant aggregate structures by limited proteolysis. Proteolytic digestion of cell lysates from N2a NM-HA^{agg} clone 7A, Δ 1-39 clone 5D, Δ 75-123 subclone 8H-23 and the corresponding soluble NM-HA expressing bulk cell lines. Cell lysates were treated with chymotrypsin at the indicated protease to total protein ratios or left untreated. For size comparison full-length and mutant NM-HA^{sol} or NM-HA^{agg} samples were loaded on the same gel. NM was detected using 4A5 anti-M domain antibody. CHY: chymotrypsin.

As there were no detectable digestion products for NM Δ 1-39 and the intensity of the full-length NM Δ 1-39 signal was not reduced with higher concentrations of chymotrypsin, the remaining protein (~ aa 40-250) appeared to be well protected within the conformer. For aggregated NM Δ 75-123 only residual soluble protein was detected in addition to the full-length NM Δ 75-123 protein (Fig. 34, upper panel). Although no additional fragments were detected for NM Δ 75-123, the intensity of the full-length NM Δ 75-123 band decreased with higher amounts of chymotrypsin, indicating that the aggregated full-length NM Δ 75-123 protein was accessible to digestion, suggesting a more loosely packed aggregate compared to NM Δ 1-39. Control group lysates of stable cell lines expressing soluble full-length and mutant NM displayed increasing levels of digestion with higher levels of chymotrypsin, demonstrating proteolytic digestion of full-length and mutant NM when peptide chains are easily accessible.

To investigate whether additionally to the aminoterminus, cleavage was also occurring at the carboxyterminus of NM, we repeated the experiment and this time used the anti HA-tag antibody to detect fragments (Fig. 35A), as the HA-tag antibody epitope contains internal chymotrypsin digestion sites (Fig. 32B).

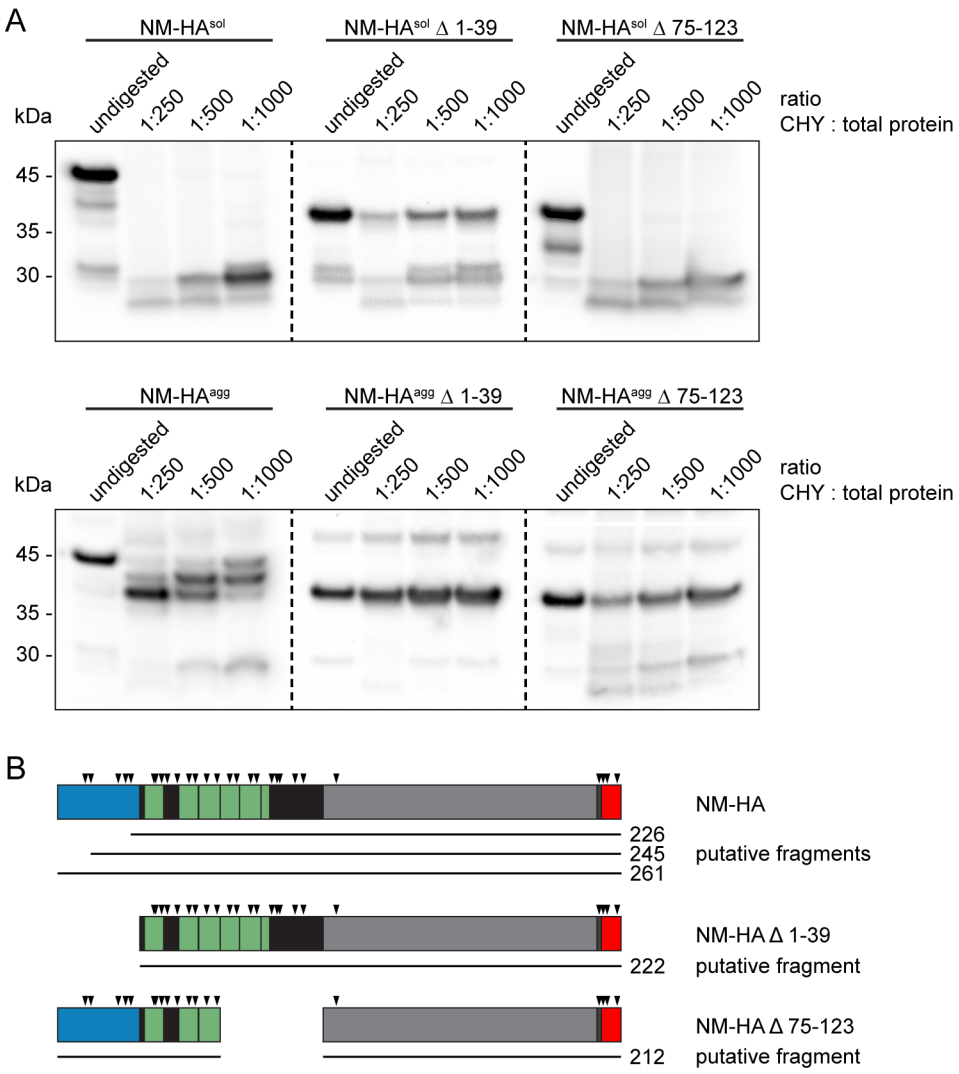

Figure 35. Detection of full-length and mutant NM proteolytic digestion fragments with the anti-HA antibody. (A) Proteolytic digestion of cell lysates from N2a NM-HA^{agg} clone 7A, Δ 1-39 clone 5D, Δ 75-123 subclone 8H-23 and the corresponding soluble NM-HA expressing bulk cell lines. Cell lysates were treated with chymotrypsin at the indicated protease to total protein ratios or left untreated. For size comparison, full-length and mutant NM-HA^{agg} and NM-HA^{sol} samples were loaded on the same gel. NM was detected using mAb anti-HA. CHY: chymotrypsin. **(B)** Putative fragments of full-length and mutant NM after digestion with chymotrypsin. Arrowheads mark preferential chymotrypsin digestion sites. Dark grey: EcoRI restriction site, red: HA-tag. Numbers refer to amino acids.

Interestingly, digestion fragments of full-length and mutant NM-HA^{sol} and NM-HA^{agg} appeared in the same pattern as when detected with the M domain antibody, indicating that, with the exception of the QNR in full-length NM, the entire NM protein including the M domain is protected within the formed aggregates (Fig. 35B). Noticeable, as the HA-tag antibody is stronger compared to the M domain antibody it is able to detect even very weak fragments on the Western blot not visible with the M domain antibody. However, additional weak fragments detected on the Western blot for the aggregated full-length NM and NM mutant proteins coincide with fragments observed in cell lysates form the respective soluble isoforms and therefore most likely originate from residual soluble protein found in the N2a NM-HA^{agg} cell populations.

To analyze the structure of NM fibrils in comparison to endogenous full-length NM aggregates, we performed limited proteolytic digestion of *in vitro* fibrillized recombinant NM (Fig. 36).

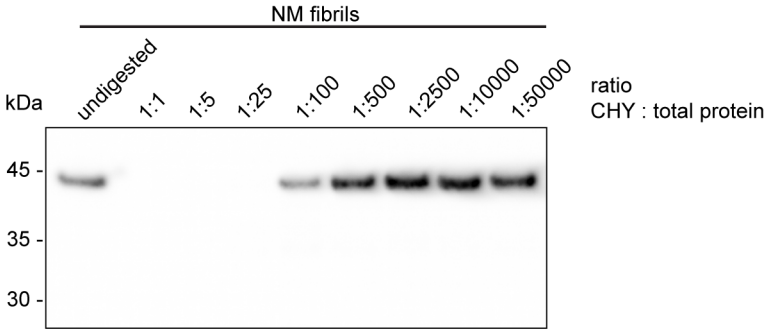

Figure 36. Limited proteolysis of recombinant NM fibrils. Western blot image of *in vitro* fibrillized recombinant NM that was digested with chymotrypsin at the indicated protease to total protein ratios or left untreated. NM was detected using 4A5 anti-M domain antibody. CHY: chymotrypsin.

As expected, no partial proteolytic digestion pattern could be detected for the tightly packed recombinant NM fibrils, indicating strong structural differences between *in vitro* fibrillized and intracellularly aggregated NM.

In summary, the results demonstrate that: (1) the proteolytic protected core region of full-length NM-HA aggregates does not include the QNR, (2) full-length NM-HA and NM-HA Δ 1-39 likely share a similar core and (3) upon deletion of the last three oligopeptide repeats and the CTN (NM-HA Δ 75-123), the protected region shifts towards the aminoterminus, now also including the QNR region.

4. Discussion

Successful prion replication requires three sequential steps: *de novo* induction of prions, fragmentation of amyloid fibrils and transmission of infectious propagons to daughter cells, and, in the case of mammalian cells, to bystander cells (Cascarina and Ross 2014). In *S. cerevisiae* these processes depend on two domains within the N domain of NM. *De novo* induction of aggregates is facilitated by the QNR and the first two repeats of the OPR, whereas Hsp104 mediated fragmentation and subsequent maintenance of the aggregate phenotype requires the entire OPR (King 2001, Parham et al. 2001, Osherovich et al. 2004, Shkundina et al. 2006). Here we demonstrate that, contrary to prion propagation in *S. cerevisiae,* the three sequential steps of prion replication and inheritance in the mammalian cell environment are encoded by only one region: the last three repeats of the OPR and the CTN (aa 75-123) (Fig. 37). Deletion of this region drastically impaired spontaneous formation of aggregates, initial aggregate induction and decoration as well as maintenance of aggregates. However, base levels of prion replication activity were still detected in mutants lacking this region, indicating that different types of aggregates can be formed, and once assembled, are capable of replication.

4.1 Spontaneous aggregation is inhibited by the QNR in mammalian cells

Although the exact structure of NM aggregates in N2a cells is not known, their ability to be seeded, their insolubility and SDS resistance strongly indicate the formation of amyloid fibrils. Though these characteristics are indicative of amyloid formation, further experiments could be performed to ensure the amyloidogenic nature of NM aggregates. Congo red staining is primarily used on histological sections to demonstrate the presence of amyloid fibrils, but was also successfully used in cell culture experiments (Sipe 1994, Kluve-Beckerman et al. 1999). While Thioflavin-T (ThT) can be used for histological stainings, it is also broadly used for *in vitro* analysis and immunofluorescence stainings of amyloid candidate proteins, as its fluorescence emission is strongly enhanced upon binding to amyloid fibrils (Biancalana and Koide 2010).

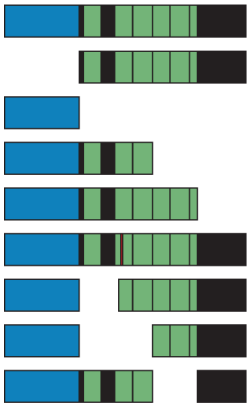

	Spontaneous aggregation	Induction of aggregates	Decoration of endogenous NM aggregates	Aggregate maintenance	Transmission to bystander cells
NM	0.09 %	62 %	++	+++	+
NM Δ 1-39	2.5 %	58 %	++	+++	+
NM Δ 39-123	0 %	5 %	-	+++	n.d.
NM Δ 75-123	0 %	1 %	+	++	+
NM Δ 98-123	0.02 %	4 %	+	+	n.d.
NM G58D	0.11 %	54 %	++	++++	n.d.
NM Δ 39-57	0.14 %	46 %	++	++	n.d.
NM Δ 39-74	0.2 %	41 %	++	++	n.d.
NM Δ 75-97	0.12 %	12 %	+	+	n.d.

Figure 37. Summary of the results. Spontaneous aggregation, fibril-mediated induction of aggregates and aggregate maintenance were studied in N2a cell lines stably expressing full-length NM or NM mutants with a carboxyterminal HA-tag. To investigate the propensity to decorate endogenous NM aggregates, N2a cell line 2CG11 producing stable NM-GFP prions was transfected with HA-tagged full-length NM and NM mutant constructs. Transmission to bystander cells was assessed using stable full-length and mutant NM aggregate-bearing cell clones cocultured with soluble NM-GFP expressing N2a cells. Decoration: "++" decoration of endogenous aggregates was detected in ≥ 50% transfectants, "+" in ≤ 5% transfectants, "-" in ≤ 1 % transfectants. Aggregate maintenance: "++++" slightly increased mitotic stability compared to the full-length NM control (fold change > - 0.5 and < 0), "+++" only slightly impaired mitotic stability (> 0 and < 0.5), "++" lower mitotic stability (> 0.5 and < 1), "+" very low mitotic stability (> 1 and < 1.5). Transmission to bystander cells: "+" transmission was observed in at least 10^3 cells, "n.d." not done.

Lately, it was proposed that in early events of amyloid formation, monomers group together to form micelle-like structures that are converted to the prion-isoform upon binding to insoluble seeds (Serio et al. 2000). This finding is supported by results of the group of Simon Alberti, which argue that formation of fibrous aggregates is preceded by protein assembly in liquid droplets (Patel et al. 2015). *In vitro* and in *S. cerevisiae,* interactions of NM monomers and interactions observed in peptide arrays, that would precede *de novo* aggregation, are mainly governed by amino acid stretches within the QNR, regions often referred to as nucleation sites (Krishnan and Lindquist 2005, Tessier and Lindquist 2007).

Interestingly, studies also identified a second region ranging from residues ~ 90-120, roughly including R5, R6, and the CTN, to be capable of forming intermolecular contacts, though interactions were found to be weaker compared to the first domain (Krishnan and Lindquist 2005, Tessier and Lindquist 2007). The subsequent step, *de novo* aggregation induced through overexpression of NM, is facilitated by the QNR and the first two repeats of the OPR, as identified by three separate studies (King 2001, Osherovich et al. 2004, Shkundina et al. 2006). In mammalian cells, spontaneous aggregation is comparable to *de novo* aggregation in yeast. Interestingly, in contrast to the previous findings in yeast, we found that in mammalian cells, spontaneous aggregation was in fact inhibited by the QNR and formation of aggregates was mainly promoted by the last three oligopeptide repeats and the CTN (aa 75-123) (Fig. 37). This suggests that *de novo* aggregation or spontaneous aggregation of NM can be facilitated by different nucleation sites in yeast and mammalian cells. Thus, the cellular environment is a factor that has to be taken into account when analyzing binding or aggregation behavior of prion or prion-like proteins.

Compiling evidence argues that the amino acid composition is the major determinant of amyloid or prion propensity (Ross, Edskes, et al. 2005, Ross, Minton, et al. 2005, Shewmaker et al. 2008). At that time, multiple studies had already reported that glutamine and more recently, asparagine residues, promote aggregation (DePace et al. 1998, Michelitsch and Weissman 2000, Perutz et al. 2002, Peters and Huang 2007, Alberti et al. 2009, Sabate et al. 2015). Interestingly, compared to the QNR, the region comprising the last three repeats and the CTN (aa 75-123) has a lower percentage of glutamine and asparagine residues (aa 75-123: 42.9 %, QNR: 55.3 %) as well as a lower N/Q ratio (aa 75-123: 0.62, QNR: 0.75) (Fig. 38). Additionally, the region encompassing residues 75-123 has a higher content of prolines compared to the QNR (aa 75-123: 8.2 %, QNR: 0 %). Proline residues have been reported to disfavor and even break β-sheets (Li et al. 1996, Adessi and Soto 2002, Lopez de la Paz and Serrano 2004) (Fig. 38). In an extensive *in vivo* assay Toombs and coworkers quantitatively assessed the compositional effects on prion formation (Toombs et al. 2010). They detected that charged residues strongly disfavor prion formation, whereas hydrophobic amino acids, with the exception of proline residues, strongly promote aggregation.

		QNR	OPR			OPR/ CTN		CTN
	Deletion region	**1-39**	**39-57**	**39-74**	**75-97**	**39-123**	**75-123**	**98-123**
	Length	39	19	36	23	85	49	26
charged	**R (Arg)**	2.6	0	0	0	1.2	2	3.8
charged	**D (Asp)**	2.6	0	2.8	0	1.2	0	0
charged	**K (Lys)**	0	0	0	0	1.2	2	3.8
polar	**S (Ser)**	7.9	5.3	2.8	0	2.4	2	3.8
polar	**Q (Gln)**	31.6	26.3	27.8	34.8	27.1	26.5	19.2
polar	**N (Asn)**	23.7	5.3	8.3	8.7	12.9	16.3	23.1
polar	**Q + N**	55.3	31.6	36.1	43.5	40	42.9	42.3
aromatic	**Y (Tyr)**	13.2	26.3	25	13	17.6	12.2	11.5
aromatic	**F (Phe)**	0	0	0	4.3	3.5	6.1	7.7
hydrophobic	**A (Ala)**	7.9	10.5	8.3	0	4.7	2	3.8
hydrophobic	**G (Gly)**	10.5	21.1	19.4	26.1	20	20.4	15.4
hydrophobic	**L (Leu)**	0	0	0	0	1.2	2	3.8
hydrophobic	**P (Pro)**	0	5.3	5.6	13	7.1	8.2	3.8

Figure 38. Amino acid composition of different deletion regions within the N domain. The position of the deletion regions and their lengths are depicted at the top in amino acid residues. The abundance of the individual residue is given in percent.

Interestingly, the last three oligopeptide repeats and the CTN comprise an increased number of hydrophobic residues (30.5 %) compared to the QNR (18.4 %) (percentages without proline residues), and a slightly reduced number of charged residues (aa 75-123: 4 %, QNR: 5.2 %) (Fig. 38). Two factors that would increase the overall prion propensity of the region comprising the last three oligopeptide repeats and the CTN. Yet, taken together with the decreased amount of glutamine and asparagine residues and the increase in proline residues, in total both regions might be similarly prionogenic. The comparison of the most significant differences in amino acid composition shows that composition alone does not suffice to determine amyloid or prion propensity. Interestingly, Toombs and coworkers made a similar observation. Though some amino acids strongly promote prion formation, these residues were not abundantly present in the known yeast PrDs (Toombs et al. 2010). Therefore, they hypothesized that PrDs are not optimized for maximum prion forming propensity, instead their composition demonstrates a balance of intrinsic disorder and prion propensity (Toombs et al. 2010).

In summary, these findings indicate that different nucleation sites are predominantly active *in vitro* and in *S. cerevisiae* compared to mammalian cells, and their position cannot sufficiently be determined by amino acid composition alone, environmental factors must be considered as well.

4.2 Template-assisted aggregation is facilitated by the last three oligopeptide repeats and the CTN in mammalian cells

In line with experiments performed in yeast, in mammalian cells the prion phenotype can also be induced by addition of exogenous seeds (Sparrer et al. 2000, King and Diaz-Avalos 2004, Tanaka et al. 2004, Krammer et al. 2009). Similar to spontaneous aggregation, also for template-assisted aggregate induction by recombinant NM fibrils the QNR played only a minor role and lowest induction rates were again observed when the last three repeats and/or the CTN were absent (aa 75-123) (Fig. 37). But even though aggregation was strongly impaired in these mutants, aggregate formation was not entirely abolished. This suggests that in the absence of the seemingly preferential site for template-assisted aggregation in mammalian cells (aa 75-123), alternative and less efficient binding sites take over. Our results show that aggregation is still possible even in NM mutant Δ 39-123, encoding only the QNR in addition to the M domain. As already shown by our initial results, the M domain itself is not capable of aggregation, which suggests that alternative sites must lie within the first 38 residues of the N domain. As earlier discussed, regions within the QNR have already been identified as possible binding or nucleation sites (Krishnan and Lindquist 2005, Tessier and Lindquist 2007), strengthening our hypothesis that the QNR functions as an alternative binding site for template-assisted aggregation in mammalian cells.

The last three repeats and/or the CTN were also crucial for decoration of pre-existing aggregates (Fig. 37). Interestingly, although in some cells aggregation could be induced in cell populations where the last three repeats and/or the CTN were deleted (≤ 5%), some aggregate puncta did not colocalize with endogenous NM-GFP prions. This suggests that even though NM-GFP aggregates can initially template the conversion into the prion isoform, aggregate conformations might differ between full-length NM and NM mutants lacking the last three repeats and/or the CTN. Yet, the strongest effect was observed when the entire OPR in addition to the CTN were

deleted (NM Δ 39-123). Less than 1 % of cells showed NM-HA colocalization with NM-GFP prions. The virtual abolishment of coaggregation in this NM mutant, suggests that, in contrast to template-assisted aggregation by NM fibrils, the QNR is not sufficient to decorate pre-existing aggregates. This finding is consistent with the study by Osherovich and coworkers, who found that for decoration of pre-existing fibrils at least the first repeat in addition to the QNR (aa 1-57) was needed (Osherovich et al. 2004). Combined, these findings demonstrate that the last three repeats and the CTN are the preferential sites for template-assisted aggregation by NM fibrils and decoration of pre-existing aggregates in mammalian cells. However, in the absence of the preferential binding site, the QNR functions as an alternative binding site for aggregate induction by NM fibrils. This site is, however, insufficient to facilitate decoration of pre-existing aggregates.

4.3 The last three oligopeptide repeats and the CTN contribute to prion maintenance in mammalian cells

Multiple studies have demonstrated that the entire OPR is a crucial region for fragmentation and maintenance of the prion phenotype in yeast (Doel et al. 1994, Parham et al. 2001, Osherovich et al. 2004, Shkundina et al. 2006). In yeast, fragmentation is mediated by the Hsp104 machinery (Chernoff et al. 1995). Our studies on the contrary, have shown that in the mammalian cell environment aggregate maintenance predominantly depends on the last three repeats of the OPR and the CTN (aa 75-123). Additionally, so far no mammalian homologue of Hsp104 has been identified (Chernoff et al. 1995), suggesting that fragmentation must be facilitated by different means in the mammalian cytosol. The independence of aggregate fragmentation from the aminoterminal OPR and Hsp104 is also reflected by the finding that the glycine to aspartic acid point mutation in the second repeat (G58D) improves prion maintenance compared to the full-length NM control. In yeast, NM G58D acts as a dominant-negative prion mutant that results in the elimination of the prion phenotype (Doel et al. 1994, Osherovich et al. 2004). The NM mutant was reported to destabilize the amyloid fiber and enhance Hsp104 mediated dissolution, leading to the observed defects in prion inheritance (DiSalvo et al. 2011). Interestingly, in yeast the G58D induced interference with the prion phenotype appears to be a strain dependent phenomenon, likely depending on the aggregate

structure of the individual variant (Derkatch et al. 1999, Verges et al. 2011). Our finding that G58D has no deteriorating effect on NM maintenance in mammalian cells, combined with the strain and conformation dependence observed in the NM mutant in yeast, implicate that NM conformers in mammalian cells differ from the predominant conformations in yeast. Thus, NM aggregates in mammalian cells, will subsequently also depend on different fragmentation machineries that have yet to be identified.

4.4 NM infectivity is not governed by the QNR or the last three oligopetide repeats and the CTN in mammalian cells

Prions in mammalian cells can infect neighboring cells and induce a self-perpetuating prion state. Yeast prions were already shown to be infectious in yeast as well as in mammalian cells (Wickner 1994, Hofmann et al. 2013). Yet, whether specific domains in NM contribute to the protein's infectivity has not been analyzed so far. In our study, we found that neither deletion of the QNR nor deletion of the last three repeats and the CTN prevented the infection of neighboring cells (Fig. 37). Although induction rates were overall low, deletion of the QNR in fact significantly increased the appearance of NM aggregates in recipient cells, suggesting that the QNR has, if any, a rather inhibiting effect. Though one out of four clones harboring NM Δ 75-123 aggregates was not infectious, no difference to full-length NM could be detected in the quantitative assessment, suggesting that the last three repeats and the CTN do not contribute to NM infectivity. Notably, infectivity experiments were performed using cell clones, and it cannot be excluded that clonal differences had an effect on induction efficiencies. Additionally, it has to be considered that the analyzed clones were amongst other factors selected for the mitotic stability of NM aggregates, which necessitates successful fragmentation of high molecular weight conformers. Fragmentation on the other hand, is also a requirement to generate small infectious entities capable of entering neighboring cells. Therefore, in the cloning process selected NM mutant aggregates might not represent the true infectious efficiencies of the NM mutants. During the maintenance experiment and the cloning process, NM mutant Δ 75-123 already showed mitotic instability that might have been facilitated through deficiencies in fragmentation. This likely also affected its infectious activities. However, one observation we made was that, regardless of the NM sequence,

overall clones with smaller, punctate aggregates appeared to have higher induction rates, indicating that at least for the analyzed clones, infectivity might have been sequence-independent. Combined, our findings indicate that NM infectivity is not governed by the QNR or the last three repeats and the CTN and follow-up experiments should be performed.

4.5 Aggregation is facilitated through different nucleation sites in mammalian cells and in *S. cerevisiae*

A striking feature of prions is the faithful propagation of strains or variants that induce distinct prion phenotypes. Prion variants have been proposed to differ in their conformations, resulting from variations in the length or position of the amyloid core and the extent of β-sheet structures (Tanaka et al. 2004, Toyama et al. 2007, Chang et al. 2008). *In vitro* fibrillized recombinant NM has been shown to contain a mixture of amyloid conformations (Glover et al. 1997, Gorkovskiy et al. 2014). Despite that great diversity, so far investigated variants *in vitro* as well as in yeast mostly contained amyloid core structures spanning the aminoterminal N domain including the QNR (Toyama et al. 2007, Luckgei et al. 2013). In our mammalian cell model, on the other hand, *in vitro* fibrillized NM induces full-length NM conformers, where the QNR is not part of the tightly packed, proteolytically protected core region. Interestingly, Chang and colleagues suggested that the successful propagation of a specific strain is affected by the genetic environment of the host and the biophysical properties of the strain (Chang et al. 2008). Thus, *in vitro*, in yeast and in the mammalian cell environment, different conformations might be dominant as a result of selective pressure. This notion agrees with two theories: (1) the mutational clone theory and (2) the "cloud" or "ensemble" model of prion variants (Collinge and Clarke 2007, Li et al. 2010) (Fig. 39). In the mutational clone theory (Fig. 39, left panel), one prion variant undergoes mutational changes, whereby it adopts a different conformation and generates a new prion variant. In the "cloud or "ensemble" model (Fig. 39, right panel), prion variants comprise a cloud of conformational species with one dominant and multiple less frequent conformers. Though several conformations coexist, only the predominant, abundant conformation will be detectable in biochemical analysis (Collinge and Clarke 2007).

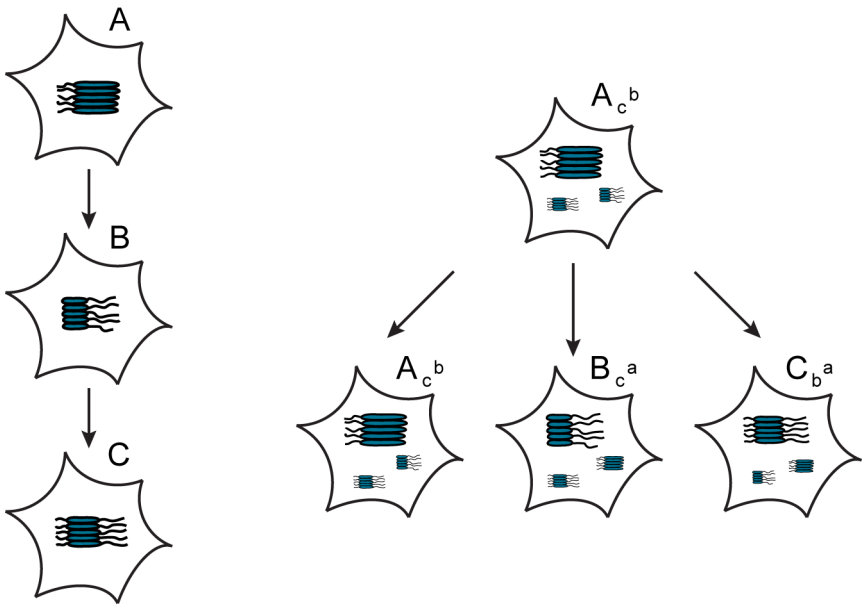

Figure 39. Mutational clone theory vs. cloud or ensemble of prion variants. Two possible theories explaining the appearance of different conformers over time. In the mutational clone theory (left panel), one prion variant undergoes mutational changes, whereby a new distinct prion variant is generated. In the "cloud" or "ensemble" model of prion variants (right panel), prion variants exist as a cloud of conformational species with one dominant conformation and multiple low-copy number conformations that might be favored by another host or environment.

However, under selective pressure in a different host or environment, another conformation might be favored and emerges. Although biochemical assays have shown that the mixture of *in vitro* fibrillized recombinant NM favors a conformation with the QNR as its amyloid core (Toyama et al. 2007, Luckgei et al. 2013), once introduced into the mammalian cell environment, conformational requirements appear to change and lead either to the interconversion into a fitter conformation or the selective amplification of a formerly low copy number conformer, most likely with the CTN as its nucleation site and core region. However, as previously discussed, NM mutant Δ 39-123, with only the QNR in addition to the N domain, also shows weak levels of aggregation, indicating that a second conformation and thus nucleation site (QNR) can be active if the predominant one is absent (Fig. 40). The adaptation of a different conformation in the absence of the predominant nucleation site (CTN) was also observed in the limited proteolysis experiment digesting NM Δ 75-123.

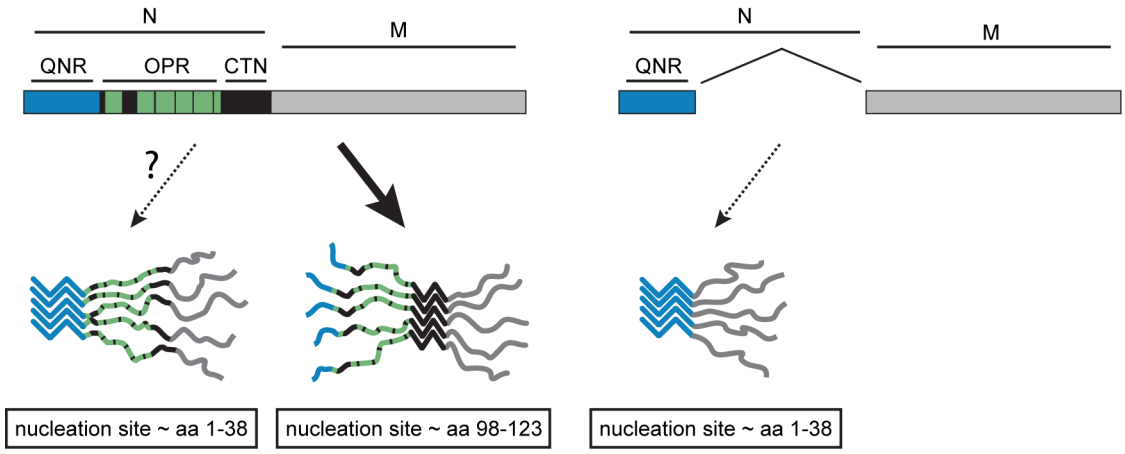

Figure 40. Putative model of NM prion nucleation and seeding. NM contains two putative nucleation sites. In the mammalian cytosol, the carboxyterminal nucleation site (CTN, aa 98-123) is favored and responsible for nucleation and template-assisted seeding (left panel). The aminoterminal nucleation site (QNR, aa 1-38) likely mediates assembly and seeding in the absence of the carboxyterminal site (right panel).

In contrast to full-length NM, no fragmentation pattern was detected for NM Δ 75-123, demonstrating that upon deletion of the last three repeats and the CTN, the amyloid conformation is altered and now also includes the QNR in its tightly packed core. Whether this second conformation with its alternative nucleation site can also be found for full-length NM in the mammalian environment, cannot be verified so far. However, the presence of two optional nucleation sites is already supported by two studies. Krishnan and Lindquist identified in 2005 two regions to form intermolecular contacts in mature NM fibrils (aa 25 - 38: head, aa 91 - 106: tail) (Krishnan and Lindquist 2005). In 2007, Tessier and colleagues identified regions spanning either residues 9-39 or 90-120 as self-nucleation elements using peptide arrays (Tessier and Lindquist 2007). Krishnan and Lindquist found that the intermolecular contacts were made in a head - head and tail - tail fashion and took this to be evidence for a β-helix amyloid fibril model, where each monomer runs along the fibril axis and forms contacts with the following monomer in an opposed orientation (Krishnan and Lindquist 2005). We, however, suggest that their finding is rather proof of the existence of two possible nucleation sites that separately arise under different environmental conditions. The interpretation of the results as evidence for a β-helix amyloid fibril model can also be called into question by the numerous studies showing proof for the in-register parallel β-sheet structure of NM fibrils (Shewmaker et al. 2006, Toyama et al. 2007, Shewmaker et al. 2009). Additionally, if two

nucleation sites were needed for a stable amyloid structure, deletion of one of the two should result in severe deficiencies in initial aggregate formation. However, the aggregation propensity of NM was not significantly altered by deletion of only the alternative, less favored nucleation site, as demonstrated in yeast (NM Δ 98-123) as well in our study in mammalian cells (NM Δ 1-39) (Osherovich et al. 2004, Shkundina et al. 2006). The suggestion that in yeast and in mammalian cells, two separate nucleation sites are predominantly active is also supported by an experiment conducted by our group in 2009 (Krammer et al. 2009). It was shown that induction of the prion phenotype in yeast with N2a NM-HA^{agg} cell extracts is possible but results in a delayed induction time. The delay in induction time could be explained by either the mutational clone or the cloud/ensemble model, but either way would likely have resulted from the need for conformational alterations due to selective pressure of a new environment.

4.6 PrionW accurately predicts the NM prion domain in mammalian cells

In recent years, tremendous progress has been made towards understanding what differentiates prion from non-prion proteins (Alberti et al. 2009, Toombs et al. 2010). The majority of this research has been based on Q/N rich prion proteins and their prionogenic behavior *in vitro* as well as in yeast. Whether, however, the same factors or parameters will drive prion formation in the mammalian cytosol has not yet been elucidated. Nevertheless, our group already showed that NM is capable of replicating in our mammalian cell model, demonstrating that the mammalian cytosol is capable of replicating Q/N rich prions. With the newly found knowledge on amyloidogenic and prionogenic behavior in yeast, algorithms have been trained to discover so far unknown prion and prion-like proteins. Though algorithms have been vastly improving, they are far from optimal yet. To discriminate between prion and non-prion proteins, two major theories have been put forward. In the first theory, amyloid formation is driven by many weak interactions that are located in a long disordered region. In the second theory, a short amyloidogenic, often hydrophobic amino acid region initially seeds amyloid formation. Algorithms like PLAAC (prion-like amino acid composition), PAPA (prion aggregation prediction algorithm) and PrionScan fall in the first group of prediction algorithms and define almost the entire N domain (PLAAC, PAPA), or in the case of PrionScan, residues 5-65, as a region with high prion propensity (Table 9).

Table 9: Disorder, β-aggregation, amyloid and prion prediction algorithms

Name ***(Prediction)***	**Description**	**Reference**	**Result for NM (aa)**
FoldIndex *(Disorder)*	Uses the algorithm by Uversky and colleagues to predict if a protein sequence is intrinsically disordered that is based on its average residue hydrophobicity and net charge.	Uversky et al. (2000) Prilusky et al. (2005) http://bip.weizmann.ac.il/fldbin/findex	1-250
Zyggregator *(β-aggregation)*	A sequence-based algorithm that predicts the aggregation propensity of proteins based on their hydrophobicity, charge and propensity to form β-sheet structures as well as environmental factors.	DuBay et al. (2004) Pawar et al. (2005) Tartaglia et al. (2008) http://www-mvsoftware.ch.cam.ac.uk/	Domains > 2 aa: 45-55, 102-107
Waltz *(Amyloids)*	Position-specific scoring matrix based on the structural and biophysical analysis of over 200 amyloid forming or non-forming hexapeptides, to identify sequences with a high propensity to nucleate amyloid formation.	Maurer-Stroh et al. (2010) http://waltz.switchlab.org/	9-18, 31-36, 45-56, 69-74, 102-108
pWaltz, PrionW *(Prions)*	Identification of PrDs that fulfill three requirements: (1) contain a protein stretch with significant prion propensity (pWaltz), (2) have a disordered structure (FoldIndex), (3) have an amino acid composition that allows the protein to retain its soluble state but still exhibit amyloid propensity scored by Sabate et al. (2015).	Sabate et al. (2015) Zambrano et al. (2015) http://bioinf.uab.cat/prionw/	98-118
Alberti et al., PLAAC *(Prions)*	Uses a hidden Markov model to identify prion-like sequences, at least 60 amino acids long, based on compositional similarities to four known yeast PrDs.	Alberti et al. (2009) Lancaster et al. (2014) http://plaac.wi.mit.edu/	~ 1-133
PAPA *(Prions)*	The algorithm determines the overall prion propensity of a protein by calculating the prion propensity of a sliding 41 amino acid window based on the prion propensity score of each amino acid and the negative FoldIndex of the region (score for disorder).	Toombs et al. (2010) Toombs et al. (2012) http://combi.cs.colostate.edu/supplements/papa/	~ 1-100

PrionScan *(Prions)*	The model uses the statistical significance of the prion propensity of amino acids obtained by analyzing 29 proteins experimentally tested as prions and 18 proteins that did not show prion characteristics defined by Alberti et al. (2009). The program runs a 60 residue window over the amino acid sequence identifying potential PrLDs with a statistically determined cutoff at 50.	Espinosa Angarica et al. (2013) Espinosa Angarica et al. (2014) http://webapps.bifi.es/prionscan	5-65

The PLAAC algorithm uses a hidden Markov model (HMM) to identify potential prions and analyzes their sequences for PrLDs and non-PrLDs (Lancaster et al. 2014). The analysis is based on findings by Alberti and colleagues who determined amino acid frequencies of PrDs of the four best-known prions of *S. cerevisiae* (including Sup35) (Alberti et al. 2009). PAPA, on the other hand, is based on an extensive *in vivo* study that quantitatively assigns prion propensity scores to each amino acid (Toombs et al. 2010, Toombs et al. 2012). The algorithm scans the protein sequence and determines prion propensity based on the overall score of the amino acids and regions of disorder (FoldIndex) (Prilusky et al. 2005). PrionScan uses a computational strategy to predict prion proteins that is also based on compositional similarities to yeast prions using the Alberti data set (Alberti et al. 2009, Espinosa Angarica et al. 2013, Espinosa Angarica et al. 2014). In contrast to other algorithms, PrionScan aims to present a database where all protein sequences in public databases are analyzed for putative PrLDs. To this end, the database is constantly updated based on the update of UniprotKB. Zyggregator, Waltz and its updated prion prediction algorithm pWaltz (prionW), on the other hand, fall into the second group and predict regions ≤ 21 residues (Table 9). Zyggregator is a sequenced-based algorithm that generates an aggregation profile of protein sequences based on the physicochemical properties of the amino acids including hydrophobicity, charge and propensity to fold into β-sheets (DuBay et al. 2004, Pawar et al. 2005, Tartaglia et al. 2008). PrionW is a web application that analyzes protein sequences for PrDs based on three parameters. First, the sequence is screened for large, disordered regions using FoldIndex (Prilusky et al. 2005). Secondly, disordered regions are analyzed for their Q/N content with the default threshold set to 25 %. In the last step, remaining

sequences are screened for PrDs using the pWaltz algorithm, an updated version of the previous Waltz algorithm to specifically detect prion rather than only amyloidogenic domains (Maurer-Stroh et al. 2010, Sabate et al. 2015, Zambrano et al. 2015). Comparing the outcomes of the algorithms with our experimental results, we found that prionW (aa 98-118) closely predicted our experimentally validated PrD in mammalian cells (aa 98-123) (Fig. 41).

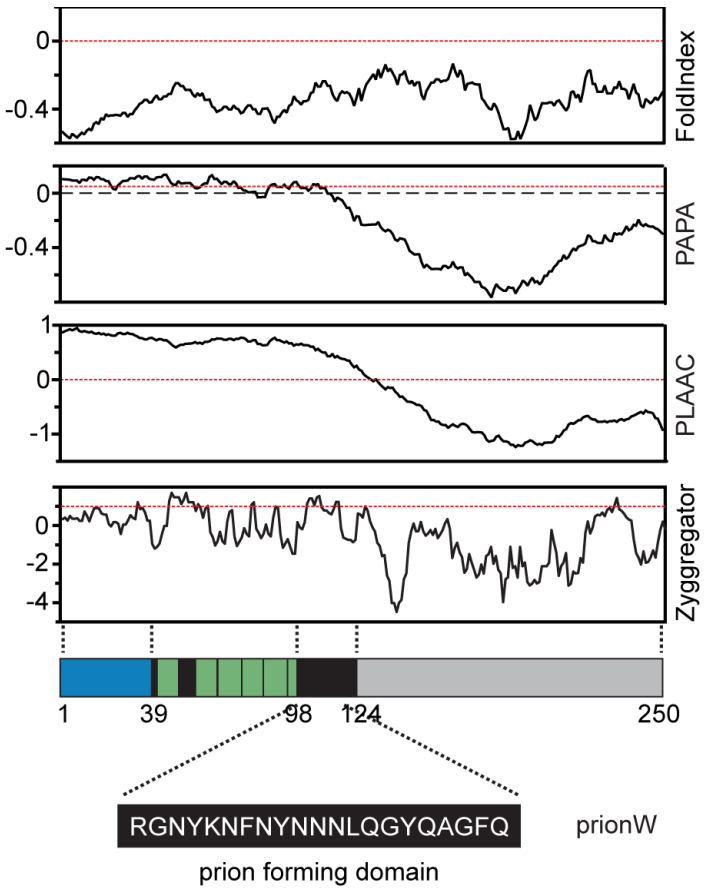

Figure 41. Results of a selection of prediction algorithms analyzing full-length NM. Predictions of disorder (FoldIndex), β-aggregation propensity (Zyggregator), prion propensity (PAPA, PLAAC) and PrD's (prionW). Images were designed using the PLAAC and Zyggregator web applications. Dotted red lines indicate individual thresholds of the algorithms: FoldIndex: < 0; PAPA; > 0.1; PLAAC: > 0, Zyggregator: > 1. The region identified as PrD by prionW is shown at the bottom.

This suggests that in the mammalian cell environment, the combination of a short region with a high prion propensity that is embedded in a larger disordered Q/N rich region is best suited to predict our PrD. Although prionW accurately predicts the PrD

active in NM in mammalian cells, it still has to be seen if it will successfully predict PrDs of to date unknown prion candidates. However, the emergence of a novel prion variant in mammalian cells, demonstrates that the dissection of structural elements that govern prion propensities has to be undertaken in the correct environment to further refine prediction algorithms and detect so far unknown prion or prion-like proteins that are active in mammalian cells.

4.7 The emergence of prion-like proteins

Tartaglia and coworkers have suggested that many proteins have coevolved with quality-control mechanisms in their cellular environment to retain their functional soluble state, but only few alterations can tip the scale towards becoming aggregation-prone (Tartaglia et al. 2007). This theory was later confirmed by Ross and colleagues, who demonstrated that only a few mutations can turn formally non-aggregating into aggregating proteins and in two incidents into proteins with prion activity (Paul et al. 2015). To date, an increasing number of proteins connected to neurodegenerative diseases has been proposed to have prion-like properties. Among these are proteins like TDP-43, FUS and TAF-15 that underlie diseases such as ALS and FTLD (King et al. 2012). TDP-43 is mainly found in the nucleus but also shuttles back and forth between nucleus and cytoplasm (Ayala et al. 2008). It functions in transcriptional regulation and splicing of RNA (Buratti and Baralle 2008, Buratti and Baralle 2010, King et al. 2012). TDP-43 contains a PrLD at its carboxyterminus and was shown to form cytoplasmic inclusions in FTLD and ALS (Brandmeir et al. 2008, Pamphlett et al. 2009). *In vitro*, full-length TDP-43 is intrinsically aggregation-prone, but aggregation can be prevented upon deletion of its PrLD that was shown to eliminate the protein's toxicity in several model systems (King et al. 2012). Several mutations linked to ALS were found within the PrLD of TDP-43 that increase its toxicity (Johnson et al. 2009). Similar to TDP-43, FUS is predominantly a nuclear protein that shuttles in and out of the nucleus and is responsible for transcriptional regulation and RNA homeostasis (Bertolotti et al. 1996, Zinszner et al. 1997, Kasyapa et al. 2005, King et al. 2012). FUS inclusions were found in the cytoplasm of ALS and FTLD patients (Kwiatkowski et al. 2009, Vance et al. 2009, Neumann et al. 2011). FUS contains a PrLD at its aminoterminus that is strongly aggregation-prone (Couthouis et al. 2011, Sun et al. 2011). Deletion of its PrLD prevents FUS from aggregating (Sun et al. 2011). TAF-15 is a nuclear protein

associated with the transcription factor II D complex and RNA polymerase II (Tan and Manley 2009). TAF-15 contains a PrLD at its aminoterminus, is aggregation-prone and found to be aggregated in the cytoplasm of ALS and FTLD patients (Couthouis et al. 2011, Neumann et al. 2011). All three proteins form cytoplasmic inclusions in neurodegenerative diseases, and were now shown to contain PrLDs. This demonstrates that to date prediction algorithms can already detect proteins that show prion-like properties in the mammalian cytosol. However, as previously discussed, algorithms are still far from optimal and many prion-like proteins remain undetected. Yet, the achievements so far show the possibilities that functional algorithms can offer and simultaneously demonstrate the need for continuous refinement of the prediction qualities to detect so far unknown prion and prion-like proteins.

4.8 Relevance

The field of prion research has been vastly developing with the discovery of yeast prions and it was through the investigation of yeast prions that the existence of PrDs was discovered. PrDs are modular regions within a protein sequence that govern the propensities required for successful prion replication. The discovery of PrDs that carry the crucial elements for prion behavior led to the development of numerous prion prediction algorithms aiming to identify so far unknown prion proteins in a genome wide search. Recently, as much as one percent of human protein-coding genes have been proposed to contain PrLDs. Among these, some have already been connected to neurodegenerative diseases like ALS and FTLD. However, up to this point, algorithms were designed based on the prionogenic behavior of proteins in either lower eukaryotes or *in vitro*. Yet, our results have shown that the environment plays a crucial role in determining the active prion variant and has to be taken into account in the continual optimization of prediction algorithms. Therefore, a profound knowledge of the compositional requirements that facilitate prion replication in mammalian cells is crucial to identify prion or prion-like proteins that may underlie diseases of so far unknown etiology in mammals.

Bibliography

Adessi, C. and C. Soto (2002) Converting a peptide into a drug: strategies to improve stability and bioavailability. *Curr Med Chem* 9(9): 963-978

Aguzzi, A. and M. Heikenwalder (2006) Pathogenesis of prion diseases: current status and future outlook. *Nature reviews. Microbiology* 4(10): 765-775

Aguzzi, A. and L. Rajendran (2009) The transcellular spread of cytosolic amyloids, prions, and prionoids. *Neuron* 64(6): 783-790

Aigle, M. and F. Lacroute (1975) Genetical aspects of [URE3], a non-mitochondrial, cytoplasmically inherited mutation in yeast. *Molecular & General Genetics MGG* 136(4): 327

Alberti, S., R. Halfmann, O. King, A. Kapila and S. Lindquist (2009) A systematic survey identifies prions and illuminates sequence features of prionogenic proteins. *Cell* 137(1): 146-158

Ayala, Y. M., P. Zago, A. D'Ambrogio, Y. F. Xu, L. Petrucelli, E. Buratti and F. E. Baralle (2008) Structural determinants of the cellular localization and shuttling of TDP-43. *J Cell Sci* 121(Pt 22): 3778-3785

Basler, K., B. Oesch, M. Scott, D. Westaway, M. Walchli, D. F. Groth, M. P. McKinley, S. B. Prusiner and C. Weissmann (1986) Scrapie and cellular PrP isoforms are encoded by the same chromosomal gene. *Cell* 46(3): 417-428

Baxa, U., V. Speransky, A. C. Steven and R. B. Wickner (2002) Mechanism of inactivation on prion conversion of the Saccharomyces cerevisiae Ure2 protein. *Proceedings of the National Academy of Sciences of the United States of America* 99(8): 5253-5260

Beringue, V., J. L. Vilotte and H. Laude (2008) Prion agent diversity and species barrier. *Veterinary research* 39(4): 47

Bertolotti, A., Y. Lutz, D. J. Heard, P. Chambon and L. Tora (1996) hTAF(II)68, a novel RNA/ssDNA-binding protein with homology to the pro-oncoproteins TLS/FUS and EWS is associated with both TFIID and RNA polymerase II. *The EMBO journal* 15(18): 5022-5031

Bessen, R. A. and R. F. Marsh (1992) Biochemical and physical properties of the prion protein from two strains of the transmissible mink encephalopathy agent. *Journal of virology* 66(4): 2096-2101

Biancalana, M. and S. Koide (2010) Molecular mechanism of Thioflavin-T binding to amyloid fibrils. *Biochimica et biophysica acta* 1804(7): 1405-1412

Brachmann, A., U. Baxa and R. B. Wickner (2005) Prion generation in vitro: amyloid of Ure2p is infectious. *The EMBO journal* 24(17): 3082-3092

Bradley, M. E. and S. W. Liebman (2004) The Sup35 domains required for maintenance of weak, strong or undifferentiated yeast [PSI+] prions. *Molecular microbiology* 51(6): 1649-1659

Brandmeir, N. J., F. Geser, L. K. Kwong, E. Zimmerman, J. Qian, V. M. Lee and J. Q. Trojanowski (2008) Severe subcortical TDP-43 pathology in sporadic frontotemporal lobar degeneration with motor neuron disease. *Acta Neuropathol* 115(1): 123-131

Bruce, M., A. Chree, I. McConnell, J. Foster, G. Pearson and H. Fraser (1994) Transmission of bovine spongiform encephalopathy and scrapie to mice: strain variation and the species barrier. *Philosophical transactions of the Royal Society of London. Series B, Biological sciences* 343(1306): 405-411

Bruce, M. E. (1993) Scrapie strain variation and mutation. *British medical bulletin* 49(4): 822-838

Buratti, E. and F. E. Baralle (2008) Multiple roles of TDP-43 in gene expression, splicing regulation, and human disease. *Front Biosci* 13: 867-878

Buratti, E. and F. E. Baralle (2010) The multiple roles of TDP-43 in pre-mRNA processing and gene expression regulation. *RNA Biol* 7(4): 420-429

Butler, D. A., M. R. Scott, J. M. Bockman, D. R. Borchelt, A. Taraboulos, K. K. Hsiao, D. T. Kingsbury and S. B. Prusiner (1988) Scrapie-infected murine neuroblastoma cells produce protease-resistant prion proteins. *Journal of virology* 62(5): 1558-1564

Cascarina, S. M. and E. D. Ross (2014) Yeast prions and human prion-like proteins: sequence features and prediction methods. *Cellular and molecular life sciences : CMLS* 71(11): 2047-2063

Castilla, J., P. Saa, C. Hetz and C. Soto (2005) In vitro generation of infectious scrapie prions. *Cell* 121(2): 195-206

Caughey, B., D. A. Kocisko, G. J. Raymond and P. T. Lansbury, Jr. (1995) Aggregates of scrapie-associated prion protein induce the cell-free conversion of protease-sensitive prion protein to the protease-resistant state. *Chemistry & biology* 2(12): 807-817

Chang, H. Y., J. Y. Lin, H. C. Lee, H. L. Wang and C. Y. King (2008) Strain-specific sequences required for yeast [PSI+] prion propagation. *Proceedings of the National Academy of Sciences of the United States of America* 105(36): 13345-13350

Chernoff, Y. O., S. L. Lindquist, B. Ono, S. G. Inge-Vechtomov and S. W. Liebman (1995) Role of the chaperone protein Hsp104 in propagation of the yeast prion-like factor [psi+]. *Science* 268(5212): 880-884

Chien, P. and J. S. Weissman (2001) Conformational diversity in a yeast prion dictates its seeding specificity. *Nature* 410(6825): 223-227

Chiti, F. and C. M. Dobson (2006) Protein misfolding, functional amyloid, and human disease. *Annual review of biochemistry* 75: 333-366

Collinge, J. and A. R. Clarke (2007) A general model of prion strains and their pathogenicity. *Science* 318(5852): 930-936

Come, J. H., P. E. Fraser and P. T. Lansbury, Jr. (1993) A kinetic model for amyloid formation in the prion diseases: importance of seeding. *Proceedings of the National Academy of Sciences of the United States of America* 90(13): 5959-5963

Coustou, V., C. Deleu, S. Saupe and J. Begueret (1997) The protein product of the het-s heterokaryon incompatibility gene of the fungus Podospora anserina behaves as a prion analog. *Proceedings of the National Academy of Sciences of the United States of America* 94(18): 9773-9778

Couthouis, J., M. P. Hart, J. Shorter, M. DeJesus-Hernandez, R. Erion, R. Oristano, A. X. Liu, D. Ramos, N. Jethava, D. Hosangadi, J. Epstein, A. Chiang, Z. Diaz, T. Nakaya, F. Ibrahim, H. J. Kim, J. A. Solski, K. L. Williams, J. Mojsilovic-Petrovic, C. Ingre, K. Boylan, N. R. Graff-Radford, D. W. Dickson, D. Clay-Falcone, L. Elman, L. McCluskey, R. Greene, R. G. Kalb, V. M. Lee, J. Q. Trojanowski, A. Ludolph, W. Robberecht, P. M. Andersen, G. A. Nicholson, I. P. Blair, O. D. King, N. M. Bonini, V. Van Deerlin, R. Rademakers, Z. Mourelatos and A. D. Gitler (2011) A yeast functional screen predicts new candidate ALS disease genes. *Proceedings of the National Academy of Sciences of the United States of America* 108(52): 20881-20890

Cox, B. S. (1965) [Psi], A cytoplasmic suppressor of super-suppressor in yeast. *Heredity* 20(4): 505-521

Cushman, M., B. S. Johnson, O. D. King, A. D. Gitler and J. Shorter (2010) Prion-like disorders: blurring the divide between transmissibility and infectivity. *J Cell Sci* 123(Pt 8): 1191-1201

DePace, A. H., A. Santoso, P. Hillner and J. S. Weissman (1998) A critical role for amino-terminal glutamine/asparagine repeats in the formation and propagation of a yeast prion. *Cell* 93(7): 1241-1252

Derkatch, I. L., M. E. Bradley, P. Zhou and S. W. Liebman (1999) The PNM2 mutation in the prion protein domain of SUP35 has distinct effects on different variants of the [PSI+] prion in yeast. *Current genetics* 35(2): 59-67

Derkatch, I. L., Y. O. Chernoff, V. V. Kushnirov, S. G. Inge-Vechtomov and S. W. Liebman (1996) Genesis and variability of [PSI] prion factors in Saccharomyces cerevisiae. *Genetics* 144(4): 1375-1386

DiSalvo, S., A. Derdowski, J. A. Pezza and T. R. Serio (2011) Dominant prion mutants induce curing through pathways that promote chaperone-mediated disaggregation. *Nature structural & molecular biology* 18(4): 486-492

Doel, S. M., S. J. McCready, C. R. Nierras and B. S. Cox (1994) The dominant PNM2- mutation which eliminates the psi factor of Saccharomyces cerevisiae is the result of a missense mutation in the SUP35 gene. *Genetics* 137(3): 659-670

Du, Z. (2011) The complexity and implications of yeast prion domains. *Prion* 5(4): 311-316

Du, Z., K. W. Park, H. Yu, Q. Fan and L. Li (2008) Newly identified prion linked to the chromatin-remodeling factor Swi1 in Saccharomyces cerevisiae. *Nature genetics* 40(4): 460-465

DuBay, K. F., A. P. Pawar, F. Chiti, J. Zurdo, C. M. Dobson and M. Vendruscolo (2004) Prediction of the absolute aggregation rates of amyloidogenic polypeptide chains. *Journal of molecular biology* 341(5): 1317-1326

Espinosa Angarica, V., A. Angulo, A. Giner, G. Losilla, S. Ventura and J. Sancho (2014) PrionScan: an online database of predicted prion domains in complete proteomes. *BMC genomics* 15: 102

Espinosa Angarica, V., S. Ventura and J. Sancho (2013) Discovering putative prion sequences in complete proteomes using probabilistic representations of Q/N-rich domains. *BMC genomics* 14: 316

Follenzi, A. and L. Naldini (2002) HIV-based vectors. Preparation and use. *Methods in molecular medicine* 69: 259-274

Fraser, H. and A. G. Dickinson (1968) The sequential development of the brain lesion of scrapie in three strains of mice. *Journal of comparative pathology* 78(3): 301-311

Gasset, M., M. A. Baldwin, D. H. Lloyd, J. M. Gabriel, D. M. Holtzman, F. Cohen, R. Fletterick and S. B. Prusiner (1992) Predicted alpha-helical regions of the prion protein when synthesized as peptides form amyloid. *Proceedings of the National Academy of Sciences of the United States of America* 89(22): 10940-10944

Gibbings, D., P. Leblanc, F. Jay, D. Pontier, F. Michel, Y. Schwab, S. Alais, T. Lagrange and O. Voinnet (2012) Human prion protein binds Argonaute and promotes accumulation of microRNA effector complexes. *Nature structural & molecular biology* 19(5): 517-524, S511

Gilks, N., N. Kedersha, M. Ayodele, L. Shen, G. Stoecklin, L. M. Dember and P. Anderson (2004) Stress granule assembly is mediated by prion-like aggregation of TIA-1. *Molecular biology of the cell* 15(12): 5383-5398

Glover, J. R., A. S. Kowal, E. C. Schirmer, M. M. Patino, J. J. Liu and S. Lindquist (1997) Self-seeded fibers formed by Sup35, the protein determinant of [PSI+], a heritable prion-like factor of S. cerevisiae. *Cell* 89(5): 811-819

Gorkovskiy, A., K. R. Thurber, R. Tycko and R. B. Wickner (2014) Locating folds of the in-register parallel beta-sheet of the Sup35p prion domain infectious amyloid. *Proceedings of the National Academy of Sciences of the United States of America* 111(43): E4615-4622

Graham, F. L., J. Smiley, W. C. Russell and R. Nairn (1977) Characteristics of a human cell line transformed by DNA from human adenovirus type 5. *The Journal of general virology* 36(1): 59-74

Griffith, J. S. (1967) Self-replication and scrapie. *Nature* 215(5105): 1043-1044

Hofmann, J. P., P. Denner, C. Nussbaum-Krammer, P. H. Kuhn, M. H. Suhre, T. Scheibel, S. F. Lichtenthaler, H. M. Schatzl, D. Bano and I. M. Vorberg (2013) Cell-to-cell propagation of infectious cytosolic protein aggregates. *Proceedings of the National Academy of Sciences of the United States of America* 110(15): 5951-5956

Johnson, B. S., D. Snead, J. J. Lee, J. M. McCaffery, J. Shorter and A. D. Gitler (2009) TDP-43 is intrinsically aggregation-prone, and amyotrophic lateral sclerosis-linked mutations accelerate aggregation and increase toxicity. *The Journal of biological chemistry* 284(30): 20329-20339

Kasyapa, C. S., P. Kunapuli and J. K. Cowell (2005) Mass spectroscopy identifies the splicing-associated proteins, PSF, hnRNP H3, hnRNP A2/B1, and TLS/FUS as

interacting partners of the ZNF198 protein associated with rearrangement in myeloproliferative disease. *Exp Cell Res* 309(1): 78-85

King, C. Y. (2001) Supporting the structural basis of prion strains: induction and identification of [PSI] variants. *Journal of molecular biology* 307(5): 1247-1260

King, C. Y. and R. Diaz-Avalos (2004) Protein-only transmission of three yeast prion strains. *Nature* 428(6980): 319-323

King, C. Y., P. Tittmann, H. Gross, R. Gebert, M. Aebi and K. Wuthrich (1997) Prion-inducing domain 2-114 of yeast Sup35 protein transforms in vitro into amyloid-like filaments. *Proceedings of the National Academy of Sciences of the United States of America* 94(13): 6618-6622

King, O. D., A. D. Gitler and J. Shorter (2012) The tip of the iceberg: RNA-binding proteins with prion-like domains in neurodegenerative disease. *Brain research* 1462: 61-80

Kluve-Beckerman, B., J. J. Liepnieks, L. Wang and M. D. Benson (1999) A cell culture system for the study of amyloid pathogenesis. Amyloid formation by peritoneal macrophages cultured with recombinant serum amyloid A. *Am J Pathol* 155(1): 123-133

Knowles, T. P., C. A. Waudby, G. L. Devlin, S. I. Cohen, A. Aguzzi, M. Vendruscolo, E. M. Terentjev, M. E. Welland and C. M. Dobson (2009) An analytical solution to the kinetics of breakable filament assembly. *Science* 326(5959): 1533-1537

Kochneva-Pervukhova, N. V., M. B. Chechenova, I. A. Valouev, V. V. Kushnirov, V. N. Smirnov and M. D. Ter-Avanesyan (2001) [Psi(+)] prion generation in yeast: characterization of the 'strain' difference. *Yeast* 18(6): 489-497

Kochneva-Pervukhova, N. V., S. V. Paushkin, V. V. Kushnirov, B. S. Cox, M. F. Tuite and M. D. Ter-Avanesyan (1998) Mechanism of inhibition of Psi+ prion determinant propagation by a mutation of the N-terminus of the yeast Sup35 protein. *The EMBO journal* 17(19): 5805-5810

Krammer, C., D. Kryndushkin, M. H. Suhre, E. Kremmer, A. Hofmann, A. Pfeifer, T. Scheibel, R. B. Wickner, H. M. Schatzl and I. Vorberg (2009) The yeast Sup35NM domain propagates as a prion in mammalian cells. *Proceedings of the National Academy of Sciences of the United States of America* 106(2): 462-467

Krauss, S. and I. Vorberg (2013) Prions Ex Vivo: What Cell Culture Models Tell Us about Infectious Proteins. *International journal of cell biology* 2013: 704546

Krishnan, R. and S. L. Lindquist (2005) Structural insights into a yeast prion illuminate nucleation and strain diversity. *Nature* 435(7043): 765-772

Kryndushkin, D. S., I. M. Alexandrov, M. D. Ter-Avanesyan and V. V. Kushnirov (2003) Yeast [PSI+] prion aggregates are formed by small Sup35 polymers fragmented by Hsp104. *The Journal of biological chemistry* 278(49): 49636-49643

Kwiatkowski, T. J., Jr., D. A. Bosco, A. L. Leclerc, E. Tamrazian, C. R. Vanderburg, C. Russ, A. Davis, J. Gilchrist, E. J. Kasarskis, T. Munsat, P. Valdmanis, G. A. Rouleau, B. A. Hosler, P. Cortelli, P. J. de Jong, Y. Yoshinaga, J. L. Haines, M. A. Pericak-Vance, J. Yan, N. Ticozzi, T. Siddique, D. McKenna-Yasek, P. C. Sapp, H. R. Horvitz, J. E. Landers and R. H. Brown, Jr. (2009) Mutations in the FUS/TLS gene on chromosome 16 cause familial amyotrophic lateral sclerosis. *Science* 323(5918): 1205-1208

Lancaster, A. K., J. P. Bardill, H. L. True and J. Masel (2010) The spontaneous appearance rate of the yeast prion [PSI+] and its implications for the evolution of the evolvability properties of the [PSI+] system. *Genetics* 184(2): 393-400

Lancaster, A. K., A. Nutter-Upham, S. Lindquist and O. D. King (2014) PLAAC: a web and command-line application to identify proteins with prion-like amino acid composition. *Bioinformatics* 30(17): 2501-2502

Li, J., S. Browning, S. P. Mahal, A. M. Oelschlegel and C. Weissmann (2010) Darwinian evolution of prions in cell culture. *Science* 327(5967): 869-872

Li, L. and S. Lindquist (2000) Creating a protein-based element of inheritance. *Science* 287(5453): 661-664

Li, S. C., N. K. Goto, K. A. Williams and C. M. Deber (1996) Alpha-helical, but not beta-sheet, propensity of proline is determined by peptide environment. *Proceedings of the National Academy of Sciences of the United States of America* 93(13): 6676-6681

Linden, R., Y. Cordeiro and L. M. Lima (2012) Allosteric function and dysfunction of the prion protein. *Cellular and molecular life sciences : CMLS* 69(7): 1105-1124

Liu, J. J., N. Sondheimer and S. L. Lindquist (2002) Changes in the middle region of Sup35 profoundly alter the nature of epigenetic inheritance for the yeast prion [PSI+]. *Proceedings of the National Academy of Sciences of the United States of America* 99 Suppl 4: 16446-16453

Lopez de la Paz, M. and L. Serrano (2004) Sequence determinants of amyloid fibril formation. *Proceedings of the National Academy of Sciences of the United States of America* 101(1): 87-92

Luckgei, N., A. K. Schutz, L. Bousset, B. Habenstein, Y. Sourigues, C. Gardiennet, B. H. Meier, R. Melki and A. Bockmann (2013) The conformation of the prion domain of Sup35p in isolation and in the full-length protein. *Angew Chem Int Ed Engl* 52(48): 12741-12744

MacLea, K. S. and E. D. Ross (2011) Strategies for identifying new prions in yeast. *Prion* 5(4): 263-268

Maurer-Stroh, S., M. Debulpaep, N. Kuemmerer, M. Lopez de la Paz, I. C. Martins, J. Reumers, K. L. Morris, A. Copland, L. Serpell, L. Serrano, J. W. Schymkowitz and F. Rousseau (2010) Exploring the sequence determinants of amyloid structure using position-specific scoring matrices. *Nature methods* 7(3): 237-242

McGlinchey, R. P., D. Kryndushkin and R. B. Wickner (2011) Suicidal [PSI+] is a lethal yeast prion. *Proceedings of the National Academy of Sciences of the United States of America* 108(13): 5337-5341

Michelitsch, M. D. and J. S. Weissman (2000) A census of glutamine/asparagine-rich regions: implications for their conserved function and the prediction of novel prions. *Proceedings of the National Academy of Sciences of the United States of America* 97(22): 11910-11915

Neumann, M., E. Bentmann, D. Dormann, A. Jawaid, M. DeJesus-Hernandez, O. Ansorge, S. Roeber, H. A. Kretzschmar, D. G. Munoz, H. Kusaka, O. Yokota, L. C. Ang, J. Bilbao, R. Rademakers, C. Haass and I. R. Mackenzie (2011) FET proteins TAF15 and EWS are selective markers that distinguish FTLD with FUS pathology from amyotrophic lateral sclerosis with FUS mutations. *Brain* 134(Pt 9): 2595-2609

Newby, G. A. and S. Lindquist (2013) Blessings in disguise: biological benefits of prion-like mechanisms. *Trends in cell biology* 23(6): 251-259

Nonaka, T., S. T. Watanabe, T. Iwatsubo and M. Hasegawa (2010) Seeded aggregation and toxicity of {alpha}-synuclein and tau: cellular models of neurodegenerative diseases. *The Journal of biological chemistry* 285(45): 34885-34898

Oesch, B., D. Westaway, M. Walchli, M. P. McKinley, S. B. Kent, R. Aebersold, R. A. Barry, P. Tempst, D. B. Teplow, L. E. Hood and et al. (1985) A cellular gene encodes scrapie PrP 27-30 protein. *Cell* 40(4): 735-746

Orgel, L. E. (1996) Prion replication and secondary nucleation. *Chemistry & biology* 3(6): 413-414

Osherovich, L. Z., B. S. Cox, M. F. Tuite and J. S. Weissman (2004) Dissection and design of yeast prions. *PLoS biology* 2(4): E86

Pamphlett, R., N. Luquin, C. McLean, S. K. Jew and L. Adams (2009) TDP-43 neuropathology is similar in sporadic amyotrophic lateral sclerosis with or without TDP-43 mutations. *Neuropathol Appl Neurobiol* 35(2): 222-225

Parham, S. N., C. G. Resende and M. F. Tuite (2001) Oligopeptide repeats in the yeast protein Sup35p stabilize intermolecular prion interactions. *The EMBO journal* 20(9): 2111-2119

Patel, A., H. O. Lee, L. Jawerth, S. Maharana, M. Jahnel, M. Y. Hein, S. Stoynov, J. Mahamid, S. Saha, T. M. Franzmann, A. Pozniakovski, I. Poser, N. Maghelli, L. A. Royer, M. Weigert, E. W. Myers, S. Grill, D. Drechsel, A. A. Hyman and S. Alberti (2015) A Liquid-to-Solid Phase Transition of the ALS Protein FUS Accelerated by Disease Mutation. *Cell* 162(5): 1066-1077

Patel, B. K., J. Gavin-Smyth and S. W. Liebman (2009) The yeast global transcriptional co-repressor protein Cyc8 can propagate as a prion. *Nature cell biology* 11(3): 344-349

Pattison, I. H. and G. C. Millson (1961) Scrapie produced experimentally in goats with special reference to the clinical syndrome. *Journal of comparative pathology* 71: 101-109

Paul, K. R., C. G. Hendrich, A. Waechter, M. R. Harman and E. D. Ross (2015) Generating new prions by targeted mutation or segment duplication. *Proceedings of the National Academy of Sciences of the United States of America* 112(28): 8584-8589

Paushkin, S. V., V. V. Kushnirov, V. N. Smirnov and M. D. Ter-Avanesyan (1997) In vitro propagation of the prion-like state of yeast Sup35 protein. *Science* 277(5324): 381-383

Paushkin, S. V., V. V. Kushnirov, V. N. Smirnov and M. D. Ter-Avanesyan (1996) Propagation of the yeast prion-like [psi+] determinant is mediated by oligomerization of the SUP35-encoded polypeptide chain release factor. *The EMBO journal* 15(12): 3127-3134

Pawar, A. P., K. F. Dubay, J. Zurdo, F. Chiti, M. Vendruscolo and C. M. Dobson (2005) Prediction of "aggregation-prone" and "aggregation-susceptible" regions in

proteins associated with neurodegenerative diseases. *Journal of molecular biology* 350(2): 379-392

Perutz, M. F., B. J. Pope, D. Owen, E. E. Wanker and E. Scherzinger (2002) Aggregation of proteins with expanded glutamine and alanine repeats of the glutamine-rich and asparagine-rich domains of Sup35 and of the amyloid beta-peptide of amyloid plaques. *Proceedings of the National Academy of Sciences of the United States of America* 99(8): 5596-5600

Peters, T. W. and M. Huang (2007) Protein aggregation and polyasparagine-mediated cellular toxicity in Saccharomyces cerevisiae. *Prion* 1(2): 144-153

Prilusky, J., C. E. Felder, T. Zeev-Ben-Mordehai, E. H. Rydberg, O. Man, J. S. Beckmann, I. Silman and J. L. Sussman (2005) FoldIndex: a simple tool to predict whether a given protein sequence is intrinsically unfolded. *Bioinformatics* 21(16): 3435-3438

Priola, S. A., J. Chabry and K. Chan (2001) Efficient conversion of normal prion protein (PrP) by abnormal hamster PrP is determined by homology at amino acid residue 155. *Journal of virology* 75(10): 4673-4680

Prusiner, S. B. (1982) Novel proteinaceous infectious particles cause scrapie. *Science* 216(4542): 136-144

Prusiner, S. B. (1998) Prions. *Proceedings of the National Academy of Sciences of the United States of America* 95(23): 13363-13383

Prusiner, S. B., D. F. Groth, D. C. Bolton, S. B. Kent and L. E. Hood (1984) Purification and structural studies of a major scrapie prion protein. *Cell* 38(1): 127-134

Rogoza, T., A. Goginashvili, S. Rodionova, M. Ivanov, O. Viktorovskaya, A. Rubel, K. Volkov and L. Mironova (2010) Non-Mendelian determinant [ISP+] in yeast is a nuclear-residing prion form of the global transcriptional regulator Sfp1. *Proceedings of the National Academy of Sciences of the United States of America* 107(23): 10573-10577

Ross, E. D., H. K. Edskes, M. J. Terry and R. B. Wickner (2005) Primary sequence independence for prion formation. *Proceedings of the National Academy of Sciences of the United States of America* 102(36): 12825-12830

Ross, E. D., A. Minton and R. B. Wickner (2005) Prion domains: sequences, structures and interactions. *Nature cell biology* 7(11): 1039-1044

Sabate, R., F. Rousseau, J. Schymkowitz and S. Ventura (2015) What makes a protein sequence a prion? *PLoS computational biology* 11(1): e1004013

Saborio, G. P., B. Permanne and C. Soto (2001) Sensitive detection of pathological prion protein by cyclic amplification of protein misfolding. *Nature* 411(6839): 810-813

Schatzl, H. M., M. Da Costa, L. Taylor, F. E. Cohen and S. B. Prusiner (1995) Prion protein gene variation among primates. *Journal of molecular biology* 245(4): 362-374

Schlumpberger, M., S. B. Prusiner and I. Herskowitz (2001) Induction of distinct [URE3] yeast prion strains. *Molecular and cellular biology* 21(20): 7035-7046

Scott, M., D. Groth, D. Foster, M. Torchia, S. L. Yang, S. J. DeArmond and S. B. Prusiner (1993) Propagation of prions with artificial properties in transgenic mice expressing chimeric PrP genes. *Cell* 73(5): 979-988

Serio, T. R., A. G. Cashikar, A. S. Kowal, G. J. Sawicki, J. J. Moslehi, L. Serpell, M. F. Arnsdorf and S. L. Lindquist (2000) Nucleated conformational conversion and the replication of conformational information by a prion determinant. *Science* 289(5483): 1317-1321

Serpell, L. C. (2000) Alzheimer's amyloid fibrils: structure and assembly. *Biochimica et biophysica acta* 1502(1): 16-30

Serpell, L. C., M. Sunde, M. D. Benson, G. A. Tennent, M. B. Pepys and P. E. Fraser (2000) The protofilament substructure of amyloid fibrils. *Journal of molecular biology* 300(5): 1033-1039

Shewmaker, F., D. Kryndushkin, B. Chen, R. Tycko and R. B. Wickner (2009) Two prion variants of Sup35p have in-register parallel beta-sheet structures, independent of hydration. *Biochemistry* 48(23): 5074-5082

Shewmaker, F., E. D. Ross, R. Tycko and R. B. Wickner (2008) Amyloids of shuffled prion domains that form prions have a parallel in-register beta-sheet structure. *Biochemistry* 47(13): 4000-4007

Shewmaker, F., R. B. Wickner and R. Tycko (2006) Amyloid of the prion domain of Sup35p has an in-register parallel beta-sheet structure. *Proceedings of the National Academy of Sciences of the United States of America* 103(52): 19754-19759

Shkundina, I. S., V. V. Kushnirov, M. F. Tuite and M. D. Ter-Avanesyan (2006) The role of the N-terminal oligopeptide repeats of the yeast Sup35 prion protein in propagation and transmission of prion variants. *Genetics* 172(2): 827-835

Shorter, J. and S. Lindquist (2005) Prions as adaptive conduits of memory and inheritance. *Nat Rev Genet* 6(6): 435-450

Si, K., Y. B. Choi, E. White-Grindley, A. Majumdar and E. R. Kandel (2010) Aplysia CPEB can form prion-like multimers in sensory neurons that contribute to long-term facilitation. *Cell* 140(3): 421-435

Si, K., S. Lindquist and E. R. Kandel (2003) A neuronal isoform of the aplysia CPEB has prion-like properties. *Cell* 115(7): 879-891

Silveira, J. R., G. J. Raymond, A. G. Hughson, R. E. Race, V. L. Sim, S. F. Hayes and B. Caughey (2005) The most infectious prion protein particles. *Nature* 437(7056): 257-261

Sipe, J. D. (1994) Amyloidosis. *Crit Rev Clin Lab Sci* 31(4): 325-354

Sondheimer, N. and S. Lindquist (2000) Rnq1: an epigenetic modifier of protein function in yeast. *Molecular cell* 5(1): 163-172

Soto, C. (2012) Transmissible proteins: expanding the prion heresy. *Cell* 149(5): 968-977

Sparrer, H. E., A. Santoso, F. C. Szoka, Jr. and J. S. Weissman (2000) Evidence for the prion hypothesis: induction of the yeast [PSI+] factor by in vitro- converted Sup35 protein. *Science* 289(5479): 595-599

Stefani, M. and C. M. Dobson (2003) Protein aggregation and aggregate toxicity: new insights into protein folding, misfolding diseases and biological evolution. *Journal of molecular medicine* 81(11): 678-699

Sun, Z., Z. Diaz, X. Fang, M. P. Hart, A. Chesi, J. Shorter and A. D. Gitler (2011) Molecular determinants and genetic modifiers of aggregation and toxicity for the ALS disease protein FUS/TLS. *PLoS biology* 9(4): e1000614

Suzuki, G., N. Shimazu and M. Tanaka (2012) A yeast prion, Mod5, promotes acquired drug resistance and cell survival under environmental stress. *Science* 336(6079): 355-359

Sweeting, B., M. Q. Khan, A. Chakrabartty and E. F. Pai (2010) Structural factors underlying the species barrier and susceptibility to infection in prion disease. *Biochemistry and cell biology = Biochimie et biologie cellulaire* 88(2): 195-202

Tan, A. Y. and J. L. Manley (2009) The TET family of proteins: functions and roles in disease. *J Mol Cell Biol* 1(2): 82-92

Tanaka, M., P. Chien, N. Naber, R. Cooke and J. S. Weissman (2004) Conformational variations in an infectious protein determine prion strain differences. *Nature* 428(6980): 323-328

Tartaglia, G. G., A. P. Pawar, S. Campioni, C. M. Dobson, F. Chiti and M. Vendruscolo (2008) Prediction of aggregation-prone regions in structured proteins. *Journal of molecular biology* 380(2): 425-436

Tartaglia, G. G., S. Pechmann, C. M. Dobson and M. Vendruscolo (2007) Life on the edge: a link between gene expression levels and aggregation rates of human proteins. *Trends Biochem Sci* 32(5): 204-206

Telling, G. C., P. Parchi, S. J. DeArmond, P. Cortelli, P. Montagna, R. Gabizon, J. Mastrianni, E. Lugaresi, P. Gambetti and S. B. Prusiner (1996) Evidence for the conformation of the pathologic isoform of the prion protein enciphering and propagating prion diversity. *Science* 274(5295): 2079-2082

Ter-Avanesyan, M. D., A. R. Dagkesamanskaya, V. V. Kushnirov and V. N. Smirnov (1994) The SUP35 omnipotent suppressor gene is involved in the maintenance of the non-Mendelian determinant [psi+] in the yeast Saccharomyces cerevisiae. *Genetics* 137(3): 671-676

Ter-Avanesyan, M. D., V. V. Kushnirov, A. R. Dagkesamanskaya, S. A. Didichenko, Y. O. Chernoff, S. G. Inge-Vechtomov and V. N. Smirnov (1993) Deletion analysis of the SUP35 gene of the yeast Saccharomyces cerevisiae reveals two non-overlapping functional regions in the encoded protein. *Molecular microbiology* 7(5): 683-692

Tessier, P. M. and S. Lindquist (2007) Prion recognition elements govern nucleation, strain specificity and species barriers. *Nature* 447(7144): 556-561

Toombs, J. A., B. R. McCarty and E. D. Ross (2010) Compositional determinants of prion formation in yeast. *Molecular and cellular biology* 30(1): 319-332

Toombs, J. A., M. Petri, K. R. Paul, G. Y. Kan, A. Ben-Hur and E. D. Ross (2012) De novo design of synthetic prion domains. *Proceedings of the National Academy of Sciences of the United States of America* 109(17): 6519-6524

Toyama, B. H., M. J. Kelly, J. D. Gross and J. S. Weissman (2007) The structural basis of yeast prion strain variants. *Nature* 449(7159): 233-237

Tuite, M. F. and B. S. Cox (2003) Propagation of yeast prions. *Nature reviews. Molecular cell biology* 4(11): 878-890

Uptain, S. M. and S. Lindquist (2002) Prions as protein-based genetic elements. *Annual review of microbiology* 56: 703-741

Uptain, S. M., G. J. Sawicki, B. Caughey and S. Lindquist (2001) Strains of [PSI(+)] are distinguished by their efficiencies of prion-mediated conformational conversion. *The EMBO journal* 20(22): 6236-6245

Uversky, V. N., J. R. Gillespie and A. L. Fink (2000) Why are "natively unfolded" proteins unstructured under physiologic conditions? *Proteins* 41(3): 415-427

Vance, C., B. Rogelj, T. Hortobagyi, K. J. De Vos, A. L. Nishimura, J. Sreedharan, X. Hu, B. Smith, D. Ruddy, P. Wright, J. Ganesalingam, K. L. Williams, V. Tripathi, S. Al-Saraj, A. Al-Chalabi, P. N. Leigh, I. P. Blair, G. Nicholson, J. de Belleroche, J. M. Gallo, C. C. Miller and C. E. Shaw (2009) Mutations in FUS, an RNA processing protein, cause familial amyotrophic lateral sclerosis type 6. *Science* 323(5918): 1208-1211

Verges, K. J., M. H. Smith, B. H. Toyama and J. S. Weissman (2011) Strain conformation, primary structure and the propagation of the yeast prion [PSI+]. *Nature structural & molecular biology* 18(4): 493-499

Walker, L. C. and M. Jucker (2015) Neurodegenerative diseases: expanding the prion concept. *Annual review of neuroscience* 38: 87-103

Wickner, R. B. (1994) [URE3] as an altered URE2 protein: evidence for a prion analog in Saccharomyces cerevisiae. *Science* 264(5158): 566-569

Wickner, R. B., F. P. Shewmaker, D. A. Bateman, H. K. Edskes, A. Gorkovskiy, Y. Dayani and E. E. Bezsonov (2015) Yeast prions: structure, biology, and prion-handling systems. *Microbiology and molecular biology reviews : MMBR* 79(1): 1-17

Zambrano, R., O. Conchillo-Sole, V. Iglesias, R. Illa, F. Rousseau, J. Schymkowitz, R. Sabate, X. Daura and S. Ventura (2015) PrionW: a server to identify proteins containing glutamine/asparagine rich prion-like domains and their amyloid cores. *Nucleic acids research* 43(W1): W331-337

Zinszner, H., J. Sok, D. Immanuel, Y. Yin and D. Ron (1997) TLS (FUS) binds RNA in vivo and engages in nucleo-cytoplasmic shuttling. *J Cell Sci* 110 (Pt 15): 1741-1750

Abbreviations

%	Percent
°C	Degree Celsius
Δ	Deletion
aa	Amino acid
AD	Alzheimer’s disease
ALS	Amyotrophic lateral sclerosis
ATCC	American type culture selection
BSA	Bovine serum albumin
BSE	Bovine spongiform encephalopathy
CHY	Chymotrypsin
CJD	Creutzfeldt-Jakob disease
CNS	Central nervous system
conj.	Conjugated
CPEB	Cytoplasmic polyadenylation element binding protein
CTN	Carboxyterminal N domain
ctrl	Control
CWD	Chronic wasting disease
DMEM	Dulbecco's modified eagle's medium
DMSO	Dimethyl sulfoxide
DNA	Deoxyribonucleic acid
E.coli	*Escherichia coli*
ECL	Enhanced chemiluminescence
EDTA	Ethylenediaminetetraacetic acid
ER	Endoplasmic reticulum
et al.	And others (" et alia")
FCS	Fetal calf serum
FFI	Fatal familial insomnia
Fig.	Figure
FTLD	Frontotemporal lobar degeneration
g	Gram
GFP	Green fluorescent protein
Glc	Glycosylated

GPI	Glycosylphosphatidylinositol
GSS	Gerstmann-Sträussler-Scheinker syndrome
h	Hour
H_2O_{bidest}	Bidistilled water
HA	Hemagglutinin
HBSS	Hank's balanced salt solution
HC	Hydrophobic core region
Hek293T/17	Human embryonic kidney cells, expressing simian virus 40 large T antigen, clone 17
HRP	Horseradish peroxidase
Hsp	Heat shock protein
IF	Immunofluorescence
Ig	Immunoglobulin
IMDM	Iscove's modified Dulbecco's medium
IPTG	Isopropyl-β-D-thiogalactopyranoside
kb	Kilobase
kDa	Kilodalton
l	Litre
LB	Lysogeny broth
M	Molar concentration
mA	Milliampere (10^{-3})
mAb	Monoclonal antibody
min	Minute
ml	Milliliter (10^{-3})
mM	Millimolar concentration (10^{-3})
N	Asparagine
n.d.	Not done
N2a	Murine neuroblastoma cell line
ng	Nanogram (10^{-9})
nm	Nanometer (10^{-9})
NM	NM domain of Sup35
NM^{agg}	Aggregated NM protein
NM^{sol}	Soluble NM protein
ns	Not significant

O/N	Overnight
OD	Optical density
OPR	Oligopeptide repeat region
pAb	Polyclonal antibody
PAGE	Polyacrylamide gel electrophoresis
PAPA	Prion aggregation prediction algorithm
PBS	Phosphate buffered saline
PCR	Polymerase chain reaction
PD	Parkinson's disease
PEG	Polyethylene glycol
PLAAC	Prion-like amino acid composition
PMCA	Protein misfolding cyclic amplification
PMD	Protein misfolding disease
PrD	Prion domain
PrLD	Prion-like domain
PRNP	Gene of the human prion protein
PrP	Prion protein
PrP^{C}	Cellular isoform of the prion protein
PrP^{Sc}	Pathogenic isoform of the prion protein
Q	Glutamine
QNR	Asparagine- and glutamine- rich region
RNA	Ribonucleic acid
rpm	Revolutions per minute
RT	Room temperature
S. cerevisiae	*Saccharomyces cerevisiae*
SD	Standard deviation
SDD-AGE	Semi-denaturing detergent - agarose gel electrophoresis
SDS	Sodium dodecyl sulfate
sec	Second
SP	Signal peptide
TDP-43	43 kDa, transactive response DNA binding protein
ThT	Thioflavin-T
Tris	Tris(hydroxymethyl)aminomethane
TSE	Transmissible spongiform encephalopathy

UV	Ultraviolet
V	Volt
WB	Western blot
µg	Microgram (10^{-6})
µl	Microlitre (10^{-6})
µm	Micrometer (10^{-6})
µM	Micromolar concentration (10^{-6})

Publications and congress contributions

Publications

Grassmann, A., Wolf, H., Bester, R., Hossinger, A., Pleschka, K., Duernberger, Y., Riemschoss, K., Liu, S., Priola, S.A., Groschup, M.H., Schätzl, H. and Vorberg, I. Involvement of alternative endocytic pathways in prion strain replication. *In revision.*

Duernberger, Y., Liu, S., Paulsen, L., Bester, R., Kuhn, P.H., Schölling, M., Lichtenthaler, S.F., Vorberg, I. Prion replication in the mammalian cytosol: Functional regions within a prion domain driving induction, propagation and inheritance. *Submitted.*

Posters

Duernberger, Y., Liu, S., Paulsen, L., Bester, R., Kuhn, P.H., Schölling, M., Lichtenthaler, S.F., Vorberg, I. (2016) Functional protein domains for cytosolic prion replication. DZNE Ph.D. Retreat, Bonn, Germany.

Duernberger, Y., Liu, S., Paulsen, L., Bester, R., Kuhn, P.H., Lichtenthaler, S.F., Vorberg, I. (2016) Prion replication in the mammalian cytosol: Functional regions within a prion domain required for induction, propagation and inheritance. Propagation in Neurodegenerative Disease Conference, Dublin, Ireland.

Duernberger, Y., Liu, S., Paulsen, L., Bester, R., Kuhn, P.H., Lichtenthaler, S.F., Vorberg, I. (2015) Prion replication in the mammalian cytosol: Functional regions within a prion domain required for induction, propagation and inheritance. DZNE Retreat, Nürburg, Germany.

Duernberger, Y., Liu, S., Paulsen, L., Bester, R., Kuhn, P.H., Lichtenthaler, S.F., Vorberg, I. (2015) Prion replication in the mammalian cytosol: Functional regions within a prion domain required for induction, propagation and inheritance. Molecular Mechanisms and Physiological Consequences of Protein Aggregation Conference, West Palm Beach, USA.

Talks

Prion replication in the mammalian cytosol: Functional regions within a prion domain required for induction, propagation and inheritance. (2016) Propagation in Neurodegenerative Disease Conference, Dublin, Ireland.